Politecnico di Torino

DEPARTMENT OF ENERGY "G. FERRARIS"
Master of Science in Energy and Nuclear Engineering

MASTER THESIS

Development of a collisional-radiative code for the interpretation of optical emission spectroscopy measurements in a helicon plasma source

at Swiss Plasma Center (EPFL, Lausanne)

Candidate:
Rita Agus

Supervisors:
Prof. Gianni Coppa
Prof. Ivo Furno (SPC)
Dr. Riccardo Agnello (SPC)

Academic Year 2018/2019

Anche 1% fa la differenza.

Acknowledgements

First of all, I would like to thank Prof. Gianni Coppa (Politecnico di Torino), for supervising this thesis from Italy and for hooking me up with the Swiss Plasma Center.
My sincere thanks goes to Professor Ivo Furno (École Polytechnique Fédérale de Lausanne) first for giving the opportunity to carry out my final research project in such a stimulating environment and then for his precious guide through it. I am very grateful also to my supervisor Riccardo Agnello (EPFL) for his continuous support, expertise and availability during these months. Thank you both for teaching me what to do research with passion and determination means.
I feel to strongly thank Dr. Christine Stolberg (EPFL) for her assistance during OES and Maurizio Giacomin (EPFL) who shared with me his experience on collisional radiative codes.
I also want to thank the whole SPC-Industrial plasmas group for welcoming me in their great team since the first day.

Abstract

Optical emission spectroscopy (OES) is a non-invasive diagnostic tool for the the characterization of a plasma source. In order to interpret the data from these measurements, it is necessary to use a collisional radiative code that, starting from the light emitted by the plasma, can translate this information into plasma parameters. The goal of this work is the development of a collisional radiative code, AtoH, for the interpretation of the spectrum of hydrogen plasma discharges performed in the Resonant Antenna Ion Device (RAID).
The first step of the project is the realization of a code that, starting from known plasma conditions, is able to estimate the population density of the excited states of atomic hydrogen, and therefore the emissivity.
Then, the results of these simulations are compared with emissivity estimated by Yacora, a web application for the simulation of atomic hydrogen spectral lines. This comparison showed that the two codes differ but the results are not far. The differences are probably due to the different number of quantum states of hydrogen taken into account in the models, and to the different collisional data.
Subsequently, the OES campaign carried on in RAID is described and the main results are reported and commented.
Finally, AtoH is used for the interpretation of the measurements and for the investigation of the effect of negative ions on the line ratios. Using a collisional radiative code for the OES interpretation means finding the plasma parameters combination that reduces the difference between the experimental emissivity and the theoretical one. The result is that, even if AtoH has some limitations, it gives as output a good approximation of plasma parameters.
However, many improvements can be done on AtoH, and they could be the basis for future work, especially the increment of the number of quantum states, the update of the H_2^+ mutual neutralization cross section when it will be available, and the addition of more collisional channels.

Keywords: Plasma physics, collisional radiative code, optical emission spectroscopy, helicon waves, negative ions source, plasma diagnostic.

Executive Summary

This Master thesis is the result of a five-month work at the Swiss Plasma Center (SPC) of École Polytechnique Fédérale de Lausanne, financed by the FuseNet association.
The objective was the development of a zero-dimensional collisional radiative code for the interpretation of optical emission spectroscopy of hydrogen discharges in a helicon plasma source available at SPC, called Resonant Antenna Ion Device (RAID). Optical emission spectroscopy is a non-invasive diagnostic that is able to characterize some of the plasma parameters, recording the emitted radiation. However, for the interpretation of the measurements, a collisional radiative code is necessary. Some collisional-radiative codes have been already developed for this purpose. However, the SPC wanted a personal interpretation code, applicable on RAID, so that it would be easy to exactly know how it works and eventually how to improve the performances.
First, a collisional-radiative population model was developed, allowing to simulate the atomic hydrogen quantum states population density and therefore the emissivity, knowing the plasma parameters (i.e., temperatures and densities of the species). The chemical species involved were H, H_2, H^-, H^+, H_2^+ and H_3^+.
The collisional radiative code was named AtoH, which stands for Atomic Hydrogen. At the same time, *atoh* is a Sudanese word meaning "anyway". Hence the code name has the double meaning of being both the acronym for its purpose, and to recall the reason why this code was developed,as a new option among the already existing models,to be used 'anyway'.
AtoH basically solves a differential system of $|20\rangle$ equations, one for each quantum state, taking into account simultaneously the spontaneous emission and all the collisional channels that could populate or depopulate a quantum state. This model was developed in MatLab.
Then, AtoH was compared to Yacora, another collisional radiative code available online. The two codes have some differences related to the number of considered quantum states, the collisional channels taken into account, the cross sectional data and the method used for the solution of the system of equations. The two models are compared both in terms of emissitivies and excitation channels. Concerning the emissivities, they give results with a constant offset at the same temperature, regardless of the electron density. This result can be linked to the different cross sectional data used. About the excitation channels, AtoH showed an overestimation of the contribution on the final quantum state $|20\rangle$ with respect to Yacora. This is mainly due to the fact that Yacora has a double number of quantum states.
Then, the OES campaign was performed at the SPC laboratories in the Resonant Antenna Ion Device (RAID). RAID is a plasma source developed for the investigation of the physics of negative ions in helicon generated plasmas. The OES setup was installed and calibrated and then the principal atomic lines of hydrogen H_α, H_β and H_γ were measured. The data analysis and also the results of the campaign at 3.5 kW and 1.5 kW were reported and commented.
Finally, AtoH was applied for the interpretation of the OES. The interpretation of these measurements can be done applying the code in an opposite way. While in the direct way the plasma parameters are given as input for the solution, these parameters can be defined, thanks to a minimization algorithm (*fminsearch*), finding the configuration that minimizes the difference between OES and AtoH. The results were not far from the expected ones, except for the H_2^+ density. This is probably due to an overestimation of the mutual neutralization cross section that involves this species. Indeed, new publications are expected for the collisional data related to this channel.

The interpretation of OES is not an easy task due to the multidimensionality of the problem that could bring to unreliable results if their are not critically checked. Anyway, the results must be interpreted as indications and not exact values, considering the simplifications of the model and the complexity of the research of an absolute minimum.
Then, an investigation on the line ratios sensitivity to the negative ions presence was carried on showing that, under particular conditions in which the mutual neutralization becomes the dominant excitation channel, the negative ions density can affect the H_α/H_β value, depending on the electron temperature and density.
Obviously, further enhancements could be done for the improvement of the performances of AtoH, especially with respect to the minimization method. A more flexible algorithm would allow to define some boundary conditions on the space of parameters, avoiding minimums without a physical meaning.

Contents

List of Figures

List of Tables

List of Abbreviations

SPC	Swiss Plasma Center
RAID	Resonant Antenna Ion Device
OES	Optical Emission Spectroscopy
CR code	Colisional Radiative code
LTE	Local Thermodynamic Equilibrium
LP	Langmuir Probe
NBI	Neutral Beam Injection

Chapter 1

Introduction

1.1 Basics of plasma physics

In Physics, a plasma is defined as a mixture of neutrals, electrons and ions that move independently [15]. Langmuir coined the term "plasma" giving birth to this Physics field. Since that moment, this scientific branch rapidly developed for several applications such as energy, microelectronics (i.e., film formation) and decontamination.
The plasma can be fully or partly ionized depending on the energy provided to the gas. This energy is stored in terms of kinetic energy or excitation of the involved species. The first characterization of a plasma is done depending on the temperature, where temperature usually refers to the the temperature of electrons. It is possible to talk about temperature of a plasma only when a thermal equilibrium among all the species is present. High temperature plasmas reach temperatures of millions of Kelvin, with the aim of achieving the fusion of hydrogen isotopes for energy production. On the other hand, low temperature plasmas are dominated by dissociation and ionization phenomena, thanks to electron temperatures of the order of few electronvolt. This work will be mainly focused on low temperature hydrogen plasmas.
The second characterization refers to the heating method, such as constant or alternating electric fields at low frequencies or radio frequencies or waves at GHz frequencies. In particular, in the case of waves-heated plasma, the frequency of the electric field is so high (GHz) that the electrons can just follow the electric field, and when an additional magnetic field is applied, also the resonant heating of electrons becomes possible.
All plasmas can be generated at low pressure or atmospheric pressure. The difference is related to the fact that the collision rate increases when increasing the pressure, approaching a condition closer to thermal equilibrium (i.e., same temperature of all the species).
Another factor that characterizes low temperature plasmas is the *ionization degree*, namely the ratio between the number of charged species and the total density of the species. Sometimes this factor is defined also as the ratio between electron density and density of the neutral species. The other two important parameters are the degree of electronegativity, that is the ratio between the density of negative ions and electrons, and the degree of dissociation that, in the case of an hydrogen plasma, is the ratio between atomic and molecular hydrogen [33].

1.2 Diagnostic in low temperature plasmas

The goal of plasma diagnostic is the determination of plasma parameters, as temperature and density of the different species involved. The easiest types of plasma diagnostic are externally accessible, like a spectrometer that records the light emitted by the plasma [35]. More complicated diagnostics (e.g., the Langmuir probes, LP) are able to directly measure the electron temperature. The LP consists of a metallic thin cylindrical electrode that, after being inserted inside the plasma

is submitted to a constant or time-varying voltage. It allows to measure the temperature of the electrons and to have an idea of the electron density distribution. Indeed, the electron density measured with this technique could be underestimated if not corrected with laser interferometry. Laser interferometry is a method that, measuring the defasage of a laser that crosses a plasma, is able to estimate the integrated value of electron density. From this result, knowing the electron density distribution thanks to the measurements with the LP, it is possible to calculate the peak value of n_e.
Other advanced diagnostics, such as two photons induced fluorescence and cavity ring down, allow to determine the density of neutral and negative ions respectively.
In this work, the attention is focused on the optical emission spectroscopy diagnostic.

1.3 Introduction to Optical Emission Spectroscopy

Optical Emission Spectroscopy (OES) is an external, relatively easy, diagnostic tool that, recording the light emitted by a plasma source, is able to give some information about its physical conditions. The study of the light emission started in 1752, when Thomas Melville firstly demonstrated that the radiation of an incandescent gas is composed by several discrete frequencies, called emission lines. Then, it was discovered that an atom exposed to white light is able to absorb only particular frequencies, the absorption lines, that exactly corresponds to the emission lines. Later, Balmer showed that the lines on the visible part of the hydrogen spectra are regular, and he described this relation with the following empirical formula.

$$\nu_{ab} = R(\frac{1}{n_a^2} - \frac{1}{n_b^2}) \quad n_a = 1, 2.., \quad n_b = 3, 4.. \tag{1.1}$$

where R is the Rydberg's constant, n_a and n_b are positive integers with $n_b > n_a$ and ν_{ab} is the frequency of an emission or absorption line. It was subsequently demonstrated that the Balmer's formula is valid for the complete hydrogen spectrum.
At the beginning of the 20th century, with the atomic hydrogen semiclassical model of Niels Bohr, the connection between atomic physics and the radiation emission was explained. In this model, the electron moves around the nucleus of its atom in circular orbits, without emitting any radiation. The allowed orbits are finite in number and a specific energy of the electron is associated to each orbit, following that the energy of the electrons is quantized. Indeed, an electron can change its orbit only if it acquires, or loses, through an electromagnetic radiation, exactly the amount of energy that corresponds to the energy difference between the two orbits. In particular, if E_i is the energy of the initial orbit and E_f the energy of the final one, the energy of the electromagnetic wave, emitted or absorbed, is equal to:

$$|E_f - E_i| = h\nu \tag{1.2}$$

where ν is the wave frequency and h is the Planck constant ($6.626 \cdot 10^{-34}$ J s).
This formula allowed to relate the radiation emitted by an atom to well defined electrons movements from an initial orbits to a final one characterized by a lower energy. Each orbit, and thus the associated energy of the electron, is quantized by an integer number n, called principal quantum number:

$$E_n = -\frac{me^4}{32\pi^2\varepsilon_0^2\hbar^2 n^2} \tag{1.3}$$

where ε_0 is the vacuum electrical permittivity ($8.85 \cdot 10^{-12}$ Fm^{-1}), e is the elementary charge ($1.602 \cdot^{-19}$ C), m is the mass of the electron ($9.11 \cdot 10^{-31}$ kg) and $\hbar$ is the reduced Planck constant ($h/2/\pi$). The integer numbers that in the Balmer's formula (1.1) define the frequency of the atomic hydrogen lines, exactly correspond to the fundamental quantum numbers n.
Therefore, it is possible to justify the emission line of the spectrum of an atom as the result of the transition of an electron between two defined quantum states.
Every element has its particular spectrum with characteristic wavelengths, thanks to the different

electronic configurations, that allows to distinguish them from each other. A first distinction can be done for atomic and molecular transitions. In the case of the molecule, more effects must be taken into account such as the interaction between different nucleus and their respective interaction with the surroundings. In this situation, indeed, the electronic states split in a set of level related to the vibration (indicated with the quantum number ν) and the rotation of the nuclei. The vibrational, rotational and electrons energy scales are well separated so that the vibrational transitions tends to the infrared, rotation emissions are in the microwave regions and electrons radiations mostly fall in the visible and UV part of the spectrum [1].
The atomic hydrogen spectrum was studied in depth, and its lines are labelled with the Greek letters in order of decreasing wavelength. The series that terminates in the ground state is called *Lyman* series and lies in the ultra-violet part of the spectrum. The Balmer series has the final quantum number $n = 2$, and its lines are denoted as H_α ($\lambda_\alpha = 656.3$ nm), H_β ($\lambda_\beta = 486.1$ nm), $H_\gamma(\lambda_\gamma = 434.0$ nm), etc. Finally, another well known series is the Paschen one, for the transitions to the quantum state $|3\rangle$ [3].

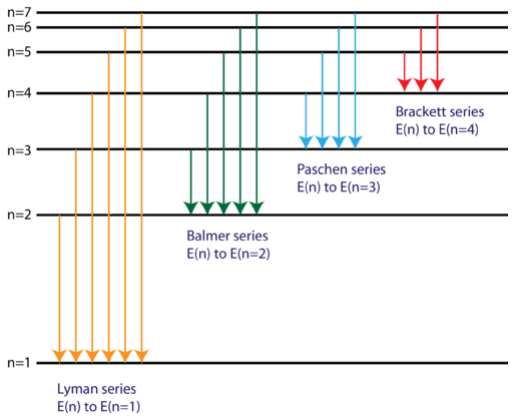

Figure 1.1: Spectral lines of atomic hydrogen [14]

The emission of a photon, related to the decay of the electron to a level with a lower energy, is a phenomenon called *spontaneous emission*. The probability per unit time that a spontaneous emission occurs is given by the Einstein coefficient A_{ij}, where $|i\rangle$ and $|j\rangle$ are the initial and final states of the electron. For atomic hydrogen these coefficients are well known and tabulated [34].
The emissivity of an atomic line radiation per unit of volume, time and solid angle, is directly proportional to the associated Einstein coefficient and to the population density of the initial state n_i. The term *population density*, indicates the density of electrons that populate a quantum state [17].

$$\epsilon_{ij} = \frac{h\nu}{4\pi} n_i A_{ij} \quad [\frac{\text{eV}}{\text{sm}^3\text{sr}}] \tag{1.4}$$

At the same time, an emission can be characterized in terms of absolute line intensity:

$$I_{ij} = n_i A_{ij} \quad [\frac{\text{ph}}{\text{m}^3\text{s}}] \tag{1.5}$$

Therefore, the line emission intensity depends only on the the population density of the excited level that in turn strongly depends on the plasma parameters.

$$n_i = f(T_e, n_e, T_{ions}, n_{ions}, \dots) \tag{1.6}$$

1.3.1 Non equilibrium plasmas

By definition, a non equilibrium plasma is a plasma in which the temperature of ions and electrons are different. This is due to the fact that, during an elastic collision, the energy that can be transmitted is proportional to the ratio of the masses of the colliding particles and therefore, the electrons can transfer a small amount of energy. When the electron density is sufficiently high ($n_e > 10^{22}$ m^{-3}), the collisions between ions and electrons are enough to establish an equilibrium between the two species. When this condition is not reached, the electrons dominate the dynamic of the plasma. The term dynamic of the plasma indicates the collisional processes that lead to the population or depopulation of a quantum state. In the case of an hydrogen plasma, the principal processes that affect the dynamic are the excitation and de-excitation process due to electron collisions. However, as well as spontaneous emission, also other processes must be taken into account for the determination of the population densities of non equilibrium plasmas.
These plasmas are far from local thermal equilibrium and therefore the population of the excited states is not described by a Maxwell-Boltzmann distribution and, in addition, the population of excited states is several order of magnitude lower than the population of the ground state. These conditions allows to assume that the ground state density is equal to the overall density of the gas.
All these ingredients are considered in what is called *population model*, for the calculation of the population density of the excited states of a chemical species [17, 12].

1.4 Population models

Three types of population models are mainly applied:

- Corona models
  This model is suitable for applications in an ionizing plasma, therefore with low electron density ($n_e \approx 10^{12}$ m^{-3}), high electron temperature ($T_e \approx 100$ eV) and negligible radiation density. The fact that the radiation density is negligible means that self-absorption is not an important phenomenon and the excitation occurs only due to electron collisions [2]. The high electron temperature guarantees that the plasma is ionizing and thus the recombining processes, that will be later explained, are negligible. This model assumes that the upward transitions are related only to electron collisions, while downward transitions are due to spontaneous emission.

- Collisional Radiative (CR) models
  This model balances the collisional and radiative processes, setting up a rate equation for each quantum state coupled with all the other states. It is a necessary instrument for electron densities higher than 10^{16} m^{-3}, since other processes, not considered in corona models, may play an important role. The purpose of this work is the development of this type of model that will be fully described in Chapter 2. It is the most complete type of model since it has no limits of applicability if all the main collisional channels are considered. It can be seen as the improvement of a corona model, where in case of atomic hydrogen the recombination, mutual neutralization and dissociative excitation processes are added.

- LTE models
  The local thermodynamic equilibrium model can be used in situations of high electron densities ($n_e > 10^{22}$ m^{-3}) where the density of excited states of atoms and molecules follows a local Boltzmann distribution function [16, 12].

1.5 Atomic hydrogen

In the case of a population model for atomic hydrogen, under particular conditions, it is possible to make some simplifications. Indeed, the effect of an excitation channel on populating or depopulating a quantum state, can be predominant or negligible depending on the electron temperature.

When the temperature is higher than a few eV, the plasma is *ionizing* and the most effective phenomena are the direct excitation from the ground state and the dissociative excitation of H_2. In the case of a *recombining* plasma, the electron temperature is $T_e \leq 1$ eV and therefore the recombination of positive ions and their mutual neutralization with H^- can be the dominant paths. All these excitation channels will be fully explained in Chapter 2.
In the case of a partially-recombining plasma, all the previous mentioned collisional processes must be taken into account. The most important excitation channels for an atomic hydrogen model and the simplifications that might be done under the related assumptions are reported in Figure 1.2.

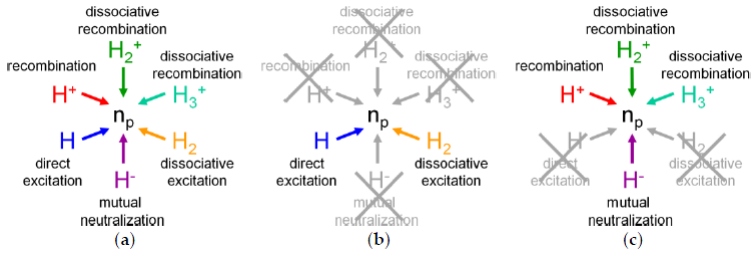

Figure 1.2: Atomic hydrogen excitation channels: (a) all the channels, (b) relevant channels in ionizing plasmas, (c) relevant channels in recombining plasmas [36].

1.6 Interpretation of optical emission spectroscopy by means of population models

The first way to use a CR code is a direct way: knowing all the plasma parameters (i.e., densities and temperatures of all the species involved) it can calculate the emissivity related to these particular conditions. Moreover, changing some of these parameters it is possible to figure out which are the channels that mostly affect the emission.
The second way is an inverse application of the model. It can be used for the interpretation of OES, and therefore for the extrapolation of the physical information contained in the emissivity recorded by the spectrometer. Indeed, knowing the values of emissivities observed during an optical emission spectroscopy campaign, the population model can be implemented to find out the values of plasma parameters that give as output the same emissivities. The collisional radiative code developed will be applied for the interpretation of OES of hydrogen discharges on the Resonant Antenna Ion Device, RAID. This device will be described in Chapter 4.

1.7 Structure of the thesis

In this project, a collisional radiative code (called *AtoH*) for the calculation of the emissivity of the Balmer lines H_α, H_β and H_γ has been developed and it will be fully illustrated in Chapter 2. Then, in Chapter 3, AtoH will be compared with another collisonal radiative code called Yacora, available online, that has been developed at the Max Plank Institute for Plasma Physics.
In Chapter 4 the resonant antenna plasma device (RAID) setup and working principles will first be introduced. Then the optical emission spectroscopy campaign on RAID will be described and the main results will be reported and commented.
Finally, on Chapter 5, the code will be applied for the interpretation of the OES measurement, in order to characterize, as much as possible, the plasma parameters.
In Chapter 6 the conclusions and the suggestions for future improvements will be reported.

Chapter 2

AtoH: population densities calculation and emissivity estimation

A flexible and handy population model was necessary for the interpretation of OES in RAID plasma device. As it will be fully explained in Chapter 4, the electrons and ions temperatures are quite different in RAID, and therefore it is defined as a non-equilibrium plasma. Moreover, the electron temperature conditions categorizes RAID as in between an ionizing and a recombining plasma. For these reasons, a complete collisional radiative code was necessary. This is *AtoH*.

2.1 Structure of the model for the calculation of the population densities

The first goal of this model is to calculate the population density distribution over the excited quantum states of atomic hydrogen. As explained in the Introduction, knowing the population density it is possible to calculate the associated emissivity. Then, this type of code could be applied for OES interpretation.
Each energy level is defined only by the fundamental quantum number, since the sub-levels, due to different possible orientations of the angular momentum and the spin of the electron, are degenerate. This means that the different quantum levels are distinguished only depending on their energy [36].
The population density can be calculated through the solution of a time dependent, 0 dimensional, system of equations. Each equation describes the time evolution of the electron density (n_i) of the single quantum state $|i\rangle$ taking into account the phenomena that populate and depopulate this energy level.
A quantum state $|i\rangle$ can be populated by:

- collisional excitation of an electron in a generic $|j\rangle$ quantum level at a lower energy;
- collisional de-excitation of an electron in a generic $|j\rangle$ quantum level at a higher energy;
- radiative decay of an electron (spontaneous emission).

The same processes can depopulate a quantum level, moving an electron to a higher or to a lower quantum state. Therefore, it is clear that all the $|j\rangle \neq |i\rangle$ quantum states inserted in the model, are involved in the equation of the $|i\rangle$ state. The contribution of a collisional process can be simply described as the product between a rate coefficient (usually denoted by the letter K), that depends on the temperature of the electrons (or the ions), and the densities of the involved species

[23]. On the other hand, the spontaneous emission contribution is expressed as the product between the density of the initial excited quantum state and a coefficient that quantifies the transition probability between the initial (i) and final (j) energy level, called Einstein coefficient (A_{ij}) [34, 35].
The differential equation with all the contribution is shown in the Formula (2.1).

$$\frac{dn_i}{dt} = \sum_{j>i} A_{ji} n_j - \sum_{j<i} A_{ij} n_i + n_e \Bigg(\sum_{j \neq i} K_{ji}(T_e) n_j - \sum_{j \neq i} K_{ij}(T_e) n_i - S_p n_p + (\alpha + \beta n_e) n_+ + n_0 K_0(T_e) + n_+ K_{DR,+}(T_{ion}) \Bigg) + n_+ n_- K_{\pm}(T_{ion}) \quad (2.1)$$

The right hand side of the equation represents:

1. population of the state $|i\rangle$ due to a spontaneous emission from the state $|j\rangle > |i\rangle$;
2. depopulation of the state $|i\rangle$ due to spontaneous emission from the state $|i\rangle$ to the state $|j\rangle < |i\rangle$;
3. population of the state $|i\rangle$ due to electron collision excitation from a a state $|j\rangle < |i\rangle$ and electron collision de-excitation from a state $|j\rangle > |i\rangle$;
4. depopulation of the state $|i\rangle$ due to electron collision excitation to a a state $|j\rangle > |i\rangle$ and electron collision de-excitation to a state $|j\rangle < |i\rangle$;
5. depopulation of the state $|i\rangle$ due to the electron collision ionization;
6. population of the state $|i\rangle$ due to two and three body positive ions recombination;
7. population of the state $|i\rangle$ due to dissociative excitation of neutral species $\Big(n_0 K_0(T_e)\Big)$ and dissociative recombination of positive ions $\Big(n_+ K_{DR,+}(T_{ion})\Big)$;
8. population of the state $|i\rangle$ due to mutual neutralization of ionic species (n_+ and n_-).

In general, as specified in the introduction, different collision processes have a different effect depending on the conditions of the plasma, and in particular depending on if it can be defined as a recombining or ionizing plasma. In ionizing plasmas, the direct excitation by electron collision is the predominant channel, while in recombining plasmas the predominant path is the recombination [37]. Since in this model both these type of channels have been inserted, it means that it is suitable for an application in both recombining and ionizing plasmas.

2.1.1 Calculation of the rate coefficients

The rate coefficients can be obtained by calculating the convolution integral of the collision quantities and the velocity distribution functions of the particles. The convolution integral allows to weight the effect of a collisional process as a function of the effective velocity (and thus energy) distribution of the involved particles.
The fundamental quantity that characterizes a collision is the cross section $\sigma(v_r)$, where (v_r) is the relative velocity of the two particles before the collision.

$$v_r = |\vec{v_1} - \vec{v_2}| \quad (2.2)$$

The cross sections are generally defined choosing as center of the coordinate system the center of mass of the system.
Thus, to obtain the rate coefficient $k_i(T)$, the parameter that defines the collision frequency as a

function of the temperature, it is necessary to integrate the cross section over the velocity distribution function of the involved particles ($f_1(v_1)$ and $f_2(v_2)$).
The expression for the reaction rate is [23]:

$$k_i = \int_0^{+\infty} f_1(v_1) f_2(v_2) \sigma(v_r) v_r \, d^3v_1 \, d^3v_2 \tag{2.3}$$

When the collision process includes an electron and a heavy particle, the relative velocity of the colliding particles can be assumed to be the velocity of the electron, as if the heavy particle is at rest, since the velocity of the electron is much higher and its mass is negligible. This is the same as saying that the center of mass, and thus the center of the reference system, is the center of the heavy particle. Under this condition, it is necessary to know only the electron distribution function, and the integral is much easier.
In the references adopted for the calculation of the rate coefficients, the cross section is always expressed as a function of the energy of the collision E, that again can be assumed to be the energy of the colliding electron in case of electrons-heavy particles collisions. Therefore, for a given energy distribution function *f(E,T)* of the electrons, the rate coefficient can be calculated doing the convolution integral of the product of the electron velocity $v(E)$ with the reaction cross section $\sigma_i(E)$ [29].
In a plasma, it is possible to assume an electron Maxwell-Boltzmann distribution if the mean distance between the electrons is higher than the de Broglie wavelength of electrons with thermal energies (Λ):

$$\Lambda = \frac{h}{\sqrt{2\pi m_e k T_e}} \tag{2.4}$$

where T_e is the electron temperature, k is the Boltzmann constant ($1.38 \cdot 10^{-23}$ $\mathrm{m^2 kgs^{-2} K^{-1}}$), m_e is the mass of an electron and h is the Planck constant.
In terms of electron density:

$$n_e << \Lambda^{-3} \tag{2.5}$$

Otherwise, a Dirac distribution function must be adopted [16]. In general, in low temperature plasmas, a deviation from a Maxwell-Boltzmann distribution can be related to:

1. a heating of the plasma due to secondary electrons that are generated by ion impact on the plasma walls;
2. a reduction of the distribution function due to dominant loss mechanisms such as dissociation and ionization [33].

Considering RAID's operating conditions, for example with an electron density between $10^{17} - 4 \cdot 10^{18}$ $\mathrm{m^{-3}}$ and an electron temperature around $1 - 5$ eV, this condition is always satisfied and a Maxwell-Boltzmann distribution can be assumed.
In terms of velocity the distribution function assumes the shape reported on Equation (2.6).

$$f(v)dv = \left(\frac{m}{2\pi k T_e}\right)^{3/2} exp\left(-\frac{m_e v^2}{2kT_e}\right) 4\pi v^2 dv \tag{2.6}$$

The corresponding energy distribution function adopted is [16]:

$$f(E, T_e)dE = 2\left(\frac{E}{\pi}\right)^{1/2} (kT_e)^{-3/2} exp\left(\frac{-E}{kT_e}\right) dE \tag{2.7}$$

Therefore, the complete integral is expressed as:

$$k_i(T_e) = \int_0^{+\infty} \sigma(E) v(E) 2\left(\frac{E}{\pi}\right)^{1/2} \left(kT_e\right)^{-3/2} exp\left(\frac{-E}{kT_e}\right) dE \tag{2.8}$$

The velocity $v(E)$, neglecting any relativistic effect, is calculated as:

$$v(E) = \sqrt{2E/m_e} \tag{2.9}$$

As far ad the collisions between particles with a comparable mass (as for example two ions) are concerned, the approximation made for the relative velocity in the case of electron-heavy mass collision is no longer valid.
In this case, in the adopted references, the cross section is expressed in terms of relative collision energy of the two particles, on a reference system centered in the center of mass. To consider the effect related to the the different masses, it is necessary to adopt a reduced mass μ [4]:

$$\mu = \frac{m_A m_B}{m_A + m_B} \tag{2.10}$$

The rate coefficient obtained, is calculated always assuming a Maxwell-Boltzmann distribution function. The formula used is always (2.8), substituting the mass with μ and integrating over the relative energy.

Rate coefficients for de-excitation collisions

As already said, the electron collision can cause an excitation or a de-excitation of atomic hydrogen. Concerning the de-excitation due to electron collision, the cross section was calculated starting from the excitation cross section and applying the principle of the detailed balance. The principle of the detailed balance can be applied assuming that transitions between any two states take place with equal frequency in both directions.
If the term a_{ij} represents the probability per unit time of a excitation from state i to state j, and assuming that the system is kept at a constant temperature T by thermal contact with a heat bath at this temperature, it follows that:

$$a_{ij} \exp\left(-\frac{E_i}{kT}\right) = a_{ji} \exp\left(-\frac{E_j}{kT}\right) \tag{2.11}$$

The transition probability for the de-excitation process is thus defined as [20]:

$$a_{ji} = a_{ij} \exp\left(\frac{E_j - E_i}{kT}\right) \tag{2.12}$$

The numerator of the exponential term is always bigger than zero since the energy of the final state E_j is bigger than the energy of the initial one E_i, and this means that increasing the temperature in the denominator, all the exponential term tends to one. As a consequence, at low temperatures the de-excitation transition probability a_{ji} is bigger than the excitation probability while increasing the temperature the two probabilities get closer in order to achieve an equilibrium condition between the two processes.
In our application, a_{ij} represents the excitation cross section due to electron collision, a_{ji} is the cross section for the inverse process, and T is the electron temperature T_e.
The energy of two different quantum states, E_i and E_j, is calculated as:

$$E_n = \frac{-m_e^4}{2n^2\hbar^2} = \frac{E_0}{n^2} \tag{2.13}$$

where E_0 is the energy of the ground state ($E_0 \approx -13.6\,\text{eV}$), $\hbar$ is the reduced Planck constant and n is the fundamental quantum number [3]. Once that the cross section has been defined, the rate coefficient is calculated, also in this case, through the convolution integral over the probability density function.

2.1.2 Collisional channels

The species that are mainly present in a low temperature hydrogen plasma and that are considered in this population model are: H, H_2, H^-, H^+, H_2^+ and H_3^+ [27].
Since the objective of this model was the application on RAID the choice of the collisional channels was related to the operating conditions of this plasma device. Thanks to the fact that the electron temperature and density is well defined on RAID, it is known that it can generate a partially-recombining plasma. This means that all the collisional processes reported in Figure 1.2 should be taken into account.
Table 2.1 shows an overview of the collisional channels that were considered in the model.

Table 2.1: Overview of the reactions inserted in the model for the hydrogen atom

Collisional process		Reference
Excitation by electron collision	$H(j) + e \longrightarrow H(i > j) + e$	[27]
De-excitation by electron collision	$H(j) + e \longrightarrow H(i < j) + e$	[27], [20]
Ionization by electron collision	$H(j) + e \longrightarrow H^+ + 2e$	[27]
Spontaneous emission	$H(j) \longrightarrow H(i < j) + h\nu$	[34]
H^+ recombination	(2 body) $H^+ + e \longrightarrow H(i) + h\nu$	[27]
	(3 body) $H^+ + 2e \longrightarrow H(i) + e$	[27]
H_2 dissociative excitation	$H_2 + e \longrightarrow H(i) + H(1) + e$	[30]
H_2^+ dissociative recombination	$H_2^+ + e \longrightarrow H(i) + H(1)$	[27]
H_3^+ dissociative recombination	$H_3^+ + e \longrightarrow H(i) + H_2$	[27]
Mutual neutralization	$H^+ + H^- \longrightarrow H(i) + H$	[27]
	$H_2^+ + H^- \longrightarrow H(i) + H_2$	[9]

It is possible to see that there is a missing reaction with respect to the CR code channels for an atomic hydrogen model reported in the Introduction (Figure 1.2). This is the H_2^+ dissociation due to a collision with an electron: $H_2^+ + e \longrightarrow H(i) + H^+ + e$. This reaction has a threshold value at a temperature of 15.2 eV [27] and therefore it was neglected in first approximation since the maximum temperature measured in RAID is lower than 5 eV.

Electron impact process

$$e + H(j) \longrightarrow e + H(i>j) \tag{2.14a}$$
$$e + H(j) \longrightarrow e + H(i<j) \tag{2.14b}$$
$$H(j) + e \longrightarrow H^+ + 2e \tag{2.14c}$$

The electron collision with the hydrogen atom can cause excitation (2.14a), de-excitation (2.14b) or ionization (2.14c).
The cross section for the excitation is distinguished between cross section for the excitation from the ground state and cross section for the transitions between excited states.
In Figure 2.1 (a), the cross section for excitation from the ground level depending on the electron energy and the correspondent rate coefficient as a function of T_e are shown. As it is possible to see, this quantity has a threshold value that increases with the quantum number of the state that is populated, since more energy is required to allow a transition to a higher quantum level. Obviously also the rate coefficient for excitation decreases with the final quantum level and it increases with the temperature in the range of interest.
The phenomenon of ionization becomes more and more important, as expected, when increasing the electron temperature. Indeed, if the electrons have more energy, this means that they can easily ionize a hydrogen atom, and, moreover, electrons in high energy levels need less energy to be removed from an atom, and thus they have a lower threshold, as shown in Figure 2.2.

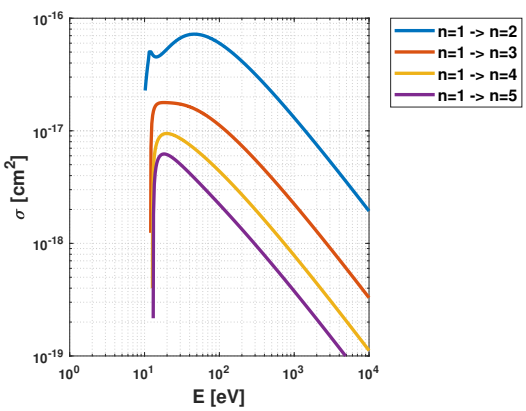

(a) Electron collision excitation cross section from the ground state to n=1,2,3,4,5

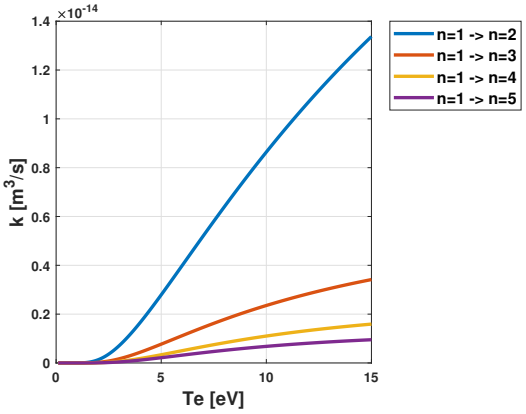

(b) Electron collision excitation rate coefficient from the ground state to n=1,2,3,4,5

Figure 2.1: Comparison between electron collision excitation cross section and rate coefficient

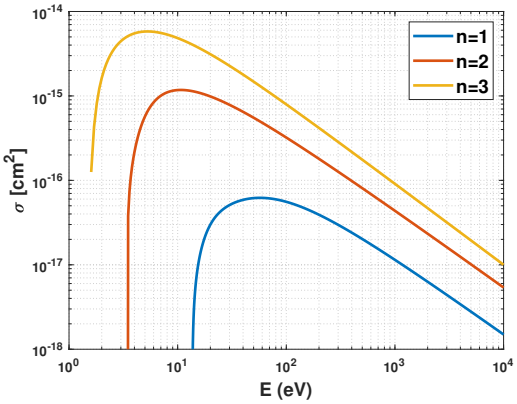

Figure 2.2: Electron impact ionization cross section of n=1,2,3 states of atomic hydrogen

Spontaneous emission

$$\mathrm{H(j)} \longrightarrow \mathrm{H}(i<j) + h\nu \tag{2.15}$$

The spontaneous emission is a radiative phenomenon for which an excited electron spontaneously moves to a lower energy state emitting a photon with an energy equal to the energy difference of the two states (neglecting the recoil energy of the atom) [17, 3]. The transitions for which the Einstein coefficient is zero are optically forbidden. The data regarding Einstein coefficient has been taken from an article of the National Institute of Standard and Technologies [34].
In order to check the the powerful of the spontaneous emission process, Figure 2.3 was realized. To obtain this graph, the effect of Einstein coefficients for the population and the depopulation of excited states was considered.
The initial population density for the hydrogen states has been set with a ground state density of the order of 10^{19} m^{-3}, and excited levels densities between $10^{12}\mathrm{m}^{-3}$ for $|2\rangle$ and $10^{8}\mathrm{m}^{-3}$ for $|20\rangle$. Figure 2.3 shows the depopulation of the states $|2\rangle - |20\rangle$, and not the ground state since its density is several order of magnitude bigger than the others.
The steady state condition in which all the excited states are empty is reached in almost 10^{-4}s.

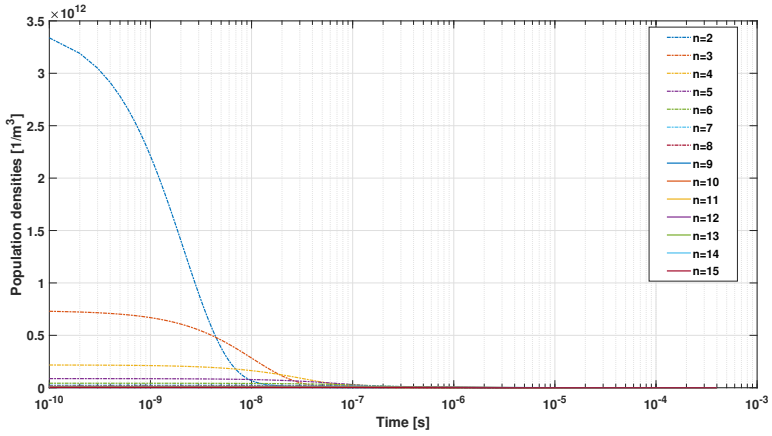

Figure 2.3: Test of the Einstein coefficient depopulating power

Two and three bodies H^+ recombination

$$H^+ + e \longrightarrow H(i) + h\nu \tag{2.16a}$$

$$H^+ + 2\,e \longrightarrow H(i) + e \tag{2.16b}$$

Each radiative (two bodies, (2.16a)) and three bodies (2.16b) electron-proton recombination generate an atom of hydrogen in an excited state [27].
The effect related to these two reactions is different because when the number of colliding particles increases from 2 to 3, the probability of a successful collision decreases, since a collision is successful if the involved particles interact with enough energy and with the right orientation [18].
This is the reason for which the three body electron-proton recombination is often assumed to be negligible. To verify that, its effect were compared with the electron impact ionization process, that is a non negligible collisional process both at low and high temperatures.
In Table 2.2 the ionization contribute and the three body recombination effect on the population of the state $|2\rangle$ at 1 eV and different electron densities are shown. The gain from the recombining path G_{rec} and the loss due to the ionization channel L_{ion} are calculated as reported on equations (2.17), where n_2 is the population density of the hydrogen quantum state $|2\rangle$ in a steady state condition, referred to the specific n_e and T_e, $k_{ion}(Te, n = 2)$ is the electron impact ionization rate coefficient for the quantum state $|2\rangle$ at T_e, n_{H^+} is the density of the protons, assumed to be constant, and $k_{3R}(T_e, n = 2)$ is the three body recombination rate coefficient that populate the state $|2\rangle$ at T_e.

$$L_{ion} = n_2 n_e k_{ion}(Te, n = 2) \quad [\mathrm{m^{-3}s^{-1}}] \tag{2.17a}$$

$$G_{rec} = n_{H^+} n_e n_e k_{3R}(T_e, n = 2) \quad [\mathrm{m^{-3}s^{-1}}] \tag{2.17b}$$

Table 2.2: Comparison between the depopulation due to electron impact ionization and population due to three body recombination on the state |2> at 1eV for different electron densities

n_e [$\mathrm{m^{-3}}$]	L_{ion} [$\mathrm{m^{-3}s^{-1}}$]	G_{rec} [$\mathrm{m^{-3}s^{-1}}$]
$1 \cdot 10^{18}$	$\approx 10^{13}$	$\approx 10^{13}$
$1 \cdot 10^{17}$	$\approx 10^{10}$	$\approx 10^{11}$
$1 \cdot 10^{16}$	$\approx 10^{7}$	$\approx 10^{9}$

Table 2.2 shows that at 1 eV, with an electron density of 10^{18} $\mathrm{m^{-3}}$, the ionization and the three body recombination process are comparable. Increasing the quantum number, for the same plasma

conditions, the two processes differ more, reaching one order of magnitude of difference. Decreasing the electron density, the two effects are no longer comparable and the ionization overcomes the recombination of at least two order of magnitude if n_e is 10^{16} m^{-3}. Likewise, increasing the electron temperature up to 5 eV, they differ of at least five orders of magnitude even if the electron density is 10^{18} m^{-3}.
The conclusion is that this phenomenon should not be neglected for applications on plasma with densities higher than 10^{17} m^{-3} or temperatures lower than, or equal to, 1 eV. In this model this process was considered, also because, it is the rate coefficient by itself that weights the effect of the processes.
Concerning the radiative recombination (2.16a), in reference [27], was directly given a formulation for the rate coefficient, in which the Sclomilch exponential integral appeared. A proper expansion of these terms has been found in reference [25].

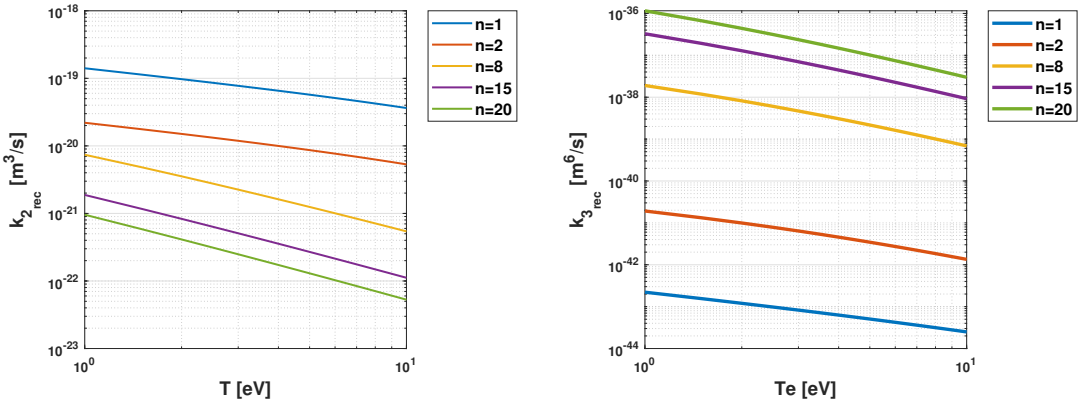

(a) Two bodies recombination rate coefficient

(b) Three bodies recombination rate coefficient

Figure 2.4: Comparison between two and three body proton - electrons recombination rate coefficient

Figure 2.4 shows the two and three bodies recombination rate coefficients. To compare them, it is important to notice the different unit of measurements. Indeed, in order insert the three bodies recombination process on the population density differential equation (2.1), this coefficient must be multiplied two times by the electron density.

H_2 dissociative excitation

$$H_2 + e \longrightarrow H(i) + H(1) + e \tag{2.18}$$

The dissociative excitation is one of the main channels that come from the collision between an electron and an excited molecule of hydrogen. The other channels are non-dissociative or they generate only two ground state atoms of hydrogen, and thus are not interesting for this application, since they do not give a contribution to the population of the excited states.
In reference [27], is stated that in a collision between molecular hydrogen and an electron the non-dissociative channel accounts for 95% of the collisional process. This means that only 5% of the total cross section can be addressed to the dissociative excitation under investigation.
In reference [31] the total dissociative excitation rate coefficient for temperatures lower than 10 10 eV is reported. In addition, in the reference [30] the same rate coefficient is discriminated as a function of the quantum number of the excited hydrogen produced, as shown in Figure 2.5. Here, the contribution on the quantum state n follows a $log(n)^{-6}$ profile, this means that the greatest effect of this dissociation channel is on the lower energy quantum states. The molecular hydrogen dissociative excitation rate coefficient has a peak at a temperature of almost 100 eV, and it decreases when reducing the temperature.

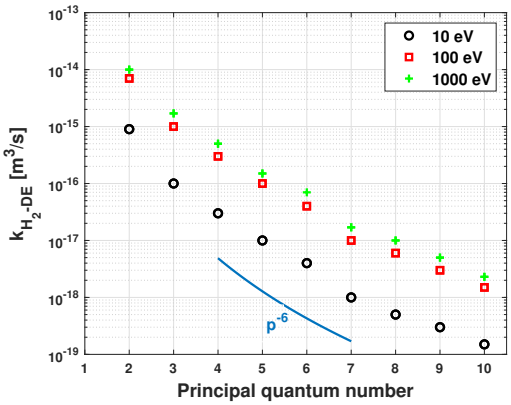

Figure 2.5: Electron impact molecular hydrogen dissociative excitation rate coefficient [30].

In the model, the rotovibrational states of molecular hydrogen are not taken into account. Indeed, in order to consider them, it in necessary to know the density of H_2 in each molecular state and to know the cross section as a function of the vibrational quantum number. As stated in [29], for the development of an atomic hydrogen model it is not necessary to couple it with a molecular hydrogen model since it would add excessive complications without a significant gain in information. For this reason, the H_2 density was not calculated by a molecular model in this application.

H_2^+ dissociative recombination

H_2^+ dissociative recombination rate coefficients are provided in reference [27] only in a form that discriminates the different initial rotovibrational states of this molecule. However, in order to insert these terms in equation (2.1), it would have been necessary to calculate a rate coefficient for each vibrational state of the molecule and at the same time to know the densities, in terms of m^{-3}, of each vibrational excited state of H_2^+ depending on the vibrational quantum number ν.
The molecule H_2^+ is the simplest molecular ion, which consists of only two protons and one electron that is perfectly shared between the two positive charges. The Schrodinger quantum mechanics equation can be analytically solved for H_2^+ thanks to its simple configuration, also due to the lack of the electron-electron repulsion. It follows that the energy associated to the molecular states can be calculated.
The first assumption that is necessary to make in order to calculate an average rate coefficient, is that all the H_2^+ molecule are in a fundamental electronic state. Knowing that, it was also possible to numerically calculate the vibrational energy of the molecule.

$$E_\nu = \hbar\omega_0(\nu + \frac{1}{2}) \tag{2.19}$$

where $\omega_0 = 8,25 \cdot 10^{-3}$ s^{-1}, referred to $|0\rangle$, and ν is the vibrational quantum number [1].
The cross sections provided in [27] are in the form $\sigma(\nu \to n)$, therefore differentiating the production of atomic hydrogen in different excited states (n) from different vibrational excited quantum states ν.
Assuming that the probability that a H_2^+ molecule is on a specific quantum state ν, can be approximated by a Maxwell-Boltzmann probability function, it is possible to calculate the total cross section that generates a hydrogen atom on a specific quantum state starting from any initial

vibrational state of the ionic molecule.

$$P_\nu = \frac{e^{\frac{-E_\nu}{RT}}}{Q} \tag{2.20a}$$

$$Q = \sum_\nu e^{\frac{-E_\nu}{RT}} \tag{2.20b}$$

$$\sigma(\forall\nu \to n=2) = \sigma(\nu=0 \to n=2)P_{\nu=0} + \sigma(\nu=1 \to n=2)P_{\nu=1} + ... + \sigma(\nu>6 \to n=2)P_{\nu\geq 6} \tag{2.20c}$$

where R is the universal gas constant (8.314 $\mathrm{Jmol^{-1}K^{-1}}$), T is the temperature of the gas and E_ν is the energy calculated with Formula (2.19).
Some cross sections behaviours as a function of the electron energy, calculated with the above described procedure, are shown in Figure 2.6.

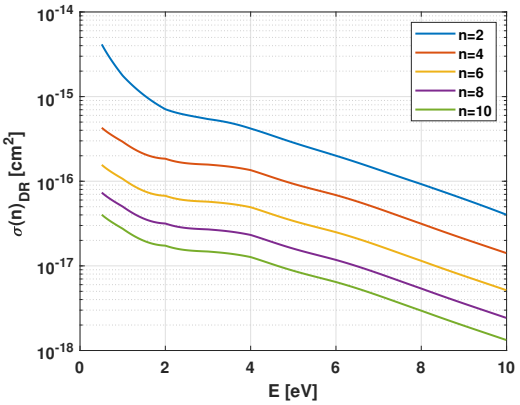

Figure 2.6: H_2^+ dissociative recombination cross section from any ν to $n = 2, 4, 6, 8, 10$

H_3^+ dissociative recombination

The H_3^+ dissociative recombination has two principal dissociation channels.

$$H_3^+ + e \longrightarrow H(i) + H_2 \tag{2.21a}$$

$$H_3^+ + e \longrightarrow 3H(1) \tag{2.21b}$$

Regarding this reactions, only total cross sections are available in literature, and they all refers to a $\nu = 0$ state of H_3^+. The products of the dissociative recombination reaction (2.21a) were theoretically investigated and it was demonstrated that only the quantum state $|2\rangle$ can be populated by this collision [22, 27, 36, 21].
Since the only contribution to the hydrogen excited states comes from (2.21a), it is the only H_3^+ channel that has been inserted in the model. The total cross section provided in reference [27] does not differentiate the effect that could come from (2.21a) or (2.21b). To do that, it was necessary to multiply the total cross section to the branching factors shown in Figure 2.7, for an energy range between 0.003 and 25 eV.

Mutual neutralization

$$H^+ + H^- \longrightarrow H(i) + H \tag{2.22a}$$

$$H_2^+ + H^- \longrightarrow H(i) + H_2 \tag{2.22b}$$

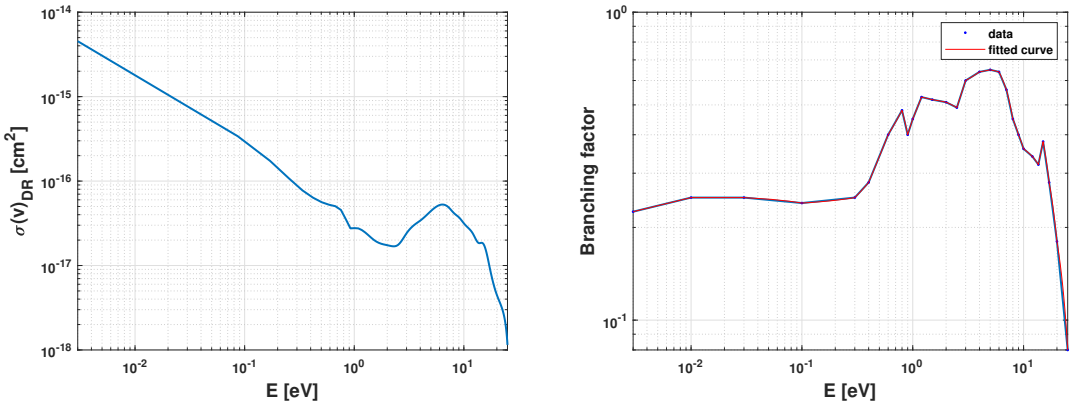

(a) Total cross section for H_3^+ dissociative recombination

(b) Branching factor for H_3^+ dissociative recombination

Figure 2.7: Profile of the total cross section for H_3^+ dissociative recombination and branching factor for the discrimination of the channel ((2.21a))

Mutual neutralization rate coefficients obviously depend on ions temperature, that in low temperature non equilibrium plasmas (such as RAID), is always quite lower than the electron temperature. It is expected to be around $900 - 1000$ K on RAID, while the electron temperature is higher than 11000 K.
About the H^- and H^+ mutual neutralization (2.22a), an interesting fact is that the final states with fundamental quantum number $n = 1$ and $n \geq 4$ are not populated by this reaction, while strong non-adiabatic transitions populate the $n = 2$ and $n = 3$ electron capture channels [27].
In reference [9] the H_2^+ and H^- mutual neutralization cross section is reported for an energy range between 0.02 eV and 10 eV and it was extrapolated for the intermediate values. However, in reference [27], is stated that the cross section estimated within a multichannel Landau-Zener model applied on reference [9] has failed, due to an inappropriate treatment of channel dynamics and coupling interactions.
Nevertheless, reference [9] is the only available data, up to now, about H_2^+ and H^- mutual neutralization, and therefore it was adopted to stall before a new publication. The only thing that reference [27] adds to the previous information is that the two mutual neutralization processes must be comparable in an energy range lower than 1 keV.

2.1.3 Validity range

The validity range of this model is clearly determined by the rate coefficients available data previously mentioned. For the upper threshold, the first limitation comes from H_3^+ dissociative recombination, since the branching factors are available only up to 25 eV. Moreover, the $H_2^+ + H^-$ mutual neutralization cross sections are available only up to 10 eV. Another limitation on the maximum temperature of applicability is the absence of H_2^+ dissociation that, as already mentioned, has a threshold at 15.2 eV [27]. Since the first application of this model was intended for RAID, it was neglected considering the device operating conditions.
Recent laboratory measurement on RAID showed the possibility of a more energetic electron population which, could increase the impact of this channel, even if it represents a small portion of the total electron density.
However, the effect can be considered negligible in comparison to the other reactions, assuming to have an electron Maxwell-Boltzmann distribution that is centered at a temperature lower than 10 eV.
The lower limit again is related to the data availability, and is of 1 eV.

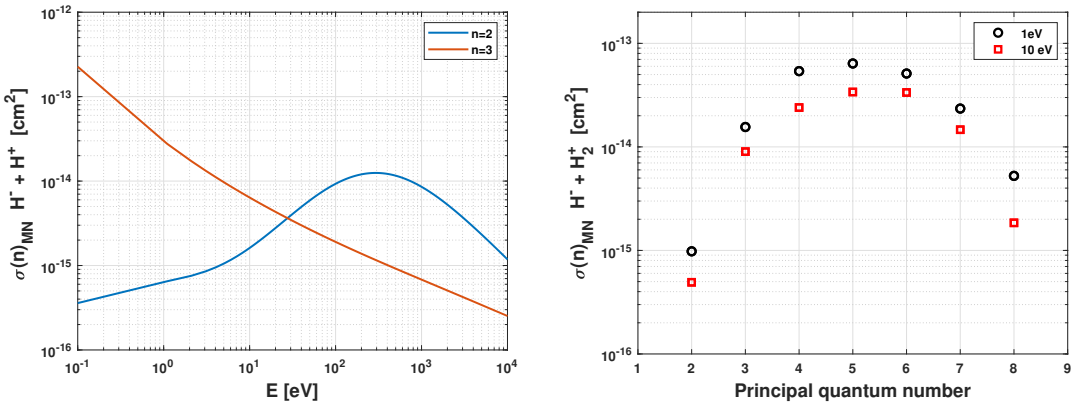

(a) $H^+ + H^-$ mutual neutralization cross section **(b)** $H_2^+ + H^-$ mutual neutralization cross section

Figure 2.8: Comparison between $H_2^+ + H^-$ and $H_2^+ + H^-$ mutual neutralization cross section

To sum up, this model can be considered reliable in a temperature range between 1 eV and 10 eV.

2.1.4 Working principles

As introduced in the section 2.1, finding the population densities means solving the system of equations in which all the excitation channels reported in Table 2.1 take action simultaneously, as in equation (2.1).
This system was defined considering 20 different energy levels for the hydrogen atom, starting from the ground state.
In order to find a solution, it is necessary to set an initial condition for each quantum state considered.
In general there are two possibilities:

1. set the densities of all the excited states in function of the initial temperature of the atomic hydrogen;

2. set only the density of the ground state equal to the total density of the hydrogen gas, and all the other densities equal to zero.

In the second condition, in the first step of the simulation the excited states are populated by the excitation of the electrons in the ground state: as soon as these levels are populated, all the collisional processes start to affect the system.
No particular differences in the results have been shown choosing the condition 1 or 2.
The density of the ground state is several orders of magnitude higher than the density of the excited states and it experiences a very small variation in comparison to its magnitude; for these reasons, it is assumed to be constant in time. It is clear that, physically, in the first instants of the simulations a small reduction of this density is expected, allowing to populate the other states, and then this density remains constant.
Again, no particular differences in the results have been shown when inserting a complete equation for the ground state or imposing this derivative equal to zero.
Therefore, the system can be synthesized as follows, with 20 equations and 553 different rate

coefficients.

$$\begin{cases} \frac{dn_i}{dt} = 0 & \text{if } |i = 1\rangle \\ \frac{dn_i}{dt} = \sum_{j>i} A_{ji} n_j - \sum_{j<i} A_{ij} n_i + n_e \Big(\sum_{j \neq i} K_{ji}(T_e) n_j - \sum_{j \neq i} K_{ij}(T_e) n_i \\ \quad -S_p n_p + (\alpha + \beta n_e) n_+ + n_0 K_0(T_e) + n_+ K_{DR,+}(T_{ion}) \Big) + n_+ n_- K_{+-}(T_{ion}) & \text{if } |i \geq 2\rangle \end{cases} \tag{2.23}$$

This system of 20 equations can be solved only if the unknowns are equal to 20: these unknowns are the population densities of all the quantum states n_i, and this means that all the other parameters that appear in Table 2.3 must be assigned.

Table 2.3: Parameters to assign for the solution of the system

Temperatures [K or eV]	Densities [m^{-3}]
T_e	n_e
T_{ions}	Positive ions : $n_{H_2^+}, n_{H_3^+}, n_{H^+}$ Negative ions : n_{H^-}
	Neutrals : n_H, n_{H_2}

The choice of these parameters strongly affects the results of the simulations. For example, they can be assigned randomly, just to investigate the impact of a particular species in a definite condition, or they can be assigned following a criterion that approaches the real conditions of the plasma under investigation, as it will be explained in the next sections.
The solver used by AtoH is the MatLab function *ode15s*, suitable for stiff differential equations. An equation is defined stiff when it includes some terms that may lead to a rapid variation of the solution. In each equation in AtoH there are predominant and less important terms depending on the electron temperature and density of the application. This this is the reason for which to solve these differential equations it is necessary this type of numerical method, with extremely small step size.

2.2 Emissivity exstimation

AtoH can calculate the emissivity, ideally, of all the lines of the atomic hydrogen emission spectrum for energy transitions between the quantum states $|1\rangle - |20\rangle$ that were inserted in the model. In OES for plasma characterization, usually, the atomic lines observed are the Balmer $H_\alpha, H_\beta, H_\gamma$ or their ratios, since they are relatively far from UV and thus more easily observable and they can furnish a high amount of information.
The emission is calculated starting from the final population densities obtained by the computations, with the following formula, in units of density of photons per unit time and solid angle.

$$\varepsilon_{ij} = \frac{1}{4\pi} A_{ij} n_i \quad [\frac{1}{\mathrm{sm^3 sr}}] \tag{2.24}$$

In the case of the Balmer lines considered for this application, the previous formula assumes the following shapes.

$$H_\alpha : \varepsilon_{32} = \frac{1}{4\pi} A_{32} n_3 \quad \lambda = 656.3\,\mathrm{nm} \tag{2.25a}$$

$$H_\beta : \varepsilon_{42} = \frac{1}{4\pi} A_{42} n_4 \quad \lambda = 486.1\,\mathrm{nm} \tag{2.25b}$$

$$H_\gamma : \varepsilon_{52} = \frac{1}{4\pi} A_{52} n_5 \quad \lambda = 434.1\,\mathrm{nm} \tag{2.25c}$$

Thus, AtoH calculates the absolute emissivity of atomic hydrogen lines but also the line ratios $\frac{H_\alpha}{H_\beta}$ and $\frac{H_\beta}{H_\gamma}$, particularly useful with non absolute calibrated spectroscopic systems.

2.3 How to use AtoH for the interpretation of OES

AtoH, as well as being a powerful instrument for the investigation of the effects of plasma parameters on the hydrogen plasma emissivity, is above all a device for the interpretation of optical emission spectroscopy measurements. Indeed, starting from OES measurements, AtoH is able to identify the combination of all the plasma species in order to obtain an estimation of the emissivity as close as possible to the experimental values. This application is well explained in Chapter 5, where AtoH is applied for the interpretation of OES on RAID.

Chapter 3

Comparison with Yacora

3.1 Introduction to Yacora

Yacora is a flexible solver, available as web application, that provides access to collisional radiative models, mainly for diagnostics in low-pressure plasmas, namely for atomic hydrogen, molecular hydrogen and helium [37, 17].
In order to calculate the emissivity of atomic hydrogen lines, for every collisional channel, the user has to choose a range of the parameters (i.e., electron, ions and gas temperatures and densities) or an exact value for each of them, and then sum all the contributions.
The Yacora result useful for the calculation of the emissivity is the population coefficient R_{op}, expressed as the ratio between the density of the quantum state p and the product between the electron density and a quasi-constant density that has been specified for each excitation channel [17].

$$R_{op} = \frac{n_p}{n_e n_0} \tag{3.1}$$

Then, in order to calculate the absolute intensity line emission I_{pq}, taking into account the contribute of all the channels, it is necessary to sum the product between the population coefficients R_{op} and the density of the species of the specific channel (i.e., $n_H R_{H,p} + n_{H2} R_{H2,p} + ..$), and multiply this factor to the electron density and the Einstein coefficient A_{pq} of the transition, as shown in Formula (3.2) [17].

$$I_{pq} = n_e(n_H R_{H,p} + n_{H2} R_{H2,p} + n_{H+} R_{H+,p} + n_{H+2} R_{H+2,p} + n_{H+3} R_{H+3,p} + n_H R_{H,p}) A_{pq} \quad [\frac{\text{ph}}{\text{m}^3\text{s}}] \tag{3.2}$$

For each population coefficient, it is necessary to request a simulation that, after being accepted, is saved in the user folder. Then the data must be manipulated by the user himself to calculate the emissivity with Formula (3.2).

3.2 Yacora simulations and comparison

Several simulations have been done in Yacora in order to obtain the population coefficient for different electron temperatures and densities and for each excitation channel. Giving that there were 7 excitation channels, and for every one were considered two electron temperatures (1 eV and 10 eV), and again for every electron temperature and every excitation channel were considered 10 values of electron densities (between 10^{17} m^{-3} and 10^{19} m^{-3}), the total number of population coefficients needed was: $7 \cdot 10 \cdot 2 = 140$.
The same parameters were fixed in Yacora and in AtoH to compare the results and they are reported in Table 3.1.

Table 3.1: Parameters used for the comparison between AtoH and Yacora.

T_e [eV]	1 - 10
n_e [m^{-3}]	1e17- 1e19
T_{ions} [K]	900
$n_{H_2^+}$ [m^{-3}]	1e17
$n_{H_3^+}$ [m^{-3}]	1e16
n_{H^+} [m^{-3}]	1e17
n_{H_2} [m^{-3}]	2e19
n_H [m^{-3}]	1e19
n_{H^-} [m^{-3}]	1e15

3.2.1 Emissivity comparison

The first comparison directly refers to the emissivity results on the three main atomic hydrogen lines H_α, H_β and H_γ. These emissivities were calculated with the parameters specified in Table 3.1. The results are reported in Figure 3.1. The two models are closer at higher temperatures than at lower temperatures, and the gap between them seems not to depend on the electron density. The offset is also different for different lines and it is summarized in Table 3.2.

Table 3.2: Offset between Yacora and AtoH emissivities estimation at 1 eV and 10 eV

	$T_e = 1\,\text{eV}$	$T_e = 10\,\text{eV}$
$H_{\alpha_{AtoH}}/H_{\alpha_{Yacora}}$	2.26	1.16
$H_{\beta_{AtoH}}/H_{\beta_{Yacora}}$	2.34	1.63
$H_{\gamma_{AtoH}}/H_{\gamma_{Yacora}}$	2.42	1.93

The discrepancy increases as the wavelength of the radiation decreases, and so it is higher for spontaneous emissions from higher quantum states. Indeed, $H_{\gamma_{AtoH}}$ represents the decay $|5> \rightarrow |2>$, while $H_{\beta_{AtoH}}$ represents the decay $|4> \rightarrow |2>$ and $H_{\alpha_{AtoH}}$ represents the decay $|3> \rightarrow |2>$. This phenomenon is probably related to the different number of quantum levels considered, since AtoH works with 20 quantum states while Yacora with 40 of them. Having less quantum states reduces the accuracy of the more energetic energy levels and with 40 states, the first 20 are assumed of being correct [36].
The different results could be related also to the following two factors:

1. the presence on Yacora of the H_2^+ dissociation process that could affect the solution at 10 eV, even if the cross section has a threshold at about 15 eV, due to the integration over the electron energy distribution;

2. the use of different references for the rate coefficients. Indeed, these coefficients are the most important ingredients of a collisional-radiative code and they can affect the solution. Different references give results that are similar but not equal, because often the cross sections can not be measured but only extrapolated, and different extrapolations often do not give the same results.

In general, since the offset is higher at lower temperatures, it is more likely that some low temperature collisional rate coefficients (like the recombining ones), have a bigger discrepancy in the two adopted references. To verify how much the number of levels affects the discrepancy, a version of AtoH with less quantum states and thus less equations has been realized. The results are illustrated in Figure 3.2. As expected, less levels leads to a bigger distance with respect the results of Yacora. Doubling the number of quantum levels and thus reaching the same number of Yacora would likely make the two lines considerably closer (see Figure 3.2).

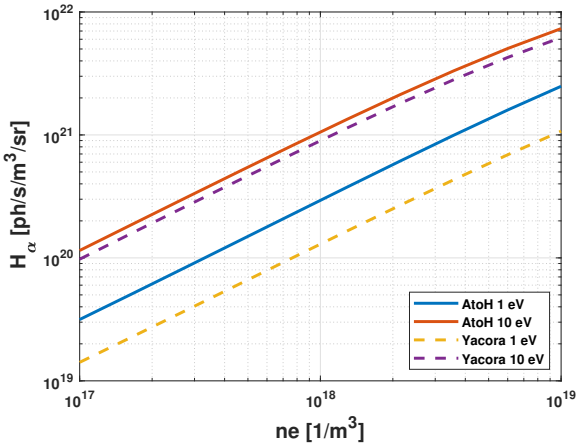

(a)

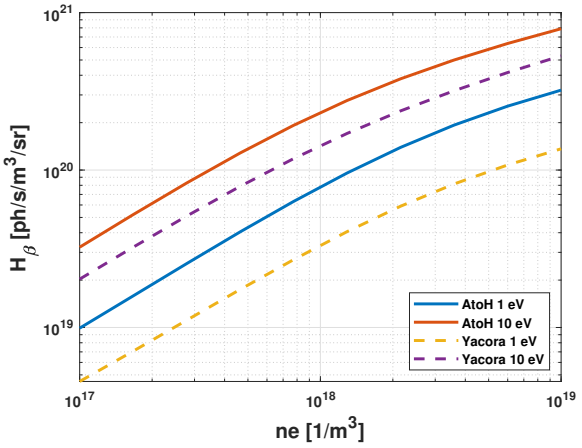

(b)

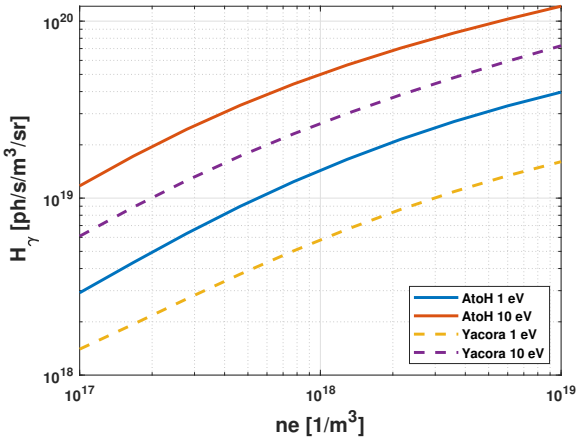

(c)

Figure 3.1: H_α (a), H_β (b), H_γ (c) emissivities in AtoH and in Yacora versus the electron density at 1 eV and 10 eV

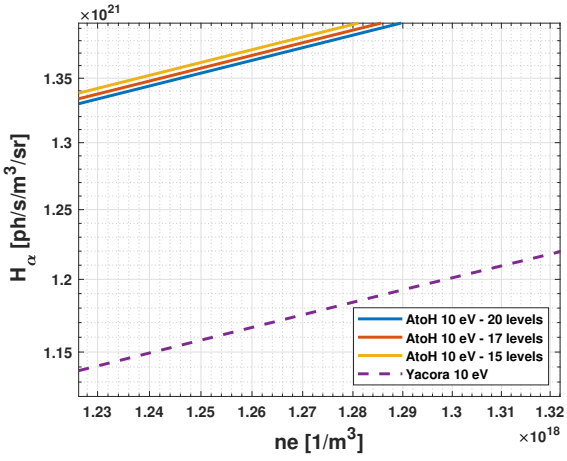

(a)

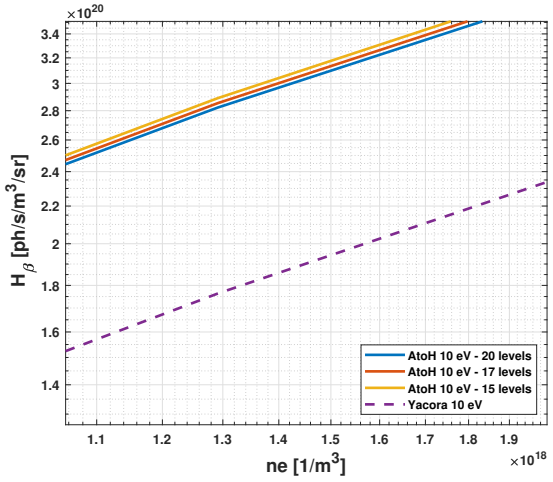

(b)

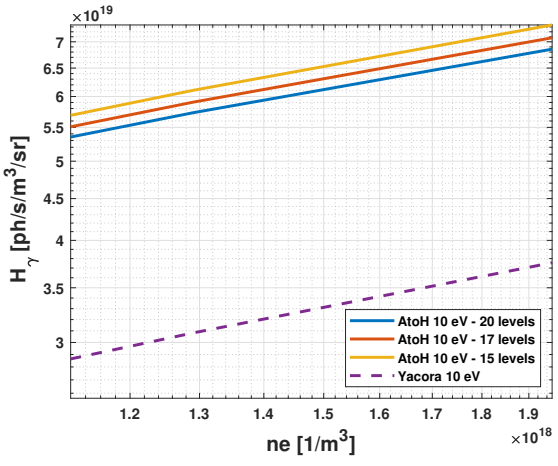

(c)

Figure 3.2: Comparison between Yacora and AtoH with |15>,|17> and |20> levels at 10 eV

3.3 Investigation of the different excitation channels

In order to identify the collisional channel in which a higher deviation is present, also AtoH has been developed in a way that it can separates the different contributions. In this way it was possible to define the contribution to the population densities of each channel and to mark the difference between the two models.
The parameters that were set for this comparison are reported in Table 3.3.

Table 3.3: Parameters used for the comparison between AtoH and Yacora separating the different excitation channels.

T_e [eV]	1 - 10
n_e [m^{-3}]	$1 \cdot 10^{17}$- $1 \cdot 10^{19}$
T_{ions} [K]	900
$n_{H_2^+}$ [m^{-3}]	$1 \cdot 10^{17}$
$n_{H_3^+}$ [m^{-3}]	$1 \cdot 10^{16}$
n_{H^+} [m^{-3}]	$1 \cdot 10^{17}$
n_{H_2} [m^{-3}]	$2 \cdot 10^{19}$
n_H [m^{-3}]	$1 \cdot 10^{19}$
n_{H^-} [m^{-3}]	$1 \cdot 10^{15}$

The first channel, here nicknamed as the *Corona channel*, considers only the electron impact effects and the spontaneous emission. This channel, on Yacora on the Web, can be considered alone but, at the same time, it is automatically considered also in all the other excitation channels. The second channel contains the two and three body recombination of H^+, the third one contains the H_2 dissociation, the fourth and fifth contain the H_2^+ and H_3^+ dissociative recombination respectively, and finally the sixth path includes the mutual neutralizations ($H_2^+ + H^-$ and $H^+ + H^-$).
At at the end of all the simulations the quantification of the effect is obtained in terms of population density of the excited states.

Table 3.4: Comparison of the contribute of different collision processes to the quantum states $|2\rangle$ and $|20\rangle$ in AtoH and Yacora.

Collisional channel	n_2 [$m^{-3}s^{-1}$]		n_{20} [$m^{-3}s^{-1}$]	
	AtoH	Yacora	AtoH	Yacora
Corona channel	$2.025 \cdot 10^{15}$	$2.224 \cdot 10^{15}$	$4.203 \cdot 10^{13}$	$2.286 \cdot 10^{12}$
H^+ recombination	$3.404 \cdot 10^{7}$	$3.823 \cdot 10^{7}$	$3.248 \cdot 10^{8}$	$3.193 \cdot 10^{9}$
H_2 dissociation	$4.480 \cdot 10^{14}$	$4.462 \cdot 10^{14}$	$2.080 \cdot 10^{12}$	$1.477 \cdot 10^{11}$
H_2^+ dissociative recombination	$2.737 \cdot 10^{13}$	$1.796 \cdot 10^{13}$	$4.255 \cdot 10^{12}$	$1.12 \cdot 10^{11}$
H_3^+ dissociative recombination	$3.293 \cdot 10^{11}$	$7.186 \cdot 10^{11}$	$1.712 \cdot 10^{08}$	$2.627 \cdot 10^{7}$
Mutual neutralization	$1.228 \cdot 10^{10}$	$8.273 \cdot 10^{9}$	$8.529 \cdot 10^{9}$	$5.921 \cdot 10^{8}$

What emerges from this analysis is that, as expected, the discrepancy is lower for lower quantum states and it increases when increasing the quantum number. Indeed, the accuracy of the model decreases for higher quantum levels, as already explained. This effect is clear especially in the case of the "*corona channel*" where it was possible to use the same cross sectional data [27] and therefore the offset is related to the different number of quantum states. Except for the mutual neutralization, the contribution to the quantum state $|2\rangle$ has the same order of magnitude for both models, while in the case of the quantum state $|20\rangle$ the contribution is one order of magnitude higher in AtoH. This order of magnitude of difference is due to the fact that, in AtoH, all the contributions are concentrated in 20 levels and this generates an overestimation of them in the highest quantum states.
In the case of mutual neutralization, the fact that also in the lower quantum state there is one

order of magnitude of difference, can be due to the problem about the $H^+ + H_2^+$ reaction rate coefficient explained in section 2.1.2.
Yacora experimented the use of a corrective factor for the mutual neutralization that takes into account the branching ratio between the mutual neutralization process that generates an excited atom (0.16) or an excited hydrogen molecule (0.84)[35]. Applying the same corrective factor in AtoH, the contribution to $|2\rangle$ reaches the same order of magnitude of Yacora and in particular it is equal to $1.965 \cdot 10^9$ $m^{-3}s^{-1}$. With this correction, also the contribution to the twentieth level is reduced to $1.365 \cdot 10^9$ $m^{-3}s^{-1}$.

3.4 Conclusions

The two models gave as output results that are not equal but comparable. This difference can be addressed to the following factors:

1. different number of quantum levels considered;
2. different references for the cross sectional data.

However Yacora, as AtoH, is a simulation model. Being closer to Yacora does not necessary mean to be close to the reality.
This should be considered as a comparison between two different population models that first of all works in a different way and, in addition, they use different cross sectional data. Due to these two reasons, even if with the same total number of quantum states, they would never give as output the same results.
On the other hand, if the comparison had shown completely different results, this meant that AtoH had some strong inaccuracy.
Despite its simplification, as it will be showed on Chapter 5, AtoH gives a good interpretation of the atomic hydrogen H_α, H_β and H_γ lines.

Chapter 4

Optical Emission Spectroscopy experimental campaign on RAID

Optical Emission spectroscopy is a non-invasive diagnostic tool that gives information about the plasma parameters, recording and analyzing the light that is emitted due to atomic and molecular radiations. Part of these transitions radiate in the visible spectra, characterizing the color of the plasma.
The spectroscopic setup consists of a lens coupling through an optical fibre bundle to a spectrometer and a detector [5]. The lens captures the light radiated from the source while the fiber bundle guides this light to the entrance slit of the spectrometer. The choice of the spectrometer, detector and lenses depends on the application.
The lenses used for OES, that collect the light from the source, are characterized by the *f number* and by the *focal length*, that usually can be regulated directly on the lens. The *f number* is inversely proportional to the amount of light that the lens is able to collect: if the light intensity is high it could saturate the sensor and therefore the *f number* should be increased to have a sharper focal plane. The *focal length* could be positive if a system converges the light or negative if it diverges the light. If the focal length is short this means that the the rays are bent more sharply, bringing them to a focus in a shorter distance.
The collected light passes trough the fiber bundle and reaches the spectrometer, also called monochromator, that consists of a sequence of entrance slit, lenses, grating and exit port. The first part of the monochromator is the collimator (the slit and the lens). The slit is at the focal plane of the lens, so that the lens will produce parallel light from the slit.
After that all the rays have become parallel, the light reaches the diffraction grating. This component spatially separates different wavelengths thanks to small groves on its surfaces that create an interference pattern. It is characterized in terms of grooves per millimetre and it mainly defines the spectral resolution of the monochromator. IUPAC defines the *resolution* in optical spectroscopy as the minimum distinguishable wavelength (or frequency) difference between two lines in a spectrum [24]. However, also the entrance slit affects the spectral resolution since a bigger slit means a higher intensity of light, but a lower resolution.
From the diffraction grating, the rays reaches the exit port. Depending on the orientation between the grating and the exit port, a particular wavelength is transmitted out from the exit slit. Then, the light is focused again by a lens and arrives to the detector. Here the photons are converted into electrons and further into a digital signal. Then this signal is sent, through a serial port, to a computer with a software for the data capturing.
An OES setup is schematically shown in Figure 4.1.
An important task during an OES campaign is the calibration of the spectroscope. The first calibration is the *wavelength calibration*, also called *relative calibration*, that consists of the calibration of the wavelength axis of the pictures taken with the camera. This alignment of the wavelength scales can be done with the use of a calibration lamp and wavelength tables.

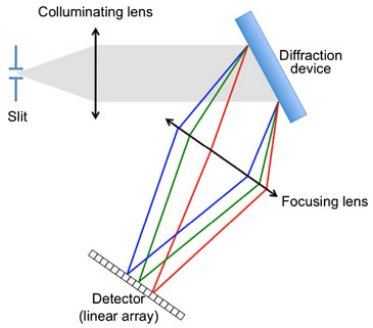

Figure 4.1: Scheme of a spectroscope working principle [6].

The system is relatively calibrated when the lines measured by the camera perfectly match the wavelengths of the lamp used. This calibration corrects the sensitivity of the system, that is the relative efficiency of detection of light as a function of the frequency or wavelength of the signal. The subsequent calibration is an *absolute calibration*, that provides, in addition, the conversion between measured signals (counts or voltage) and $\frac{\text{ph}}{\text{m}^3\text{s}}$. An absolutely calibrated spectra gives access to more plasma parameters and therefore this effort is compensated by an increase in information. A standard source with a continuous spectrum and a known spectral intensity distribution is needed for this purpose. In this way, the acquired spectrum can be compared to the known one, in order to correct the acquisition in terms of absolute intensity [12].
The spectral lines are always broadened, and this is related to the finite resolution of the spectrometer and to intrinsic physical causes. The main physical causes of spectral line broadening are pressure broadening due to collisions of the emitters with neighboring particles and Doppler broadening [26]. Moreover, also the stark broadening can give a non negligible contribution and it has been demonstrated, with a recent and appropriate perturbation propagation model, that its effect is comparable to the Doppler broadening in case of strong magnetic fields [19, 11].
The broadening is quite interesting in OES since it provides information about the plasma parameters. In particular, stark broadening, that is a line broadening effect due to the local electric field generated by electrons and ions in the plasma. Stark broadening causes a Lorentzian line shape and it allows to estimate the electron density. Doppler broadening is related to the thermal motion of the emitting atoms or ions and this can be related to the ion temperature; e.g., in case of a Maxwellian velocity distribution, the line shape obtained is Gaussian and the width yields to the ion/atom temperature [26].
Moreover, the rotation of the plasma can be proved by the Doppler shift, namely the modification of the wavelength due to a velocity of the emission source with respect to the observer. The wavelength is decreased if the radiator is moving towards the observer (*blueshifted*) or it is increased in the opposite condition (*redshifted*). This can be verified more easily on H_α since the Doppler effect is proportional to the wavelength [8].
Another application of OES is related to the negative ions (H^-) densities distribution. Indeed, there exists a combination of plasma parameters for which all the collisional channels become negligible except for the mutual neutralization, and therefore for a fixed value of electron temperature and electron density, the line ratio $\frac{H_\alpha}{H_\beta}$ is directly correlated to the density ratio $\frac{H^-}{H}$ [13].

4.1 RAID plasma device

The Resonant Antenna Ion Device (RAID) is a helicon plasma source developed at the Swiss Plasma Center of École Polytechnique Fédérale de Lausanne. The purpose of this device is helicon plasma physics investigation for the production of negative ions. The helicon wave technology is indeed one of the best candidates of the next generation negative ions sources for neutral beam injection (such as for DEMO and beyond).

The plasma in RAID is mostly heated through helicon waves. A helicon wave is a low frequency wave of the whistler family. In low temperature plasmas and in presence of a magnetic field, it is possible to excite the helicon modes. If this condition is reached the helicon wave can be coupled with the plasma, generating a resonant heating. While in vacuum the wavelength of these waves is of the order of meters, in the plasma it is reduced to tens of centimetres. The ways in which the helicon wave deposits the energy on the plasma are not well know yet. The two main hypotheses are a wave-particle collision where the particles are negative ions and electrons, or a particle-particle collision where the wave interacts with the negative charges increasing their collision probability.
RAID is a cylindrical stainless steel vacuum vessel 1.5 m long and with a diameter of 40 cm. The vacuum system can reach a pressure of 10^{-6} mbar. The vessel is surrounded by six water cooled copper coils that can produce an axial magnetic field up to 800 G. In one side of the vessel there is the antenna, while in the opposite one a target. The axial magnetic field, and thus the helicon wave goes from the antenna to the target. The purposes of the target is to protect the walls of the chamber and to define a boundary condition on the plasma. During the optical emission spectroscopy, the used target was a floating one with a floating potential of 45 V.
The frequency of the antenna that generates the helicon wave is 13.56 MHz. The shape of the plasma, generated by the propagation of the helicon wave, is a horizontal column with a diameter of about 6 cm [7].
The plasma discharges can be done in hydrogen, deuterium, argon, helium, neon and nitrogen. For an hydrogen discharge, the power of the radio-frequency antenna can reach 8 kW, with a density of gas inside of about 10^{19} m^{-3}.
The profiles of electron temperature and density on RAID are shown in Figure 4.2. These profiles were measured in the same position in which the OES was carried on, with vertical scans done with the Langmuir probe correct with lasers interferometry.

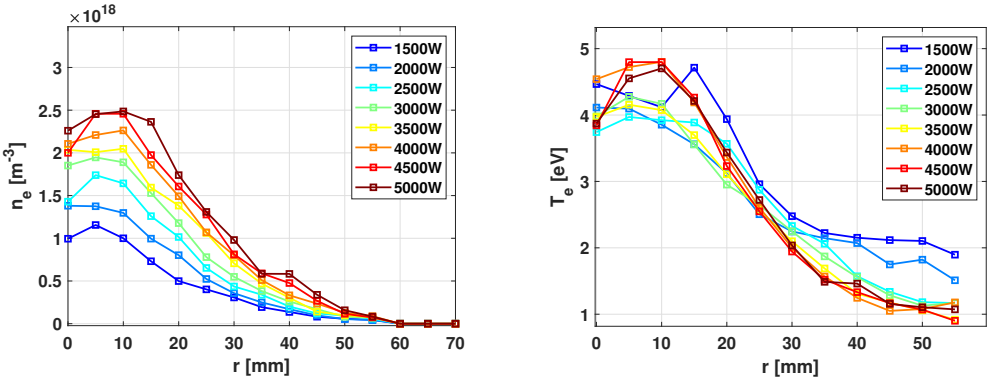

(a) Electron density **(b)** Electron temperature

Figure 4.2: Electron temperature and electron density profiles of an hydrogen plasma on RAID at different powers

The peaks correspond to the regions in which the helicon wave mainly deposits the energy. Increasing the power, the effect of this resonant heating seems to be more evident in the ionization rather than the heating of electrons. This is an advantage for a negative ion source. Indeed, the generation of negative ions occurs in two ways: surface and volume processes. During the surface production the negative ions are the result of the collision of a neutral hydrogen atom or an ion H^+ with a surface. The volumetric production consists on the dissociative attachment reaction between an ro-vibrationally excited H_2 molecule and an electron.

$$H_2(\nu) + e \longrightarrow H^- + H \tag{4.1}$$

The efficiency of this reaction increases with the vibrational state of the molecular hydrogen.

Highly molecular excited states needs electron temperatures higher than 10 eV. However, if the electron temperature is higher than 2 eV the detachment of the poorly bound extra captured electron becomes more probable [5]. In RAID, in the shell with higher temperature and electron density, the vibrationally excited $H_2(\nu)$ is produced. Then, the negative ions are produced and they are mainly concentrated in the external area, where the temperature is lower than 2 eV (see Figure 4.3 and 4.2).
Therefore, on RAID, when the electron density increases more than the electron temperature means that the dissociative attachment process efficiency increases more than the electron detachment one.

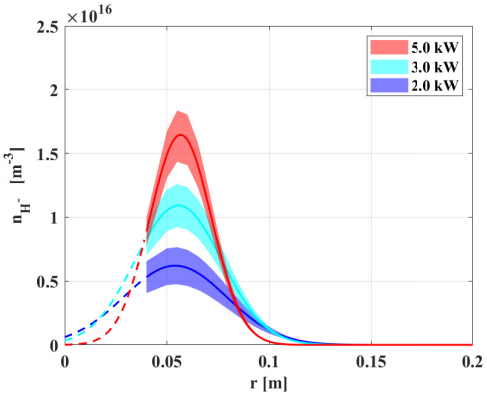

Figure 4.3: Negative ions profiles on RAID at different powers [10].

Figure 4.3 illustrates the negative ions density measured with laser based techniques. On the basis of above, the H^- density is higher in the plasma edge where the depletion is less efficient due to lower temperatures.

4.2 Preparation of the campaign and description of the equipment

A Navitar lens (*f number* 1.4, *focal length* 35 mm) was used. The 2.5 m fiber bundle was made of a linear array of 20 fibers and was fixed close to the lens in an arc rail motorized support. The arc rail allowed movements in a vertical direction (y) in order to look at different positions inside the vacuum chamber. The In-House spectrometer had a grating with 2400 lines/mm and a wavelength range from 400 nm to 700 nm. The grating of the spectrometer was motorized so that it was possible to orientate it for different wavelengths through a software. The used detector was an *Andor Ixon Ultra EMCCD* camera.

- Alignment
  The alignment of the monochromator has been done in the optics laboratory using laser diffraction. This phase is necessary to guarantee that, moving the grating, each angle corresponds to a specific wavelength.
  First, it is necessary to choose an Experimental Reference Line (ERL), and this can be done aligning a laser beam so that it passes through the small hole of a target. The objective is adjusting the monochromator, in three dimensional space, so that the ERL (and thus the laser beam) passes through the center of the entrance slit and simultaneously strikes the geometric and optical centers of the camera, grating, collimator and exit slit [28].
  When the spectrometer is aligned, the beam passes exactly through two holes of two equal targets, one between the laser and the entrance slit, and the second over the exit slit.

- Relative and absolute calibration
  First, the wavelength calibration has been done with a Neon pencil lamp. The relative cal-

ibration allows to align the wavelength scale thanks to the exposure to a well know source.

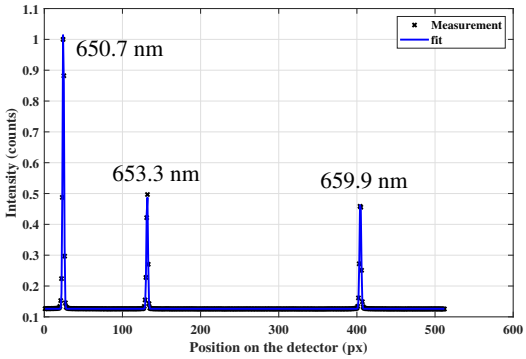

Figure 4.4: Wavelength calibration with a Neon lamp

Figure 4.4 illustrates the intensity collected as a function of the position on the detector. Knowing the wavelengths of the Neon spectral lines was possible to relate the position on the detector to a specific wavelength. From the relative calibration was found that the spectral resolution of the system was of 0.07 nm and the spectral window was of 12.4 nm. Moreover, the instrumental broadening was dominant, and it made impossible to measure the Stark and Doppler broadening.
The absolute calibration allowed to correct the absolute emissivity by using a Ulbricht LabSphere, that is an ideal Lambertian source. A Lambertian source is a light source with a brightness that is always the same, regardless the observer's angle of view. Since the emission of this source (E_{cal}) was well known, measuring the signal on the detector during the calibration (S_{cal}), it was possible to calculate the response of the spectroscopic system (R_{esp}) with the following formula:

$$S_{cal} = R_{esp} E_{cal} \tag{4.2}$$

Therefore, after the measurement, it was possible to correct the signal and calculate the real emission from the plasma, dividing the signal by the response of the spectroscopic system.

$$E_{real} = \frac{S_{plasma}}{R_{esp}} \tag{4.3}$$

- Setup layout

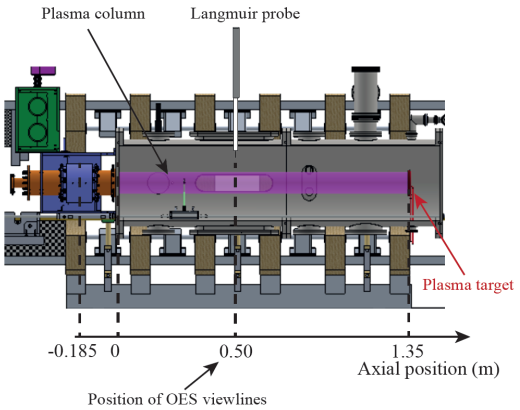

Figure 4.5: Representation of the OES window on RAID

The support for the fiber bundle and the lenses was mounted, as mentioned before, on a motorized arc rail. The lens looked inside of the vacuum chamber from an horizontal window made of quartz, almost at the axial center of the vacuum vessel (see Figure 4.5).
The movement of the lens with the arc rail allowed to look at different coordinates of the plasma. In particular, data were recorded at the center of the column and in both the lower and upper edge, in order to confirm the plasma symmetry.
Thanks to the three different scanning angles adopted, the field of view on the vertical direction y was between -70 mm and $+70$ mm. The spatial resolution was of 3.5 mm and this is the actual collecting area of one fiber. To define this value, the fiber bundle was backlit in order to project the collecting area on a sheet of paper inside of the vacuum vessel, as shown in Figure 4.6.

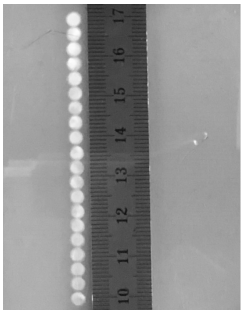

Figure 4.6: Spatial resolution of the fiber bundle in RAID

In order to prevent back reflections from the walls of the vacuum vessel, an Atakar black foil, known as the blackest paper in the world, was fixed inside the chamber, exactly behind the lens view.
The emissivity measured by each of the 20 fibers can be examined separately. This allowed to find out the orientation of the view line that refers to each measurement and to know exactly the point of the plasma column at which every fiber was looking.

- Measurements procedure
  The lines observed were atomic lines of hydrogen: H_α, H_β, H_γ, one at a time. Each line was observed at the three different positions already mentioned and at different powers: 1.5 kW, 2.5 kW, 3 kW, 3.5 kW, 5 kW.
  Only the data obtained at 3500 W and 1500 W will be reported here.

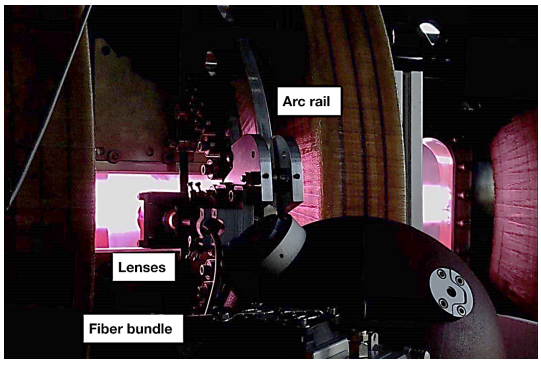

Figure 4.7: Picture of the OES setup aligned to the center of the plasma column

In Figure 4.7, the OES setup during the operations is shown. It is possible to distinguish the hydrogen plasma column, at which the lens is pointed. Hold by same support, over the arc rail, there is also the fiber bundle, connected to the spectrometer. This configuration

was the central one, that allowed to record the hottest area of the the column, where also the highest emissivity occurred.

- Data analysis
  The second part of the measurement campaign consisted in the data analysis.
  The data analysis is the conversion of the figures taken with the camera, in emissivity (i.e., ph/s/m^3), taking into account all the corrections of the spectra that come from the calibration and from the OES setup (e.g., the potential absorption of the window).
  An example of raw data is reported in Figure 4.8. From the absolute calibration was known how to convert the counts in ph/s/m^2.

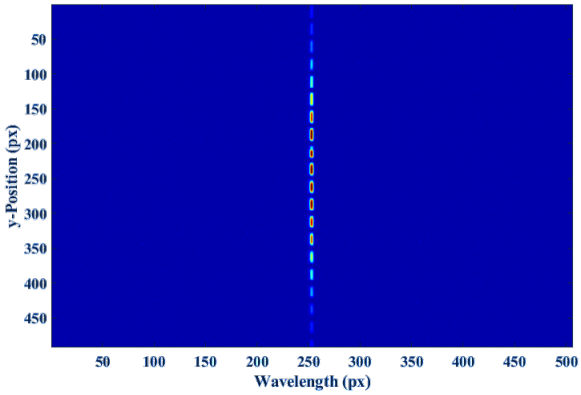

Figure 4.8: Example of OES row data

These emissivities were values integrated over the view line of the optical fiber (ph/s/m^2). Figure 4.9 (a) exhibits the integrated values of emissivities as a function of the vertical position y. The three angles indicated in the legend correspond to the three positions of the arc rail. As previously mentioned, the three position covered all the plasma column between -70 mm and $+70$ mm.

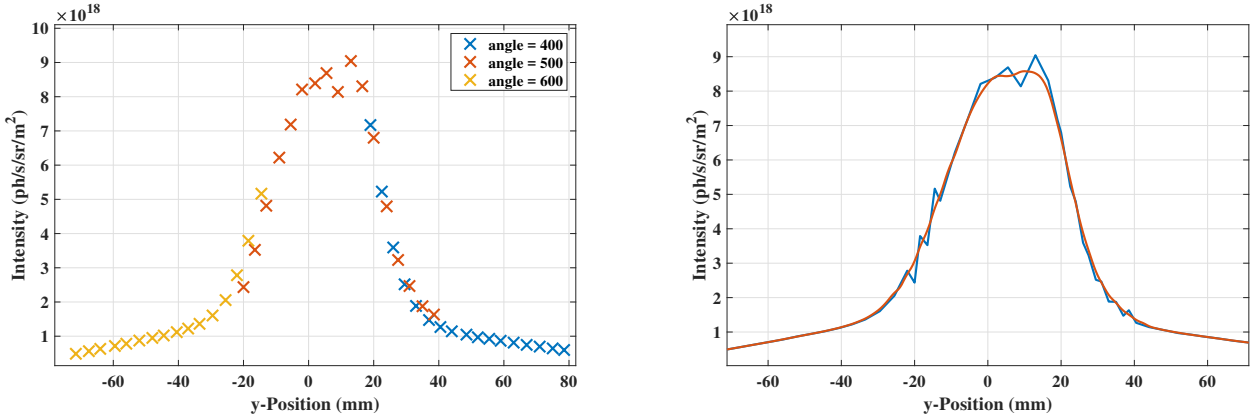

(a) Field of view

(b) Smoothing for IAT

Figure 4.9: OES data analysis: field of view (a), and smoothing procedure for the Inverse Abel Transform

The integrated values contained all the information that is collected on the line sight of the optical fiber. In order to obtain the emissivities in ph/s/m^3, as a function of a radial

distance from the center of the plasma r, an Inverse Abel Transform was necessary. The Abel transform is limited to applications with axially symmetric geometries [32].
To proceed with this mathematical process, it was necessary to smooth the curve. The line profile can be approximated by a Gaussian (Figure 4.9 (b)).

4.3 Results of the campaign

At this point, after the IAT, the H_α, H_β, H_γ emissivities and line ratios profiles were well defined. The results at 3500W and 1500W are reported and commented here.
It should be remarked that the line ratios are expressed in terms of $\frac{\text{eV}}{\text{eV}}$. This means that the emissivities are taken into account considering the energy contribution (in eV) that comes from each photon. Therefore, the line ratios expressed in terms of $\frac{\text{eV}}{\text{eV}}$ or $\frac{\text{ph}}{\text{ph}}$ are different. In a nutshell, the number of photons have been multiplied by the energy of the emission, that is equal to 2.0 eV for an H_α photon, 2.5 eV for an H_β photon, and 2.86 eV for an H_γ photon.

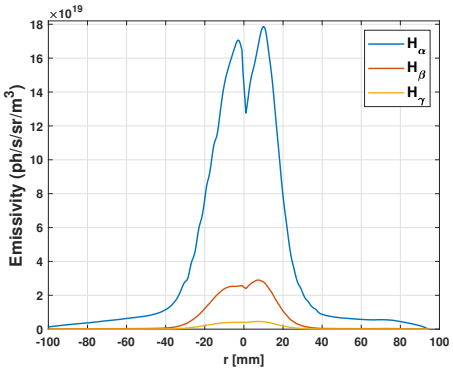

(a) Intensities of the hydrogen lines H_α, H_β, H_γ at 3500W

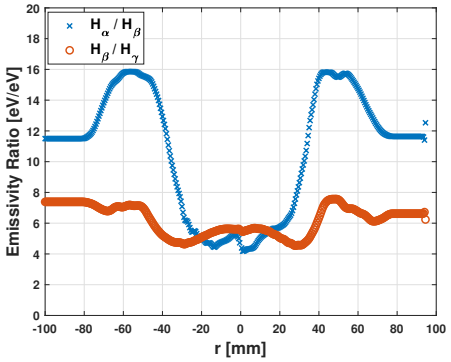

(b) Line ratios H_α H_β and H_β H_γ at 3500W

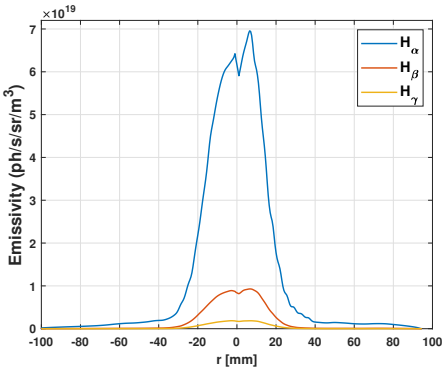

(c) Intensities of the hydrogen lines H_α, H_β, H_γ at 1500W

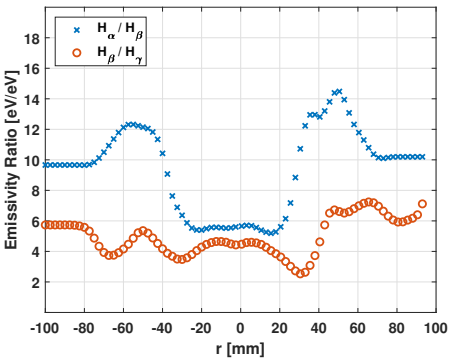

(d) Line ratios H_α H_β and H_β H_γ at 1500W

Figure 4.10: Intensities and line ratios at 3500W and at 1500W obtained with OES

The H_α line is the brightest emission line and can differ by one or two orders of magnitude in comparison to the other two lines. The absolute intensity decreases when increasing the quantum number of the initial state, approaching the UV region. The differences among these lines are related to the fact that the population density of the energy levels, as the decay probabilities (Einstein coefficients), decreases when increasing the fundamental quantum number n. The Einstein coefficients for the investigated emission lines are reported in Table 4.1. Figure 4.10 shows that,

as expected, the absolute intensity of the emission is related to the power of the antenna. This is due to the fact that a higher power generates, in general, a higher electron density and a higher electron temperature, and this causes higher excited states population densities.

Table 4.1: Decay probabilities for the involved hydrogen lines

Transition	Einstein coefficient [s^{-1}]
H_α , $\|3\rangle \rightarrow \|2\rangle$	$4.4101 \cdot 10^7$
H_β , $\|4\rangle \rightarrow \|2\rangle$	$8.4193 \cdot 10^6$
H_γ , $\|5\rangle \rightarrow \|2\rangle$	$2.5304 \cdot 10^6$

In general, while the absolute emissivity follows the profiles of electron temperature and density in the plasma (shown in Figure 4.2), the line ratio faces a completely different behaviour. All the absolute emissivity profiles experience a peak at almost 10 mm from the center of the column as $n_e(r)$ and $T_e(r)$ do, and then they drop. However, also the line ratios profiles can be related to the plasma parameter. In particular, a T_e reduction as an n_e growth, causes an increase of the line ratios [13].
On the basis of the above, and focusing the analysis on the first 45 mm of plasma, the H_α/H_β profile seems to be dominated by the electron temperature profile because it always grows since the electron temperature always decreases. On the other hand H_β/H_γ, starting from the center of the axis, rises slightly due to the electron density growth and then it drops due to electron density decreases.
The H_α/H_β behaviour can be related also to the concentration of negative ions. Indeed, an increase in the ratio H^-/H may cause an increase on H_α/H_β. Therefore, the increase of this line ratio in the region at about 55 mm can be related to both the electron temperature reduction and the negative ions increasing concentration.
Even if with different orders of magnitude, all the absolute emissivities follow a similar profile, as shown in Figure 4.11. These graphs report the normalized profiles of absolute intensity, namely the ratio between the absolute emissivity and the maximum recorded value of the referred line.

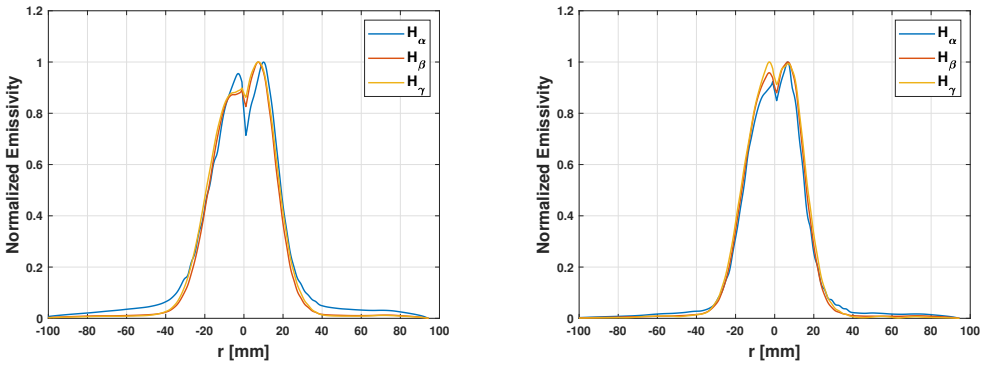

(a) Normalized emissivities at 3500W **(b)** Normalized emissivities at 1500W

Figure 4.11: Normalized values of the emissivities of the lines H_α, H_β, H_γ at 3500W and 1500W

In conclusion, it is important to specify the uncertainty that is related to the absolute emissivity measured, that is about 30% in the central region up to 15 mm and almost 15% between 15 and 60 mm.

Chapter 5

AtoH results: OES interpretation and negative ions investigation

Interpreting an OES measure means characterizing the plasma parameters through the recorded radiation.
The characterization of the plasma is usually done in one of two ways. The first method is based on the assumption that the plasma emissivity is related only to the electron temperature and electron density and therefore all the other parameters are fixed. The second process of interpretation is iterative, and characterizes the plasma fixing the lowest possible number of parameters.

5.1 Estimation of T_e and n_e

AtoH has been applied to plot the emissivity variation as a function of n_e and/or T_e. Also the densities of the other chemical species were made to change as a function of one of these two parameters. Obviously, unless a precise relationship is known between all the densities and T_e or n_e, this estimation with the emissivity can be very rough. At the same time, it is not credible to assume constant values of all the species changing the electron temperature and electron density. The densities of the species involved in AtoH were expressed as a function of n_e (Table 5.1), and therefore, the variation on emissivity depending on the electron density for different electron temperatures is observed.

Table 5.1: Density ratios of a generic low temperature plasma as a function of n_e

Density ratios
$n_{H^-}/n_e = 0.1$
$n_H/n_{H_2} = 0.5$
$n_{H3^+}/(n_e + n_{H-}) = 0.01$
$n_{H2^+}/(n_{H^-} + n_e - n_{H_3^+})$ =1/11
$n_{H^+}/(n_{H_2^+}) = 10$

The density of the gas n_{H_2} was assumed to be constant and equal to $2 \cdot 10^{19}\mathrm{m}^{-3}$ and the ions temperature was set at 1000 K. Moreover, the ions density ratios were set in order to respect the plasma neutrality between positive and negative charges.

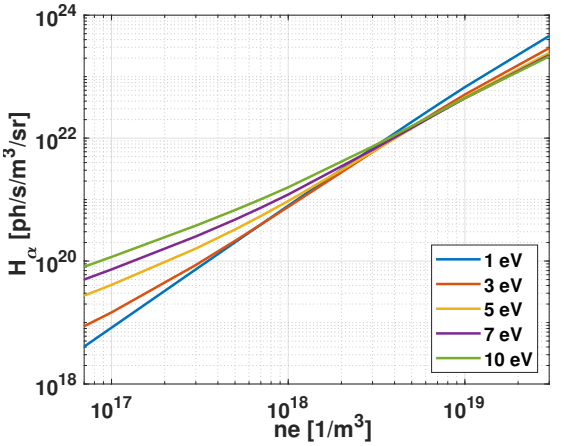

(a)

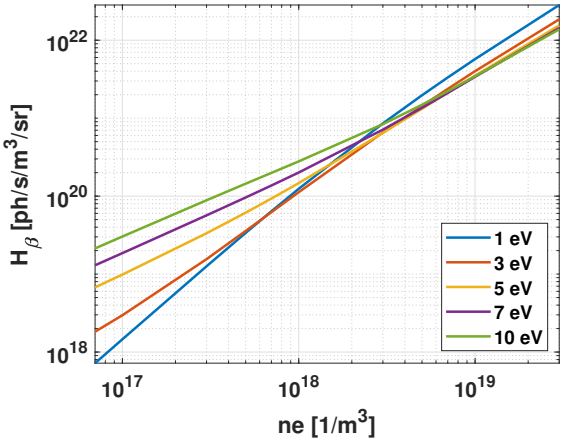

(b)

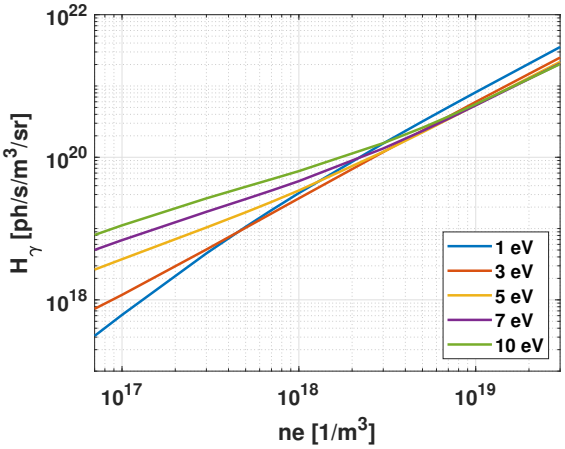

(c)

Figure 5.1: Graphs for the estimation the electron density or temperature in function of H_α, H_β and H_γ

The plots, created with the results of AtoH, are reported in Figure 5.1. In order to use these results it is necessary to know at least one variable between n_e or T_e, in order to identify a point in the figure and determine the missing one.
As expected, the emissivity increases when increasing the temperature or the density of electrons. For n_e lower than 10^{18} m^{-3}, the effect of the electron temperature on the radiation emitted is predominant. Indeed, a higher electron temperature means more energetic electrons, and thus a more probable excitation of the hydrogen atoms in higher energy levels, therefore, since the spontaneous emission is proportional to the excited states population density, the growth in electron temperature causes an increase in the radiation emitted.
Above an electron density of 10^{18} m^{-3}, the emissivity has almost the same value even with different temperatures. This means that, in these conditions, the electron density effect predominates. Increasing the electron density means increasing the concentration of electrons per unit volume, and therefore having a higher number of collisions (and thus excitation), due to the fact that the particles are closer.
The conclusion is that these types of graphs are useful for the estimation of the electron density or electron temperature in function of the emissivity measured, but only for electron densities lower than about 10^{18} m^{-3}. Moreover, these graphs have been realized with the assumptions reported in Table 5.1 and they can be adjusted depending on the properties of the plasma under investigation.

5.2 OES interpretation by means of iterations

A more precise way for OES interpretation consists in iterations over the space of all the parameters of the system of equations (i.e., densities and temperature of the species).
Starting from the results of an OES campaign, the unknown parameters are iteratively changed, in order to find the condition for which the combination of all the parameters reduces the difference between the experimental values and the emissivities calculated though the simulations.
This application required an inverse approach: the goal is not the calculation of the emissivity but the identification of the combination of parameters that allows to reach a specific result.
It is clear that the more the conditions of the plasma under investigation are known, the less the unknowns for the iterations are. Having less unknowns means having a faster minimization and reduces the probability to find a local minimum during the iterations.

5.2.1 Definition of the χ^2

The χ^2 is used in Statistics to compare the expected and the observed frequencies of a measurement and verify how close they are. Here, the χ^2 is simply referred as the sum of the square of the difference between the experimental values and the expected results of each line emissivity (i.e., the results of the simulations) divided by the expected values.
Indicating the results that come from the simulations as $H_{\alpha,S}, H_{\beta,S}, H_{\gamma,S}$, and the observed values with OES as $H_{\alpha,OES}, H_{\beta,OES}, H_{\gamma,OES}$, the χ^2 can be defined as:

$$\chi^2 = \frac{(H_{\alpha,OES} - H_{\alpha,S})^2}{H_{\alpha,S}} + \frac{(H_{\beta,OES} - H_{\beta,S})^2}{H_{\beta,S}} + \frac{(H_{\gamma,OES} - H_{\gamma,S})^2}{H_{\gamma,S}} \tag{5.1}$$

The χ^2 is minimized by finding the right combination of temperature and densities of all the species.
One of the suitable MatLab functions, used for this application, is *fminsearch*. This function uses a simplex algorithm to find the optimal combination of parameters.

5.2.2 Application on RAID

In the case of RAID, it is possible to reduce the number of parameters for the minimization since the axial and radial profile of electron temperature and density have been measured with Langmuir

probes and interferometry. The same is valid for the negative ions distribution, measured with laser-based techniques [10]. All these results were reported in the previous chapter in Figures 4.2 and 4.3. The parameters that have been left free to vary are the densities of the chemical species H, H_2, H^- (where the measurements were not available), H^+, H_2^+ and H_3^+.
Fixing the electron temperature and density and the negative ions density means choosing a precise point on the plasma radial profile. All the different ionic species are assumed to stay at the same temperature T_{ions}, that in RAID conditions is assumed to be about 1000 K.
Four points on RAID plasma column were chosen. One at 40 mm, two in an intermediate position (i.e., 10 and 20 mm) and one at the center of the column.
The initial values are fundamental for the convergence of the system and for this reason they were regulated on the basis of previous results from COMSOL simulations on RAID, developed at the Swiss Plasma Center. These ratios are reported in Table 5.2.

Table 5.2: Expected values of species ratios on RAID.

Density ratios	r=0 [mm]	r=10 [mm]	r=20 [mm]	r=40 [mm]
n_{H^-}/n_e	0.001	0.0014	0.0018	0.0299
n_H/n_{H_2}	0.4	0.21	0.020	0.01
$n_e/(n_{H_2}+n_H)$	0.0752	0.0664	0.0576	0.0163
$n_{H3^+}/(n_{H_2^+}+n_{H^+}+n_{H_3^+})$	0.05	0.225	0.4	0.75
$n_{H2^+}/(n_{H_2^+}+n_{H^+}+n_{H_3^+})$	0.06	0.0825	0.105	0.15
$n_{H^+}/(n_{H_2^+}+n_{H^+}+n_{H_3^+})$	0.89	0.6925	0.495	0.10

Starting from the measurements of electron density and the estimation of the electronegativity degree (Table 5.2), it is possible to have an idea of the density of negative ions in all the positions. Then, the total amount of positive charges can be calculated by summing the densities of electrons and negative ions, in order to maintain the plasma neutrality. Therefore, the density of each positive ion species can be estimated by multiplying this amount by the ratios reported in Table 5.2.
Several attempts for the minimization of the χ^2 were done.
The interpretation of optical emission spectroscopy is not an easy task, since often it is possible to find a mathematical solution of the problem (i.e., a minimum) that is not physically representative of the system. As stated in reference [37], the results of a CR code can be ambiguous due to the strongly multidimensional character of the problem. Therefore, it was suggested to always critically check the results with, for example, the results on a similar plasma with known parameters.
The OES results chosen for the interpretation were those at 3.5kW and at 5kW. At 3.5kW, the negative ions density was extrapolated from the measurements at 3 kW and 5 kW shown in Figure 4.3.
Table 5.3 shows the values of electron density and temperature fixed for the minimization at 3.5kW.

Table 5.3: Values of electron density and temperature that were fixed for the minimization at 3.5 kW.

Position	n_e [m^{-3}]	T_e [eV]
r=0 mm	$2.112 \cdot 10^{18}$	3.97
r=10 mm	$2.05 \cdot 10^{18}$	4.074
r=20 mm	$1.38 \cdot 10^{18}$	3.11
r=40 mm	$3.33 \cdot 10^{17}$	1.31

In Table 5.4 the best results in terms of densities of the chemical species are reported.

Then, Table 5.5 shows a comparison among the absolute emissivities measured with OES, the results of AtoH (calculated with the densities of the species of Table 5.4) and the associated χ^2.

Table 5.4: Results of OES interpretation in RAID at 3.5 kW (the * remarks that this value was fixed during the minimization).

Position	H^-[m^{-3}]	H^+ [m^{-3}]	H_2^+ [m^{-3}]	H_3^+ [m^{-3}]	H_2 [m^{-3}]	H [m^{-3}]
r=0 mm	$9.28 \cdot 10^{14}$	$9.95 \cdot 10^{17}$	$2.12 \cdot 10^{16}$	$1.63 \cdot 10^{17}$	$2.07 \cdot 10^{19}$	$1.11 \cdot 10^{18}$
r=10 mm	$3.63 \cdot 10^{15}$	$1.87 \cdot 10^{17}$	$4.68 \cdot 10^{16}$	$2.37 \cdot 10^{17}$	$1.95 \cdot 10^{19}$	$1.3 \cdot 10^{18}$
r=20 mm	$4.28 \cdot 10^{15}$	$1.31 \cdot 10^{18}$	$5.27 \cdot 10^{15}$	$4.16 \cdot 10^{17}$	$2.63 \cdot 10^{19}$	$3.43 \cdot 10^{18}$
r=40 mm	$9.95 \cdot 10^{15*}$	$1.6 \cdot 10^{17}$	$1.35 \cdot 10^{15}$	$2.89 \cdot 10^{17}$	$3.05 \cdot 10^{19}$	$3.38 \cdot 10^{17}$

Table 5.5: Comparison between OES results and the emissivities calculated with the densities conditions obtained by the minimization and associated χ^2 at 3.5 kW.

Position	Emissivity from OES [$\frac{ph}{m^3 ssr}$]		Emissivity from AtoH [$\frac{ph}{m^3 ssr}$]	χ^2
r=0 mm	H_α	$1.24 \cdot 10^{20}$	$1.17 \cdot 10^{20}$	$4.73 \cdot 10^{17}$
	H_β	$2.34 \cdot 10^{19}$	$2.23 \cdot 10^{19}$	
	H_γ	$3.85 \cdot 10^{18}$	$3.84 \cdot 10^{18}$	
r=10 mm	H_α	$1.79 \cdot 10^{20}$	$1.63 \cdot 10^{20}$	$2.58 \cdot 10^{17}$
	H_β	$2.79 \cdot 10^{19}$	$2.81 \cdot 10^{19}$	
	H_γ	$4.14 \cdot 10^{18}$	$4.13 \cdot 10^{18}$	
r=20 mm	H_α	$7.82 \cdot 10^{19}$	$7.82 \cdot 10^{19}$	$3.38 \cdot 10^{15}$
	H_β	$1.07 \cdot 10^{19}$	$1.01 \cdot 10^{19}$	
	H_γ	$1.88 \cdot 10^{18}$	$1.97 \cdot 10^{18}$	
r=40 mm	H_α	$8.76 \cdot 10^{18}$	$8.75 \cdot 10^{18}$	$1.49 \cdot 10^{16}$
	H_β	$4.45 \cdot 10^{17}$	$4.34 \cdot 10^{17}$	
	H_γ	$6.26 \cdot 10^{16}$	$1.01 \cdot 10^{17}$	

In order to make the comparison clearer in Figure 6.1 the densities profiles obtained with the minimization at 3.5 kW are reported in a graphical form.

The molecular hydrogen acquires a higher density in the external position and a lower one in the centre. This is probably due to the H_2-electron collision dissociation that has a bigger rate coefficient in the central position, due to a higher electron temperature.
As predicted also by the already mentioned COMSOL simulations on RAID, the H_3^+ is predominant in the external position, while the H^+ is dominant in the central one.
In order to verify how much the parameters are sensible to a different power, the minimization was done also taking advantage of the OES measurements at 5 kW. Since the central position is critical regarding the OES data analysis, this time the minimization was carried on only at the coordinates 10 mm, 20 mm and 40 mm.
In Table 5.6 the values of electron density and temperature fixed for the minimization at 5 kW are reported.

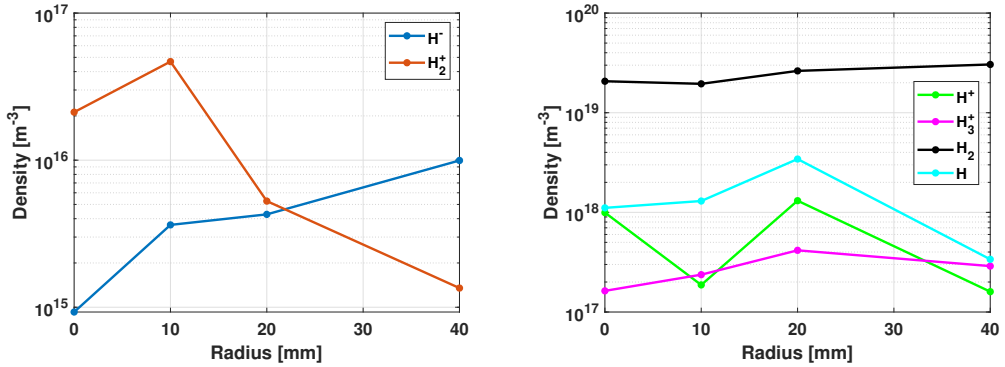

(a) Density of H^- and H_2^+ **(b)** Density of H^+, H_3^+, H_2 and H

Figure 5.2: Density of H^-, H_2^+, H^+, H_3^+, H_2 and H obtained with the minimization at 3.5 kW

Table 5.6: Values of electron density and temperature that were fixed for the minimization at 5 kW.

Position	n_e [m^{-3}]	T_e [eV]
r=10 mm	$2.49 \cdot 10^{18}$	4.702
r=20 mm	$1.74 \cdot 10^{18}$	3.44
r=40 mm	$5.83 \cdot 10^{17}$	1.15

In Table 5.7 the best results in terms of densities of the chemical species are reported.

Table 5.7: Results of OES interpretation in RAID at 5 kW (the * remarks that this value was fixed during the minimization).

Position	H^-[m^{-3}]	H^+ [m^{-3}]	H_2^+ [m^{-3}]	H_3^+ [m^{-3}]	H_2 [m^{-3}]	H [m^{-3}]
r=10 mm	$4.83 \cdot 10^{15}$	$8.34 \cdot 10^{17}$	$1.39 \cdot 10^{16}$	$3.49 \cdot 10^{16}$	$2.21 \cdot 10^{19}$	$9.68 \cdot 10^{18}$
r=20 mm	$5.31 \cdot 10^{15}$	$6.48 \cdot 10^{17}$	$6.25 \cdot 10^{15}$	$2.79 \cdot 10^{16}$	$2.37 \cdot 10^{19}$	$1.9 \cdot 10^{18}$
r=40 mm	$9.98 \cdot 10^{15*}$	$5.42 \cdot 10^{17}$	$1.24 \cdot 10^{15}$	$1.93 \cdot 10^{16}$	$1.18 \cdot 10^{19}$	$9.1 \cdot 10^{17}$

The absolute emissivities measured with OES and the results obtained with the minimization (calculated with the densities of the species in Table 5.7) and the associated χ^2 are compared in Table 5.8.

In Figure 6.2 the densities profiles obtained with the minimization at 5 kW are reported in a graphical form.

Table 5.8: Comparison between OES results and the emissivities calculated with the densities conditions obtained by the minimization and associated χ^2 at 5 kW.

Position	Emissivity from OES $[\frac{ph}{m^3 ssr}]$		Emissivity from AtoH $[\frac{ph}{m^3 ssr}]$	χ^2
r=10 mm	H_α	$3.53 \cdot 10^{21}$	$3.28 \cdot 10^{21}$	$4.54 \cdot 10^{15}$
	H_β	$3.34 \cdot 10^{19}$	$3.8 \cdot 10^{19}$	
	H_γ	$4.75 \cdot 10^{18}$	$1.73 \cdot 10^{18}$	
r=20 mm	H_α	$3.42 \cdot 10^{20}$	$3.14 \cdot 10^{20}$	$1.11 \cdot 10^{17}$
	H_β	$1.378 \cdot 10^{19}$	$5.77 \cdot 10^{19}$	
	H_γ	$2.38 \cdot 10^{18}$	$1.09 \cdot 10^{18}$	
r=40 mm	H_α	$2.73 \cdot 10^{19}$	$2.30 \cdot 10^{19}$	$4.93 \cdot 10^{15}$
	H_β	$7.67 \cdot 10^{17}$	$5.02 \cdot 10^{17}$	
	H_γ	$1.20 \cdot 10^{17}$	$1.16 \cdot 10^{17}$	

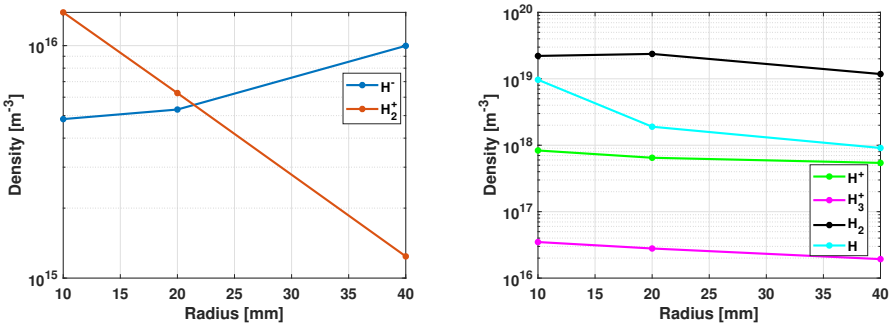

(a) Density of H^- and H_2^+ **(b)** Density of H^+, H_3^+, H_2 and H

Figure 5.3: Density of H^-, H_2^+, H^+, H_3^+, H_2 and H obtained with the minimization at 5 kW

The density of negative ions obtained is not far from expectation and, as expected, there is a higher production at 5 kW than at 3.5 kW. Indeed, increasing the power in RAID, the peak of temperature and density increases but the temperature in the edge of the plasma remains low, generating more vibrationally excited H_2 in the center and, at the same time, keeping the same rate of depletion in the edge.
At both powers, the H_2 density fluctuates around $2 \cdot 10^{19}$ m^{-3}. Instead, the H density decreases of an order of magnitude in the edge of the plasma column where, as expected, the dissociation is lower than in the central positions.
The H_2^+ and H^+ densities do not show particular variations between the two powers, while the H_3^+ is lower at 3.5 kW.
A second attempt was made fixing the molecular hydrogen density to $2 \cdot 10^{19}$ m^{-3} in all the positions. The result is that the χ^2 was not reduced and the values of densities of the other species were further from the expected values than in the previous attempt. Keeping a constant value of $2 \cdot 10^{19}$ m^{-3} always caused an additional reduction of the density of H_2^+ in comparison to the first case. On the other hand, the H_3^+ density faced an unattended increase.
It is important to remark that the $H_2^+ + H^-$ mutual neutralization cross section was corrected with a factor of 0.16 suggested in the reference [37]. In all the positions under investigation, a density of H_2^+ lower than the expected one was observed. Applying this coefficient, how Yacora does, the consumption of H_2^+ is reduced giving as output a slightly higher density, but this density is still lower than the expected value. However, this factor has been calculated for a particular experimental condition and this does not mean that it can be valid for every type of plasma. Anyway, more research is necessary on this field to identify a valid rate coefficient for the mutual neutralization between H_2^+ and H^-.

These results should be considered as indications and not exact values, taking into account all the simplifications of the model, the uncertainties of the measurements and of the cross sectional data and the complexity of the research of an absolute minimum. Indeed, as it has been already demonstrated, these types of processes could bring to some local and not absolute minima. It is possible that entire regions in the space of parameters are flat and therefore they successfully minimize the χ^2 even with different values of density [17].

5.3 Negative ions investigation with AtoH

When in a plasma there is a condition for which only the collisional channel related to one species is dominant, the radiation emitted can be directly related to the presence of this species.
This can be seen as a particular way for OES interpretation that, however, is valid only under strict conditions. This is the same concept for which in high temperature plasmas the corona models can be used as population densities model, neglecting all the other excitation channels.
When the electron temperature is higher than 1 eV and the electron density is lower than 10^{19} m^{-3} the recombination is negligible. Moreover, the dissociative excitation and dissociative recombination can be ignored if H/ $H_2 > 0.1$, H/ $H_2^+ > 1000$ or H^+/ $H_2^+ > 10$. Under these conditions, the negative ions mutual neutralization can be assumed to be the only relevant path [13]. The

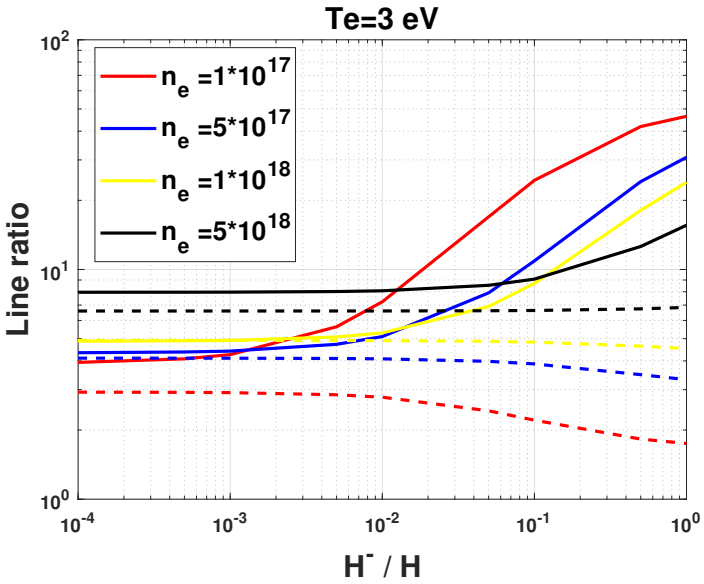

Figure 5.4: H_α/H_β (continuous line) and H_β/H_γ (dashed line) dependence on the negative ions density if the mutual neutralization is the dominant path

sensibility to the negative ions is shown in Figure 5.4, referring to an electron temperature of 3 eV for different electron densities. When the previously mentioned relationships are followed, the line ratio H_α/H_β (continuous line) is sensitive to the ratio H^-/H and thus to the negative ions presence. The sensitivity to a high ratio H^-/H decreases with an electron density increase.
As already explained in Chapter 2, the $H^+ + H^-$ mutual neutralization populates only the quantum states |2> and |3> and therefore a higher negative ions densities causes a higher H_α emission. The negative ions can undergo also another neutralization path with the positive ions H_2^+. This process populates the state $|4\rangle$ with a higher probability than $|3\rangle$, but gives an increment on both H_α and H_β emission. To take into account the effects of both the collisional processes, and also because it is affected by less uncertainties, the negative ion density effect on the emissivity has been connected to the line ratios.
Up to now, on RAID, it has not been localized a point in which the all the collisional processes can

be neglected except for the mutual neutralization. Indeed, even in the external positions of the plasma column, the density ratios required for the validity of the previous graph are not respected, and for this reason it was not possible to apply this type of analysis on this device.
Anyway, this is another demonstration of the great flexibility of AtoH and of its capability to investigate on a particular excitation channel.

Chapter 6

Conclusions and future improvements

The first part of this work was focused on the development of an atomic hydrogen collisional radiative code, AtoH. Taking into account that the first application of the code had to be the helicon plasma source RAID, the collisional channels have been chosen. 20 quantum states were considered and all the collisional channels were taken into account simultaneously. The population density differential equation of each quantum state was coupled with all the other states. A MatLab function for the calculation of the rate coefficients as a function of the electrons or ions temperature was implemented for each collisional channel. At this point all the ingredients were ready for the implementation of the system of equations. Giving as input the density of the involved species (electron, positive and negative ions) and the associated temperatures, AtoH gives as output the related population density of all the excited states of atomic hydrogen. Knowing these values, it was possible to calculate the absolute emission of the atomic hydrogen lines. The attention was mainly focused on H_α, H_β and H_γ.
AtoH was then compared to Yacora, an atomic hydrogen collisional radiative code available online. The two codes have a completely different approach to the problem. Yacora considers only one collisional channel at a time and, to know the final emissivities, it is necessary to calculate them by means of weighting factors called population coefficients. Moreover, the other two differences are that Yacora takes into account a quantum state number that is two times the number of states of AtoH and that Yacora has a broaden applicability range in terms of electron temperature, since it can also take into account the H_2^+ dissociation that has a threshold at 15.2 eV. In addition, the cross sectional data used are not the same and this increases the probability to obtain different results.
However the comparison showed that even if it is a simplified model, AtoH results are not far from the Yacora ones, giving the advantage to consider all the excitation channels simultaneously.
The comparison between the two models was done first on the emissivity. Changing the electron temperature and electron density and keeping the same values of the other chemical species, the two models showed an offset that is constant with respect to the electron density and depends only on the electron temperature. The discrepancy increases for the emission lines that involve higher quantum states. At 1 eV the offset was of 2.36 on H_α, 2.34 on H_β and 2.42 on H_γ. At 10 eV the discrepancy is lower and respectively of 1.16 on H_α, 1.63 on H_β and 1.93 on H_γ. The lower discrepancy at higher temperature suggests that the difference could be related to the low temperature processes and thus the recombining ones. However, since it has not been possible to use the same collisional data for these processes, it could be difficult to state if this discrepancy is simply related to the different sources or it has another origin. Moreover, it is important to remark that reducing the number of quantum values considered by AtoH was also tried. Since reducing them the emissivity is further from what is predicted by Yacora, it could likely happen that increasing the number of levels from 20 to 40 the results will be closer.

The second comparison was focused on the single excitation channels. AtoH has been developed to work as Yacora, considering only one excitation channel per time. What emerged from this analysis was that the contributions of the channels were quite close for the quantum state $|2\rangle$, while there was a difference of one order of magnitude on the last quantum state ($|20\rangle$). Again, this could be mainly related to the number of quantum states considered: since in AtoH the final one is $|20\rangle$ the contribution on it will be overestimated since there are not upper levels where the electrons can be spread.
Subsequently, RAID plasma device was described as the optical emission spectroscopy campaign carried on it. The results of this campaign were reported and commented for two powers: 1.5 kW and 3.5 kW. Then, AtoH was applied to plot few graphs of emissivities as a function of the electron temperature and density in a generic plasma.
Finally, the interpretation of the OES measurement at 3.5 kW and 5 kW was made. This method is based on the application of a minimization algorithm that has the objective to find the combination of densities of the involved species on the plasma reactions, that minimizes the deviation between the OES measurements and the emissivities obtained with the simulations. At the end of this procedure, theoretically, the densities of the chemical species that were present in that operating condition can be assumed to be those that minimizes the offset. The complexity of this procedure is related to the fact that only three emissivities H_α, H_β and H_γ are know from OES, while the densities of the chemical species involved, assuming to know the electron density and temperature, are six. In order to reduce the space of parameters the negative ions density was fixed in the positions in which it was measured (on the edge of the plasma column). Then, also the density of molecular hydrogen was fixed but this attempt did not helped on the reduction of the χ^2.
The results of the minimization, in terms of density of the involved species as a function of the radius, in Figures 6.1 and 6.2 are reported for 3.5 kW and 5 kW, respectively.

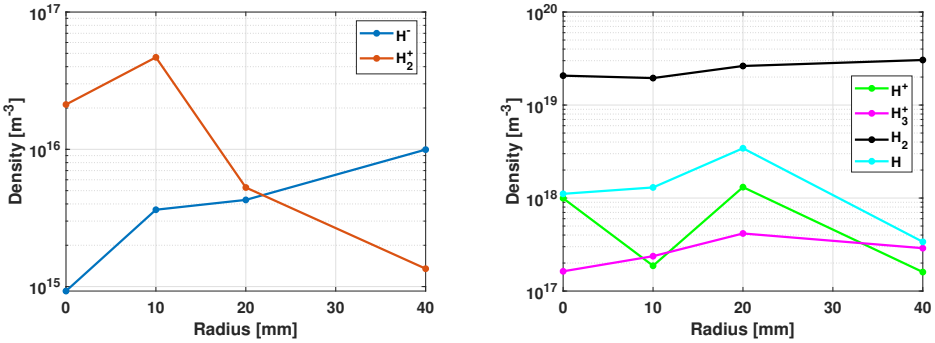

(a) Density of H^- and H_2^+ **(b)** Density of H^+, H_3^+, H_2 and H

Figure 6.1: Density of H^-, H_2^+, H^+, H_3^+, H_2 and H obtained with the minimization at 3.5 kW

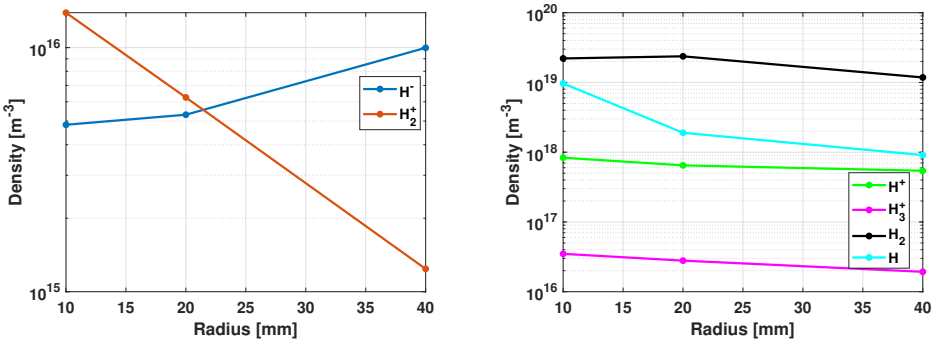

(a) Density of H^- and H_2^+ **(b)** Density of H^+, H_3^+, H_2 and H

Figure 6.2: Density of H^-, H_2^+, H^+, H_3^+, H_2 and H obtained with the minimization at 5 kW

The minimization processes offered good results for the approximation of the chemical species involved, in the sense that they were close to the expected ones.
The only species with a value quite lower than the expectations was the H_2^+. The reason of that should be searched on the cross sectional data related to this species, that is the most problematic. Indeed, the mutual neutralization data available is not reliable, as stated in what it is considered the most reliable report about low temperature processes, due to an inappropriate treatment of the channels dynamics. Nevertheless this is the only data available now. Moreover, the dissociative recombination cross section was averaged over the initial vibrational states of the molecule H_2^+ since it was not possible to discriminate, in the system of equations, the contribution of each vibrational state, because it means to know the density of H_2^+ in each vibrational quantum state. Anyway, the results must be interpreted as guide values and not exact densities, considering that is not possible to identify if the minimum founded was a local or an absolute one. Indeed, it would be possible that entire regions of parameters exist, were several local minimum which all bring to the minimization of the χ^2 are concentrated.
As last application, AtoH has been made to work for the investigation of the sensitivity of the line ratios to the presence of negative ions, plotting the behaviour of these curves as a function of H^-/H.

6.1 Future improvements

The first improvement on the existing code could be, as soon as new collisional data will be available, the review of the H_2^+ mutual neutralization and dissociative excitation cross sections. Concerning the dissociative excitation, a different averaging method of the cross section over the vibrational states can be applied to test if the results improve.
Then, a great improvement of AtoH could be done implementing the equation for other excited states of hydrogen (up to $|40\rangle$ for example) and eventually verify if the results are closer to Yacora and if the minimization gives as result a lower χ^2.
Moreover, it could be possible to add other reactions that are effective at higher temperatures (e.g., the H_2^+ dissociation) in order to expand the applicability range. Indeed, even if AtoH is applied for temperatures lower than the threshold of 15.2 eV, considering the electron energy distribution function, there could be a portion of electrons able to activate this process.
In addition, another important step for the optimization of AtoH could be focused on the minimization process. Indeed, the MatLab function *fminsearch* used for the minimization does not allow to restrict the parameters for the interaction into a known interval. This restriction would allow to focus on a region of the space close to the minimum and thus reduce the time for the iterations and avoid solutions without physical sense, like negative densities. The new minimization algorithm should be suitable for a differential system of equations and it should allow the restriction of the space of parameters. An example are the genetic algorithms, that allow to define more limit conditions for the minimization.
Finally, if it were possible to measure the density of neutrals in the plasma, this would reduce the number of unknowns during the minimization and allow to fully characterize the ionic species in the plasma. The point value of atomic hydrogen density can be measured with the two-photon excitation laser induced fluorescence (LIF). Knowing the density of atomic hydrogen and estimating the dissociation degree it could be possible to know the value of H_2.

Bibliography

[1] G.B. Bachelet and V.D.P. Servedio. *Elementi di fisica atomica, molecolare e dei solidi.* Aracne, 2017.

[2] K. Behringer and U. Fantz. The influence of opacity on hydrogen excited-state population and applications to low-temperature plasmas. *New Journal of Physics*, 2:23–23, sep 2000.

[3] B. H. Bransden and C. J. Joachain. *Physics of atoms and molecules.* Harlow : Prentice Hall, 2nd ed edition, 2003. Previous ed.: 1983.

[4] B.H. Bransden. *Atomic collision theory.* Lecture Notes and Supplements in Physics Series. Benjamin/Cummings Publishing Company, Advanced Book Program, 1983.

[5] M. Claudio. *Poloidal CX visible light plasma rotation diagnostics in TCV.* PhD thesis, Lausanne, 2017.

[6] C. Crevoisier. 7.11 - use of hyperspectral infrared radiances to infer atmospheric trace gases. In Shunlin Liang, editor, *Comprehensive Remote Sensing*, pages 345 – 387. Elsevier, Oxford, 2018.

[7] I. Furno et al. Helicon wave-generated plasmas for negative ion beams for fusion. *EPJ Web Conf.*, 157:03014, 2017.

[8] I.I. Sobelman et al. *Excitation of atoms and broadening of spectral lines.* Springer series in chemical physics. Springer-Verlag, 1981.

[9] M. J. J. Eerden et al. Cross section for the mutual neutralization reaction $h_2^+ + h^-$, calculated in a multiple-crossing landau-zener approximation. *Phys. Rev. A*, 51:3362–3365, Apr 1995.

[10] R. Agnello et al. Negative ion characterization in a helicon plasma source for fusion neutral beams by cavity ring-down spectroscopy and langmuir probe laser photodetachment. *Submitted for pubblication to Nuclear Fusion*, 2019.

[11] S. Wang et al. Balmer h, hand hspectral lines intensities in high-power RF hydrogen plasmas. *Plasma Science and Technology*, 16(3):219–222, mar 2014.

[12] U. Fantz. Basics of plasma spectroscopy. *Plasma Sources Science and Technology*, 15(4):S137–S147, oct 2006.

[13] U. Fantz and D. Wnderlich. A novel diagnostic technique for h-(d-) densities in negative hydrogen ion sources. *New Journal of Physics*, 8(12):301–301, dec 2006.

[14] Ck-12 foundation. Spectral lines of hydrogen, 2019.

[15] J. P. Freidberg. *Plasma Physics and Fusion Energy.* Cambridge University Press, 2007.

[16] T. Fujimoto. *Plasma Spettroscopy.* Oxford Science Publications, 1980.

[17] M. Giacomin. *Application of collisional radiative models for atomic and molecular hydrogen to a negative ion source for fusion.* PhD thesis, Universita' degli studi di Padova, 9 2017.

[18] F. A. Gianturco. *Atomic and Molecular Collision Theory*. Springer US, 1 edition, 1982.

[19] H. R. Griem. Stark broadening of higher hydrogen and hydrogen-like lines by electrons and ions. *The Astrophysical Journal*, 132:883, 1960.

[20] M.J. Klein. Principle of detailed balance. *Phys. Rev.*, 97:1446–1447, Mar 1955.

[21] K. C. Kulander and M. F. Guest. Excited electronic states of h3and their role in the dissociative recombination of h3. *Journal of Physics B: Atomic and Molecular Physics*, 12(16):L501–L504, aug 1979.

[22] M. Larsson. Dissociative recombination of h3+ and d5+. *Philosophical Transactions of the Royal Society A: Mathematical, Physical and Engineering Sciences*, 377(2154), 2019.

[23] M.A. Lieberman and A.J. Lichtenberg. *Principles of Plasma Discharges and Materials Processing*. Wiley, 2005.

[24] A. D. McNaught and A. Wilkinson. *Compendium of Chemical Terminology, 2nd ed. (the "Gold Book")*. Lecture Notes and Supplements in Physics Series. Blackwell Scientific Publications, 1997.

[25] A. Milton. *Handbook of Mathematical Functions, With Formulas, Graphs, and Mathematical Tables,*. Dover Publications, Inc., New York, NY, USA, 1974.

[26] NIST. Atomic spectroscopy, spectral line shape - nist, 2019.

[27] D. Reiter, R. K. Janev, and U. Samm. Collision processes in low-temperature hydrogen plasmas. (JUEL–4105), 2003.

[28] M. A. Sainz and D. M. Coleman. Experimental alignment of a spectrometer system using laser diffraction. *Appl. Spectrosc.*, 35(6):564–567, Nov 1981.

[29] J.S. Santoso. *Production of Negative Hydrogen Ions in a High-Powered Helicon Plasma Source*. PhD thesis, College of Science, Research School of Physics and Engineering, Plasma Research Laboratory, 7 2018.

[30] K. Sawada, K. Eriguchi, and T. Fujimoto. Hydrogen-atom spectroscopy of the ionizing plasma containing molecular hydrogen: Line intensities and ionization rate. *Journal of Applied Physics*, 73:8122–8125, jun 1993.

[31] K. Sawada and Fujimoto T. Effective ionization and dissociation rate coefficients of molecular hydrogen in plasma. *Journal of Applied Physics*, 78(5):2913–2924, 1995.

[32] M. Smith, R. Dennis Keefer, and S.I. Sudharsanan. Abel inversion using transform techniques. *Journal of Quantitative Spectroscopy and Radiative Transfer*, 39(5):367 – 373, 1988.

[33] A. von Keudell and V. Schulz von der Gathen. Foundations of low-temperature plasma physics—an introduction. *Plasma Sources Science and Technology*, 26(11):113001, oct 2017.

[34] W. L. Wiese and J. R. Fuhr. Publisher's note: accurate atomic transition probabilities for hydrogen, helium, and lithium [j. phys. chem. ref. data 38, 565 (2009)]. *Journal of Physical and Chemical Reference Data*, 38(4):1129–1129, 2009.

[35] D. Wnderlich, S. Dietrich, and U. Fantz. Application of a collisional radiative model to atomic hydrogen for diagnostic purposes. *Journal of Quantitative Spectroscopy and Radiative Transfer*, 110(1):62 – 71, 2009.

[36] D. Wnderlich and U. Fantz. Evaluation of state-resolved reaction probabilities and their application in population models for he, h, and h2. *Atoms*, 4(4), 2016.

[37] D. Wnderlich, M. Giacomin, R. Ritz, and U. Fantz. Yacora on the web: Online collisional radiative models for plasmas containing h, h2 or he. *Journal of Quantitative Spectroscopy and Radiative Transfer*, page 106695, 10 2019.

Appendix A

AtoH

This appendix contains the main programs developed to obtain the results described in this thesis. In particular, Section A.1 consists of an example the MatLab code used for the minimization described in Chapter 5. First is reported the principal code and then the one in which the emissivities are calculated at each iteration. Section A.2 contains the MatLab function core of AtoH, namely the differential system of equations solved for the population model, as described in Chapter 2.

A.1 Minimization

```
clear all
close all
clc


%% 3500 W

% external position r=40 mm

    Te=1.309; %eV
    Te_K=Te*11604.525;% K
    ne=3.33e17; %1/m3
    nHm=9.95e15; %1/m3
    Tp=1000; %K
    H_alpha_meas_e=8.7617138e+18; %ph/s/sr/m3
    H_beta_meas_e=4.4548961e+17;
    H_gamma_meas_e=6.2645682e+16;

    H_meas_e=[H_alpha_meas_e H_beta_meas_e H_gamma_meas_e];

% Calculation of the rate coefficients at the requested temperatures
m(1)=electrons(Te_K);
m(2)=protons(Tp);
m(3)=diss_rec_H2p(Te_K);
m(4)=diss_rec_H3p(Te_K);
m(5)=mutual_neutr_H2p(Tp);
m(6)=mutual_neutr_Hp(Tp);
m(7)=two_body_Hp_rec(Te); % in eV
m(8)=three_body_Hp_rec(Te); % in eV
m(9)=H2_diss(Te); % in eV because the fit is in eV

H_code_e=@(nhp,nh2p,nh3p,nh,nh2) H_emissivity_e(nhp,nh2p,nh3p,nh,nh2); % Definition of the function

x0_e=[3.4295e+16, 5.1443e+16, 2e17, 2.5721e+17]; % Initial values

options = optimset('MaxIter',200,'Display','final','Display','notify');
```

```
[ions_e,min_chi_square_e]=fminsearch(@(nh)(norm( (H_meas_e-H_code_e(abs(nh(1)),abs(nh(2)),abs(nh(3)
    ),abs(nh(4)),abs(nh(5)) ) )./sqrt(H_code_e(abs(nh(1)),abs(nh(2)),abs(nh(3)),abs(nh(4)),abs(nh
    (5)) ) ) )).^2,x0_e,options);

save('densities_e','ions_e');
save('min_chi_square_e','min_chi_square_e');
```

A.1.1 MATLAB function for calculation of the emissivities during the minimization

```
function H_line=H_emissivity_e(nHp,nH2p,nH3p,nH,nH2)
% esternal position r=40 mm p=3500 W
Te=1.309; %eV
Te_K=Te*11604.525;% K
ne=3.33e17; %1/m3
nHm=9.95e15;


Tp=1000; %K


        ec=importdata('AA.txt'); % Einstein Coefficients

        fid=fopen('parameters.txt','w'); % Exportation of the parameters for the solution of the
            system
        fprintf(fid,'%1.15e %1.15e %1.15e %1.15e %1.15e %1.15e %1.15e %1.15e %1.15e\r\n',Te,ne,Tp,
            nH2,nH,nHm,nH3p,nH2p,nHp,nH2);
        fclose(fid);

          tt=(0:1e-11:0.8e-4);
          [Tout,Yout]=ode15s(@dH,tt,[nH; 0;0;0;0;0;0;0;0;0;0;0;0;0;0;0;0;0;0;0;0;]); % Solution of
              the system of differential equations

          II2=zeros(1,3);

          % Calculation of the Balmer lines emissivities
                        for jk=3:5
                            II2(jk-2)= Yout(end,jk)*ec(jk,2)/(4*pi); %ph/m3/s/sr
                        end


                        H_line(1)= II2(1); % H_alpha
                        H_line(2)= II2(2); % H_beta
                        H_line(3)= II2(3); % H_gamma


end
```

A.2 MATLAB function for definition of the differential system of equations

```
function [HH]=dH(t,Hn)

% Parameters Importation
    prop=importdata('parameters.txt');
% Te=prop(1);
    ne=prop(2);
% Tp=prop(3);
    nH2=prop(4);
% nH=prop(5);
```

```
    nHm=prop(6);
    nH3p=prop(7);
    nH2p=prop(8);
    nHp_ex=0;
    nHp=prop(9);


%% Electron excitation and de-excitation

% Excitation rate coefficients
  ke=importdata('rate_coefficients_electron_ex_and_tr.txt');

% The rate coefficients are defined in this way to allow to change easily the number of
% quantum states considered and to check faster the correctness of the
% equations

        k12=ke(1);
        k13=ke(2);
        k14=ke(3);
        k15=ke(4);
        k16=ke(5);
        k17=ke(6);
        k18=ke(7);
        k19=ke(8);
        k1_10=ke(9);
        k1_11=ke(10);
        k1_12=ke(11);
        k1_13=ke(12);
        k1_14=ke(13);
        k1_15=ke(14);
        k1_16=ke(15);
        k1_17=ke(16);
        k1_18=ke(17);
        k1_19=ke(18);
        k1_20=ke(19);


        k23=ke(20);
        k24=ke(21);
        k25=ke(22);
        k26=ke(23);
        k27=ke(24);
        k28=ke(25);
        k29=ke(26);
        k210=ke(27);
        k211=ke(28);
        k212=ke(29);
        k213=ke(30);
        k214=ke(31);
        k215=ke(32);
        k216=ke(33);
        k217=ke(34);
        k218=ke(35);
        k219=ke(36);
        k220=ke(37);



        k34=ke(38);
        k35=ke(39);
        k36=ke(40);
        k37=ke(41);
        k38=ke(42);
        k39=ke(43);
        k310=ke(44);
        k311=ke(45);
        k312=ke(46);
```

```
k313=ke(47);
k314=ke(48);
k315=ke(49);
k316=ke(50);
k317=ke(51);
k318=ke(52);
k319=ke(53);
k320=ke(54);



k45=ke(55);
k46=ke(56);
k47=ke(57);
k48=ke(58);
k49=ke(59);
k410=ke(60);
k411=ke(61);
k412=ke(62);
k413=ke(63);
k414=ke(64);
k415=ke(65);
k416=ke(66);
k417=ke(67);
k418=ke(68);
k419=ke(69);
k420=ke(70);


k56=ke(71);
k57=ke(72);
k58=ke(73);
k59=ke(74);
k510=ke(75);
k511=ke(76);
k512=ke(77);
k513=ke(78);
k514=ke(79);
k515=ke(80);
k516=ke(81);
k517=ke(82);
k518=ke(83);
k519=ke(84);
k520=ke(85);


k67=ke(86);
k68=ke(87);
k69=ke(88);
k610=ke(89);
k611=ke(90);
k612=ke(91);
k613=ke(92);
k614=ke(93);
k615=ke(94);
k616=ke(95);
k617=ke(96);
k618=ke(97);
k619=ke(98);
k620=ke(99);


k78=ke(100);
k79=ke(101);
k710=ke(102);
k711=ke(103);
k712=ke(104);
```

```
k713=ke(105);
k714=ke(106);
k715=ke(107);
k716=ke(108);
k717=ke(109);
k718=ke(110);
k719=ke(111);
k720=ke(112);



k89=ke(113);
k810=ke(114);
k811=ke(115);
k812=ke(116);
k813=ke(117);
k814=ke(118);
k815=ke(119);
k816=ke(120);
k817=ke(121);
k818=ke(122);
k819=ke(123);
k820=ke(124);


k910=ke(125);
k911=ke(126);
k912=ke(127);
k913=ke(128);
k914=ke(129);
k915=ke(130);
k916=ke(131);
k917=ke(132);
k918=ke(133);
k919=ke(134);
k920=ke(135);

k1011=ke(136);
k1012=ke(137);
k1013=ke(138);
k1014=ke(139);
k1015=ke(140);
k1016=ke(141);
k1017=ke(142);
k1018=ke(143);
k1019=ke(144);
k1020=ke(145);


k1112=ke(146);
k1113=ke(147);
k1114=ke(148);
k1115=ke(149);
k1116=ke(150);
k1117=ke(151);
k1118=ke(152);
k1119=ke(153);
k1120=ke(154);


k1213=ke(155);
k1214=ke(156);
k1215=ke(157);
k1216=ke(158);
k1217=ke(159);
k1218=ke(160);
k1219=ke(161);
```

```
        k1220=ke(162);


        k1314=ke(163);
        k1315=ke(164);
        k1316=ke(165);
        k1317=ke(166);
        k1318=ke(167);
        k1319=ke(168);
        k1320=ke(169);

        k1415=ke(170);
        k1416=ke(171);
        k1417=ke(172);
        k1418=ke(173);
        k1419=ke(174);
        k1420=ke(175);

        k1516=ke(176);
        k1517=ke(177);
        k1518=ke(178);
        k1519=ke(179);
        k1520=ke(180);

        k1617=ke(181);
        k1618=ke(182);
        k1619=ke(183);
        k1620=ke(184);

        k1718=ke(185);
        k1719=ke(186);
        k1720=ke(187);

        k1819=ke(188);
        k1820=ke(189);

        k1920=ke(190);

% De-excitation rate coefficients
        kd=importdata('rate_coefficients_electron_de_ex.txt');
% k2-1 k3-1 k4-1 k5-1 k3-2 k4-2 k5-2 k4-3 k5-3 k5-4 ... [m^3/s]
        k21=kd(1);
        k31=kd(2);
        k41=kd(3);
        k51=kd(4);
        k61=kd(5);
        k71=kd(6);
        k81=kd(7);
        k91=kd(8);
        k10_1=kd(9);
        k11_1=kd(10);
        k12_1=kd(11);
        k13_1=kd(12);
        k14_1=kd(13);
        k15_1=kd(14);
        k16_1=kd(15);
        k17_1=kd(16);
        k18_1=kd(17);
        k19_1=kd(18);
        k20_1=kd(19);

        k32=kd(20);
        k42=kd(21);
        k52=kd(22);
        k62=kd(23);
        k72=kd(24);
        k82=kd(25);
```

```
k92=kd(26);
k102=kd(27);
k11_2=kd(28);
k122=kd(29);
k132=kd(30);
k142=kd(31);
k152=kd(32);
k162=kd(33);
k172=kd(34);
k182=kd(35);
k192=kd(36);
k202=kd(37);



k43=kd(38);
k53=kd(39);
k63=kd(40);
k73=kd(41);
k83=kd(42);
k93=kd(43);
k103=kd(44);
k11_3=kd(45);
k123=kd(46);
k133=kd(47);
k143=kd(48);
k153=kd(49);
k163=kd(50);
k173=kd(51);
k183=kd(52);
k193=kd(53);
k203=kd(54);



k54=kd(55);
k64=kd(56);
k74=kd(57);
k84=kd(58);
k94=kd(59);
k104=kd(60);
k11_4=kd(61);
k124=kd(62);
k134=kd(63);
k144=kd(64);
k154=kd(65);
k164=kd(66);
k174=kd(67);
k184=kd(68);
k194=kd(69);
k204=kd(70);


k65=kd(71);
k75=kd(72);
k85=kd(73);
k95=kd(74);
k105=kd(75);
k11_5=kd(76);
k125=kd(77);
k135=kd(78);
k145=kd(79);
k155=kd(80);
k165=kd(81);
k175=kd(82);
k185=kd(83);
k195=kd(84);
```

```
      k205=kd(85);


      k76=kd(86);
      k86=kd(87);
      k96=kd(88);
      k106=kd(89);
      k11_6=kd(90);
      k126=kd(91);
      k136=kd(92);
      k146=kd(93);
      k156=kd(94);
      k166=kd(95);
      k176=kd(96);
      k186=kd(97);
      k196=kd(98);
      k206=kd(99);


      k87=kd(100);
      k97=kd(101);
      k107=kd(102);
      k11_7=kd(103);
      k127=kd(104);
      k137=kd(105);
      k147=kd(106);
      k157=kd(107);
      k167=kd(108);
      k177=kd(109);
      k187=kd(110);
      k197=kd(111);
      k207=kd(112);



      k98=kd(113);
      k108=kd(114);
      k11_8=kd(115);
      k128=kd(116);
      k138=kd(117);
      k148=kd(118);
      k158=kd(119);
      k168=kd(120);
      k178=kd(121);
      k188=kd(122);
      k198=kd(123);
      k208=kd(124);


      k109=kd(125);
      k11_9=kd(126);
      k129=kd(127);
      k139=kd(128);
      k149=kd(129);
      k159=kd(130);
      k169=kd(131);
      k179=kd(132);
      k189=kd(133);
      k199=kd(134);
      k209=kd(135);

      k1110=kd(136);
      k1210=kd(137);
      k1310=kd(138);
      k1410=kd(139);
      k1510=kd(140);
      k1610=kd(141);
```

```
        k1710=kd(142);
        k1810=kd(143);
        k1910=kd(144);
        k2010=kd(145);


        k1211=kd(146);
        k1311=kd(147);
        k1411=kd(148);
        k1511=kd(149);
        k1611=kd(150);
        k1711=kd(151);
        k1811=kd(152);
        k1911=kd(153);
        k2011=kd(154);


        k1312=kd(155);
        k1412=kd(156);
        k1512=kd(157);
        k1612=kd(158);
        k1712=kd(159);
        k1812=kd(160);
        k1912=kd(161);
        k2012=kd(162);


        k1413=kd(163);
        k1513=kd(164);
        k1613=kd(165);
        k1713=kd(166);
        k1813=kd(167);
        k1913=kd(168);
        k2013=kd(169);

        k1514=kd(170);
        k1614=kd(171);
        k1714=kd(172);
        k1814=kd(173);
        k1914=kd(174);
        k2014=kd(175);

        k1615=kd(176);
        k1715=kd(177);
        k1815=kd(178);
        k1915=kd(179);
        k2015=kd(180);

        k1716=kd(181);
        k1816=kd(182);
        k1916=kd(183);
        k2016=kd(184);

        k1817=kd(185);
        k1917=kd(186);
        k2017=kd(187);

        k1918=kd(188);
        k2018=kd(189);

        k2019=kd(190);


%% Ionization rate coefficients
        k_ion_p=importdata('proton_ionization_rate_coefficients.txt');
        k_ion_e=importdata('electron_ionization_rate_coefficients.txt');
```

```
%% Mutual neutralization H- H+ rate coefficients
    kmn=importdata('mutual_neutr_Hp_rate_coefficients_2_3.txt');
    k_mn2=kmn(1);
    k_mn3=kmn(2);


%% Mutual neutralization H- H2+ rate coefficients

    kmn_h2p=importdata('rate_coefficients_MN_h2p.txt');

    k_mn2_h2p=kmn_h2p(1);
    k_mn3_h2p=kmn_h2p(2);
    k_mn4_h2p=kmn_h2p(3);
    k_mn5_h2p=kmn_h2p(4);
    k_mn6_h2p=kmn_h2p(5);
    k_mn7_h2p=kmn_h2p(6);
    k_mn8_h2p=kmn_h2p(7);


%% Dissociative recombination H2+ rate coefficients

    kdr=importdata('dissociative_recombination_H2p_rate_coefficients.txt');

%% Dissociative recombination H3+

    kdr_h3p=importdata('rate_coefficients_DR_h3p.txt','w');

%% DISSOCIATION OF H2 rate coefficients

    k_dis_h2=importdata('rate_coefficients_H2_diss.txt');

%% Two and three body recombination of H+

        k_three_body=importdata('rate_coefficients_3body_rec.txt');
        k_two_body=importdata('rate_coefficients_2body_rec.txt');



    ec=importdata('AA.txt'); %einsten coefficient
    %ec is a matrix (r,c): in each cell is reported the
    % probability from the state |r> to the state |c>

    %% definition of the system of equations


        e1=0; %
        e2= nH3p*ne*kdr_h3p + k_dis_h2(1)*nH2*ne + k_mn2_h2p*nHm*nH2p + ne*nH2p*kdr(1)+ nHm*nHp*
             k_mn2 + ne*nHp*(k_three_body(1)*ne + k_two_body(1) ) + Hn(1)*(k12*ne+k12_p*nHp_ex) - Hn
             (2)* ( nHp_ex*(k_ion_p(2)+ k220_p + k219_p + k218_p + k217_p + k216_p + k215_p + k214_p
              + k213_p + k212_p + k211_p + k210_p + k29_p + k28_p + k27_p + k26_p + k25_p + k24_p +
             k23_p + k21_p )+ ne*(k_ion_e(2)+ k220 + k219 + k218 + k217 + k216 + k215 + k214 + k213
             + k212 + k211 + k210 + k29 + k28 + k27 + k26 + k25 + k24 + k23 + k21 )+ ec(2,1) ) + Hn
             (3)*( ec(3,2)+ne*k32+nHp_ex*k32_p) + Hn(4)*( ec(4,2)+ne*k42+nHp_ex*k42_p) + Hn(5)*(ec
             (5,2)+ne*k52+nHp_ex*k52_p) + Hn(6)*(ec(6,2)+ne*k62+nHp_ex*k62_p)+ Hn(7)*(ec(7,2)+ne*k72
             +nHp_ex*k72_p) + Hn(8)*(ec(8,2)+ne*k82+nHp_ex*k82_p) + Hn(9)*(ec(9,2)+ne*k92+nHp_ex*
             k92_p)+ Hn(10)*(ec(10,2)+ne*k102+nHp_ex*k102_p) + Hn(11)*(ec(11,2)+ne*k11_2+nHp_ex*
             k11_2_p)+ Hn(12)*(ec(12,2)+ne*k122+nHp_ex*k122_p) + Hn(13)*(ec(13,2)+ne*k132+nHp_ex*
             k132_p)+ Hn(14)*(ec(14,2)+ne*k142+nHp_ex*k142_p)+ Hn(15)*(ec(15,2)+ne*k152+nHp_ex*
             k152_p) + Hn(16)*(ec(16,2)+ne*k162+nHp_ex*k162_p) + Hn(17)*(ec(17,2)+ne*k172+nHp_ex*
             k172_p) + Hn(18)*(ec(18,2)+ne*k182+nHp_ex*k182_p)+ Hn(19)*(ec(19,2)+ne*k192+nHp_ex*
             k192_p) + Hn(20)*(ec(20,2)+ne*k202+nHp_ex*k202_p);
        e3= k_dis_h2(2)*nH2*ne + k_mn3_h2p*nHm*nH2p + ne*nH2p*kdr(2)+ nHm*nHp*k_mn3 + ne*nHp*(
             k_three_body(2)*ne + k_two_body(2) ) + Hn(1)*(k13*ne+k13_p*nHp_ex) + Hn(2)* ( ne*k23+
             nHp_ex*k23_p) - Hn(3)*( nHp_ex*(k_ion_p(3)+ k320_p + k319_p + k318_p + k317_p + k316_p
             + k315_p + k314_p + k313_p + k312_p + k311_p + k310_p + k39_p + k38_p + k37_p + k36_p +
              k35_p + k34_p + k32_p + k31_p ) + ne*(k_ion_e(3)+ k320 + k319 + k318 + k317 + k316 +
```

```
     k315 + k314 + k313 + k312 + k311 + k310 + k39 + k38 + k37 + k36 + k35 + k34 + k32 + k31
      )+ec(3,2)+ec(3,1)) + Hn(4)*( ec(4,3)+ne*k43 +nHp_ex*k43_p) + Hn(5)*(ec(5,3)+ne*k53 +
     nHp_ex*k53_p)+ Hn(6)*(ec(6,3)+ne*k63 +nHp_ex*k63_p)+ Hn(7)*(ec(7,3)+ne*k73 +nHp_ex*
     k73_p) + Hn(8)*(ec(8,3)+ne*k83 +nHp_ex*k83_p) + Hn(9)*(ec(9,3)+ne*k93 +nHp_ex*k93_p)+
     Hn(10)*(ec(10,3)+ne*k103 +nHp_ex*k103_p) + Hn(11)*(ec(11,3)+ne*k11_3 +nHp_ex*k11_3_p)+
     Hn(12)*(ec(12,3)+ne*k123 +nHp_ex*k123_p) + Hn(13)*(ec(13,3)+ne*k133+nHp_ex*k133_p)+ Hn
     (14)*(ec(14,3)+ne*k143 +nHp_ex*k123_p)+ Hn(15)*(ec(15,3)+ne*k153 +nHp_ex*k153_p) + Hn
     (16)*(ec(16,3)+ne*k163+nHp_ex*k163_p) + Hn(17)*(ec(17,3)+ne*k173+nHp_ex*k173_p) + Hn
     (18)*(ec(18,3)+ne*k183+nHp_ex*k183_p)+ Hn(19)*(ec(19,3)+ne*k193+nHp_ex*k193_p) + Hn(20)
     *(ec(20,3)+ne*k203+nHp_ex*k203_p) ;
e4= k_dis_h2(3)*nH2*ne + k_mn4_h2p*nHm*nH2p + ne*nH2p*kdr(3)+ ne*nHp*(k_three_body(3)*ne +
     k_two_body(3) ) + Hn(1)*(k14*ne+k14_p*nHp_ex) + Hn(2)* ( ne*k24 + nHp_ex*k24_p) + Hn(3)
     *( ne*k34 + nHp_ex*k34_p) - Hn(4)*( nHp_ex*( k_ion_p(4)+ k420_p + k419_p + k418_p +
     k417_p + k416_p + k415_p + k414_p + k413_p + k412_p + k411_p + k410_p + k49_p + k48_p +
      k47_p + k46_p + k45_p + k43_p + k42_p + k41_p )+ ne*(k_ion_e(4) + k420 + k419 + k418 +
      k417 + k416 + k415 + k414 + k413 + k412 + k411 + k410 + k49 + k48 + k47 + k46 + k45 +
     k43 + k42 + k41 )+ec(4,3)+ec(4,2)+ec(4,1)) + Hn(5)*(ec(5,4)+ne*k54 +nHp_ex*k54_p)+ Hn
     (6)*(ec(6,4)+ne*k64 +nHp_ex*k64_p)+ Hn(7)*(ec(7,4)+ne*k74 +nHp_ex*k74_p) + Hn(8)*(ec
     (8,4)+ne*k84 +nHp_ex*k84_p) + Hn(9)*(ec(9,4)+ne*k94 +nHp_ex*k94_p)+ Hn(10)*(ec(10,4)+ne
     *k104 +nHp_ex*k104_p) + Hn(11)*(ec(11,4)+ne*k11_4 +nHp_ex*k11_4_p)+ Hn(12)*(ec(12,4)+ne
     *k124 +nHp_ex*k124_p) + Hn(13)*(ec(13,4)+ne*k134 +nHp_ex*k134_p)+ Hn(14)*(ec(14,4)+ne*
     k144 +nHp_ex*k144_p)+ Hn(15)*(ec(15,4)+ne*k154 +nHp_ex*k154_p)+ Hn(16)*(ec(16,4)+ne*
     k164+nHp_ex*k164_p) + Hn(17)*(ec(17,4)+ne*k174+nHp_ex*k174_p) + Hn(18)*(ec(18,4)+ne*
     k184+nHp_ex*k184_p)+ Hn(19)*(ec(19,4)+ne*k194+nHp_ex*k194_p) + Hn(20)*(ec(20,4)+ne*k204
     +nHp_ex*k204_p) ;
e5= k_dis_h2(4)*nH2*ne + k_mn5_h2p*nHm*nH2p + ne*nH2p*kdr(4)+ ne*nHp*(k_three_body(4)*ne +
     k_two_body(4) ) + Hn(1)*(k15*ne+k15_p*nHp_ex) + Hn(2)* ( ne*k25 + nHp_ex*k25_p ) + Hn
     (3)*( ne*k35 + nHp_ex*k35_p) + Hn(4)*( ne*k45 + nHp_ex*k45_p) - Hn(5)*(ec(5,4)+ ec(5,3)
     +ec(5,2)+ec(5,1)+ ne*(k_ion_e(5) + k520 + k519 + k518 + k517 + k516 + k515 + k514 +
     k513 + k512 + k511 + k510 + k59 + k58 + k57 + k56 + k54 + k53 + k52 + k51 ) + nHp_ex*(
     k_ion_p(5)+ k520_p + k519_p + k518_p + k517_p + k516_p + k515_p + k514_p + k513_p +
     k512_p + k511_p + k510_p + k59_p + k58_p + k57_p + k56_p + k54_p + k53_p + k52_p +
     k51_p )) + Hn(6)*(ec(6,5)+ne*k65 +nHp_ex*k65_p)+ Hn(7)*(ec(7,5)+ne*k75 +nHp_ex*k75_p) +
      Hn(8)*(ec(8,5)+ne*k85+nHp_ex*k85_p) + Hn(9)*(ec(9,5)+ne*k95+nHp_ex*k95_p)+ Hn(10)*(ec
     (10,5)+ne*k105+nHp_ex*k105_p) + Hn(11)*(ec(11,5)+ne*k11_5+nHp_ex*k11_5_p)+ Hn(12)*(ec
     (12,5)+ne*k125+nHp_ex*k125_p) + Hn(13)*(ec(13,5)+ne*k135+nHp_ex*k135_p) + Hn(14)*(ec
     (14,5)+ne*k145+nHp_ex*k145_p)+ Hn(15)*(ec(15,5)+ne*k155+nHp_ex*k155_p) + Hn(16)*(ec
     (16,5)+ne*k165+nHp_ex*k165_p) + Hn(17)*(ec(17,5)+ne*k175+nHp_ex*k175_p) + Hn(18)*(ec
     (18,5)+ne*k185+nHp_ex*k185_p)+ Hn(19)*(ec(19,5)+ne*k195+nHp_ex*k195_p) + Hn(20)*(ec
     (20,5)+ne*k205+nHp_ex*k205_p);
e6= k_dis_h2(5)*nH2*ne + k_mn6_h2p*nHm*nH2p + ne*nH2p*kdr(5)+ ne*nHp*(k_three_body(5)*ne +
     k_two_body(5) ) + Hn(1)*(k16*ne+k16_p*nHp_ex) + Hn(2)* ( ne*k26 + nHp_ex*k26_p) + Hn(3)
     *( ne*k36 + nHp_ex*k36_p) + Hn(4)*( ne*k46 + nHp_ex*k46_p) + Hn(5)*(ne*k56 + nHp_ex*
     k56_p) - Hn(6)*(ec(6,5)+ec(6,4)+ ec(6,3)+ec(6,2)+ec(6,1)+ne*(k_ion_e(6)+ k620 + k619 +
     k618 + k617 + k616 + k615 + k614 + k613 + k612 + k611 + k610 + k69 + k68 + k67 + k65 +
     k64+ k63+ k62+ k61 ) + nHp_ex*(k_ion_p(6)+ k620_p + k619_p+ k618_p + k617_p + k616_p +
     k615_p + k614_p+ k613_p + k612_p + k611_p + k610_p + k69_p + k68_p + k67_p + k65_p +
     k64_p + k63_p + k62_p + k61_p )) + Hn(7)*(ec(7,6)+ne*k76+nHp_ex*k76_p) + Hn(8)*(ec(8,6)
     +ne*k86+nHp_ex*k86_p) + Hn(9)*(ec(9,6)+ne*k96+nHp_ex*k96_p)+ Hn(10)*(ec(10,6)+ne*k106+
     nHp_ex*k106_p) + Hn(11)*(ec(11,6)+ne*k11_6+nHp_ex*k11_6_p) + Hn(12)*(ec(12,6)+ne*k126+
     nHp_ex*k126_p) + Hn(13)*(ec(13,6)+ne*k136+nHp_ex*k136_p) + Hn(14)*(ec(14,6)+ne*k146+
     nHp_ex*k146_p)+ Hn(15)*(ec(15,6)+ne*k156+nHp_ex*k156_p) + Hn(16)*(ec(16,6)+ne*k166+
     nHp_ex*k166_p) + Hn(17)*(ec(17,6)+ne*k176+nHp_ex*k176_p) + Hn(18)*(ec(18,6)+ne*k186+
     nHp_ex*k186_p)+ Hn(19)*(ec(19,6)+ne*k196+nHp_ex*k196_p) + Hn(20)*(ec(20,6)+ne*k206+
     nHp_ex*k206_p);
e7= k_dis_h2(6)*nH2*ne + k_mn7_h2p*nHm*nH2p + ne*nH2p*kdr(6)+ ne*nHp*(k_three_body(6)*ne +
     k_two_body(6) ) + Hn(1)*(k17*ne+k17_p*nHp_ex) + Hn(2)* ( ne*k27 + nHp_ex*k27_p ) + Hn
     (3)*( ne*k37 + nHp_ex*k37_p) + Hn(4)*( ne*k47 + nHp_ex*k47_p) + Hn(5)*(ne*k57 + nHp_ex*
     k57_p) + Hn(6)*(ne*k67 + nHp_ex*k67_p) - Hn(7)*(ec(7,6)+ec(7,5)+ec(7,4)+ ec(7,3)+ec
     (7,2)+ec(7,1)+ne*(k_ion_e(7) + k720 + k719 + k718 + k717 + k716 + k715 + k714 + k713 +
     k712 + k711 + k710 + k79 + k78 + k76 + k75 + k74+ k73+ k72+ k71 ) + nHp_ex*( k_ion_p(7)
     + k720_p + k719_p + k718_p + k717_p + k716_p + k715_p + k714_p + k713_p + k712_p +
     k711_p + k710_p + k79_p + k78_p + k76_p + k75_p + k74_p + k73_p + k72_p + k71_p )) + Hn
     (8)*(ec(8,7)+ne*k87+nHp_ex*k87_p) + Hn(9)*(ec(9,7)+ne*k97+nHp_ex*k97_p) + Hn(10)*(ec
     (10,7)+ne*k107+nHp_ex*k107_p) + Hn(11)*(ec(11,7)+ne*k11_7+nHp_ex*k11_7_p) + Hn(12)*(ec
     (12,7)+ne*k127+nHp_ex*k127_p) + Hn(13)*(ec(13,7)+ne*k137+nHp_ex*k137_p) + Hn(14)*(ec
     (14,7)+ne*k147+nHp_ex*k147_p)+ Hn(15)*(ec(15,7)+ne*k157+nHp_ex*k157_p) + Hn(16)*(ec
```

```
     (16,7)+ne*k167+nHp_ex*k167_p) + Hn(17)*(ec(17,7)+ne*k177+nHp_ex*k177_p) + Hn(18)*(ec
     (18,7)+ne*k187+nHp_ex*k187_p)+ Hn(19)*(ec(19,7)+ne*k197+nHp_ex*k197_p) + Hn(20)*(ec
     (20,7)+ne*k207+nHp_ex*k207_p);
e8= k_dis_h2(7)*nH2*ne + k_mn8_h2p*nHm*nH2p + ne*nH2p*kdr(7)+ ne*nHp*(k_three_body(7)*ne +
     k_two_body(7) ) + Hn(1)*(k18*ne+k18_p*nHp_ex) + Hn(2)* ( ne*k28 + nHp_ex*k28_p ) + Hn
     (3)*( ne*k38 + nHp_ex*k38_p) + Hn(4)*( ne*k48 + nHp_ex*k48_p) + Hn(5)*(ne*k58 + nHp_ex*
     k58_p) + Hn(6)*(ne*k68 + nHp_ex*k68_p) + Hn(7)*(ne*k78 + nHp_ex*k78_p) - Hn(8)*(ec(8,7)
     +ec(8,6)+ec(8,5)+ec(8,4)+ ec(8,3)+ec(8,2)+ec(8,1)+ne*(k_ion_e(8)+ k820 + k819 + k818 +
     k817 + k816 + k815 + k814 + k813 + k812 + k811 + k810 + k89 + k87 +k86 + k85 + k84+ k83
     + k82+ k81 ) + nHp_ex*(k_ion_p(8)+ k820_p + k819_p + k818_p + k817_p + k816_p + k815_p
     + k814_p + k813_p + k812_p + k811_p + k810_p + k89_p + k87_p +k86_p + k85_p + k84_p +
     k83_p + k82_p + k81_p )) +Hn(9)*(ec(9,8)+ne*k98+nHp_ex*k98_p) + Hn(10)*(ec(10,8)+ne*
     k108+nHp_ex*k108_p) + Hn(11)*(ec(11,8)+ne*k11_8+nHp_ex*k11_8_p) + Hn(12)*(ec(12,8)+ne*
     k128+nHp_ex*k128_p) + Hn(13)*(ec(13,8)+ne*k138+nHp_ex*k138_p)+ Hn(14)*(ec(14,8)+ne*k148
     +nHp_ex*k148_p)+ Hn(15)*(ec(15,8)+ne*k158+nHp_ex*k158_p) + Hn(16)*(ec(16,8)+ne*k168+
     nHp_ex*k168_p) + Hn(17)*(ec(17,8)+ne*k178+nHp_ex*k178_p) + Hn(18)*(ec(18,8)+ne*k188+
     nHp_ex*k188_p)+ Hn(19)*(ec(19,8)+ne*k198+nHp_ex*k198_p) + Hn(20)*(ec(20,8)+ne*k208+
     nHp_ex*k208_p);
e9= k_dis_h2(8)*nH2*ne + ne*nH2p*kdr(8)+ ne*nHp*(k_three_body(8)*ne + k_two_body(8) ) + Hn
     (1)*(k19*ne+k19_p*nHp_ex) + Hn(2)* ( ne*k29 + nHp_ex*k29_p ) + Hn(3)*( ne*k39 + nHp_ex*
     k39_p) + Hn(4)*( ne*k49 + nHp_ex*k49_p) + Hn(5)*(ne*k59 + nHp_ex*k59_p) + Hn(6)*(ne*k69
      + nHp_ex*k69_p) + Hn(7)*(ne*k79 + nHp_ex*k79_p) + Hn(8)*(ne*k89 + nHp_ex*k89_p) - Hn
     (9)*(ec(9,8)+ec(9,7)+ec(9,6)+ec(9,5)+ec(9,4)+ ec(9,3)+ec(9,2)+ec(9,1)+ne*(k_ion_e(9)+
     k920 + k919 + k918 + k917 + k916 + k915 + k914 + k913 + k912 + k911 + k910 + k98+ k97 +
     k96 + k95 + k94+ k93+ k92+ k91 ) + nHp_ex*(k_ion_p(9)+ k920_p + k919_p + k918_p +
     k917_p + k916_p + k915_p + k914_p + k913_p + k912_p + k911_p + k910_p + k98_p + k97_p +
      k96_p + k95_p + k94_p + k93_p + k92_p + k91_p )) + Hn(10)*(ec(10,9) + ne*k109 + nHp_ex
     *k109_p) + Hn(11)*(ec(11,9)+ne*k11_9+ nHp_ex*k11_9_p) + Hn(12)*(ec(12,9)+ne*k129+
     nHp_ex*k129_p) + Hn(13)*(ec(13,9)+ne*k139+ nHp_ex*k139_p)+ Hn(14)*(ec(14,9)+ne*k149+
     nHp_ex*k149_p) + Hn(15)*(ec(15,9)+ne*k159+ nHp_ex*k159_p) + Hn(16)*(ec(16,9)+ne*k169+
     nHp_ex*k169_p) + Hn(17)*(ec(17,9)+ne*k179+nHp_ex*k179_p) + Hn(18)*(ec(18,9)+ne*k189+
     nHp_ex*k189_p)+ Hn(19)*(ec(19,9)+ne*k199+nHp_ex*k199_p) + Hn(20)*(ec(20,9)+ne*k209+
     nHp_ex*k209_p);
e10= k_dis_h2(9)*nH2*ne + ne*nH2p*kdr(9)+ ne*nHp*(k_three_body(9)*ne + k_two_body(9) ) + Hn
     (1)*(k1_10*ne+k1_10_p*nHp_ex) + Hn(2)* ( ne*k210 + nHp_ex*k210_p ) + Hn(3)*( ne*k310 +
     nHp_ex*k310_p) + Hn(4)*( ne*k410 + nHp_ex*k410_p) + Hn(5)*(ne*k510 + nHp_ex*k510_p) +
     Hn(6)*(ne*k610 + nHp_ex*k610_p) + Hn(7)*(ne*k710 + nHp_ex*k710_p) + Hn(8)*(ne*k810 +
     nHp_ex*k810_p) + Hn(9)*(ne*k910 + nHp_ex*k910_p) - Hn(10)*(ec(10,9)+ec(10,8)+ec(10,7)+
     ec(10,6)+ec(10,5)+ec(10,4)+ ec(10,3)+ec(10,2)+ec(10,1)+ne*(k_ion_e(10) + k1020 + k1019
     + k1018 + k1017 + k1016 + k1015 + k1014 + k1013 + k1012 + k1011 + k109 + k108+ k107 +
     k106 + k105 + k104+ k103+ k102+ k10_1 ) + nHp_ex*(k_ion_p(10)+ k1020_p + k1019_p +
     k1018_p + k1017_p + k1016_p + k1015_p + k1014_p + k1013_p + k1012_p + k1011_p + k109_p
     + k108_p+ k107_p +k106_p + k105_p + k104_p + k103_p + k102_p + k10_1_p )) + Hn(11)*(ec
     (11,10)+ne*k1110+ nHp_ex*k1110_p) + Hn(12)*(ec(12,10)+ne*k1210 + nHp_ex*k1210_p) + Hn
     (13)*(ec(13,10)+ne*k1310+ nHp_ex*k1310_p) + Hn(14)*(ec(14,10)+ne*k1410+ nHp_ex*k1410_p)
      + Hn(15)*(ec(15,10)+ne*k1510+nHp_ex*k1510_p) + Hn(16)*(ec(16,10)+ne*k1610+nHp_ex*
     k1610_p) + Hn(17)*(ec(17,10)+ne*k1710+nHp_ex*k1710_p) + Hn(18)*(ec(18,10)+ne*k1810+
     nHp_ex*k1810_p)+ Hn(19)*(ec(19,10)+ne*k1910+nHp_ex*k1910_p) + Hn(20)*(ec(20,10)+ne*
     k2010+nHp_ex*k2010_p);
e11= k_dis_h2(10)*nH2*ne + ne*nH2p*kdr(10)+ ne*nHp*(k_three_body(10)*ne + k_two_body(10) ) +
      Hn(1)*(k1_11*ne+k1_11_p*nHp_ex) + Hn(2)* ( ne*k211 + nHp_ex*k211_p ) + Hn(3)*( ne*k311
      + nHp_ex*k311_p) + Hn(4)*( ne*k411 + nHp_ex*k411_p) + Hn(5)*(ne*k511 + nHp_ex*k511_p)
     + Hn(6)*(ne*k611 + nHp_ex*k611_p) + Hn(7)*(ne*k711 + nHp_ex*k711_p) + Hn(8)*(ne*k811 +
     nHp_ex*k811_p) + Hn(9)*(ne*k911 + nHp_ex*k911_p) + Hn(10)*(ne*k1011 + nHp_ex*k1011_p) -
      Hn(11)*(ec(11,10)+ec(11,9)+ec(11,8)+ec(11,7)+ec(11,6)+ec(11,5)+ec(11,4)+ ec(11,3)+ec
     (11,2)+ec(11,1)+ne*( k_ion_e(11)+ k1120 + k1119 + k1118 + k1117 + k1116 + k1115 + k1114
      + k1113 + k1112 + k1110 + k11_9 + k11_8+ k11_7 +k11_6 + k11_5 + k11_4+ k11_3+ k11_2+
     k11_1 ) + nHp_ex*(k_ion_p(11)+ k1120_p + k1119_p + k1118_p+ k1117_p + k1116_p + k1115_p
      + k1114_p + k1113_p+ k1112_p + k1110_p + k11_9_p + k11_8_p + k11_7_p + k11_6_p +
     k11_5_p + k11_4_p + k11_3_p + k11_2_p + k11_1_p )) + Hn(12)*(ec(12,11)+ne*k1211 +
     nHp_ex*k1211_p) + Hn(13)*(ec(13,11)+ne*k1311 + nHp_ex*k1311_p) + Hn(14)*(ec(14,11)+ne*
     k1411 + nHp_ex*k1411_p) + Hn(15)*(ec(15,11)+ne*k1511 + nHp_ex*k1511_p)+ Hn(16)*(ec
     (16,11)+ne*k1611+nHp_ex*k1611_p) + Hn(17)*(ec(17,11)+ne*k1711+nHp_ex*k1711_p) + Hn(18)
     *(ec(18,11)+ne*k1811+nHp_ex*k1811_p)+ Hn(19)*(ec(19,11)+ne*k1911+nHp_ex*k1911_p) + Hn
     (20)*(ec(20,11)+ne*k2011+nHp_ex*k2011_p);
e12= k_dis_h2(11)*nH2*ne + ne*nH2p*kdr(11)+ ne*nHp*(k_three_body(11)*ne + k_two_body(11) ) +
      Hn(1)*(k1_12*ne+k1_12_p*nHp_ex) + Hn(2)* ( ne*k212 + nHp_ex*k212_p ) + Hn(3)*( ne*k312
```

```
 + nHp_ex*k312_p) + Hn(4)*( ne*k412 + nHp_ex*k412_p) + Hn(5)*(ne*k512 + nHp_ex*k512_p)
+ Hn(6)*(ne*k612 + nHp_ex*k612_p) + Hn(7)*(ne*k712 + nHp_ex*k712_p) + Hn(8)*(ne*k812 +
nHp_ex*k812_p) + Hn(9)*(ne*k912 + nHp_ex*k912_p) + Hn(10)*(ne*k1012 + nHp_ex*k1012_p) +
 Hn(11)*(ne*k1112 + nHp_ex*k1112_p ) - Hn(12)*(ec(12,11)+ec(12,10)+ec(12,9)+ec(12,8)+ec
(12,7)+ec(12,6)+ec(12,5)+ec(12,4)+ ec(12,3)+ec(12,2)+ec(12,1)+ne*(k_ion_e(12)+ k1220 +
k1219 + k1218 + k1217 + k1216 + k1215 + k1214 + k1213 + k1211 + k1210 + k129 + k128+
k127 +k126 + k125 + k124+ k123+ k122+ k12_1 ) + nHp_ex*(k_ion_p(12)+ k1220_p + k1219_p
+ k1218_p + k1217_p + k1216_p + k1215_p + k1214_p + k1213_p + k1211_p + k1210_p +
k129_p + k128_p + k127_p + k126_p + k125_p + k124_p + k123_p + k122_p + k12_1_p )) + Hn
(13)*(ec(13,12)+ne*k1312 + nHp_ex*k1312_p) + Hn(14)*(ec(14,12)+ne*k1412 + nHp_ex*
k1412_p) + Hn(15)*(ec(15,12)+ne*k1512+ nHp_ex*k1512_p)+ Hn(16)*(ec(16,12)+ne*k1612+
nHp_ex*k1612_p) + Hn(17)*(ec(17,12)+ne*k1712+nHp_ex*k1712_p) + Hn(18)*(ec(18,12)+ne*
k1812+nHp_ex*k1812_p)+ Hn(19)*(ec(19,12)+ne*k1912+nHp_ex*k1912_p) + Hn(20)*(ec(20,12)+
ne*k2012+nHp_ex*k2012_p);
e13= k_dis_h2(12)*nH2*ne + ne*nH2p*kdr(12)+ ne*nHp*(k_three_body(12)*ne + k_two_body(12) ) +
 Hn(1)*(k1_13*ne+k1_13_p*nHp_ex) + Hn(2)* ( ne*k213 + nHp_ex*k213_p ) + Hn(3)*( ne*k313
 + nHp_ex*k313_p) + Hn(4)*( ne*k413 + nHp_ex*k413_p) + Hn(5)*(ne*k513 + nHp_ex*k513_p)
+ Hn(6)*(ne*k613 + nHp_ex*k613_p) + Hn(7)*(ne*k713 + nHp_ex*k713_p) + Hn(8)*(ne*k813 +
nHp_ex*k813_p) + Hn(9)*(ne*k913 + nHp_ex*k913_p) + Hn(10)*(ne*k1013 + nHp_ex*k1013_p) +
 Hn(11)*(ne*k1113 + nHp_ex*k1113_p) + Hn(12)*(ne*k1213 + nHp_ex*k1213_p) - Hn(13)*(ec
(13,12)+ec(13,11)+ec(13,10)+ec(13,9)+ec(13,8)+ec(13,7)+ec(13,6)+ec(13,5)+ec(13,4)+ ec
(13,3)+ec(13,2)+ec(13,1)+ne*(k_ion_e(13)+ k1320 + k1319 + k1318 + k1317 + k1316 + k1315
 + k1314 + k1312 + k1311 + k1310 + k139 + k138+ k137 +k136 + k135 + k134+ k133+ k132+
k13_1 )+ nHp_ex*( k_ion_p(13)+ k1320_p + k1319_p + k1318_p + k1317_p + k1316_p +
k1315_p + k1314_p + k1312_p + k1311_p + k1310_p + k139_p + k138_p + k137_p + k136_p +
k135_p + k134_p + k133_p + k132_p + k13_1_p ) ) + Hn(14)*(ec(14,13)+ne*k1413 + nHp_ex*
k1413_p) + Hn(15)*(ec(15,13)+ne*k1513+ nHp_ex*k1513_p)+ Hn(16)*(ec(16,13)+ne*k1613+
nHp_ex*k1613_p) + Hn(17)*(ec(17,13)+ne*k1713+nHp_ex*k1713_p) + Hn(18)*(ec(18,13)+ne*
k1813+nHp_ex*k1813_p)+ Hn(19)*(ec(19,13)+ne*k1913+nHp_ex*k1913_p) + Hn(20)*(ec(20,13)+
ne*k2013+nHp_ex*k2013_p);
e14= k_dis_h2(13)*nH2*ne + ne*nH2p*kdr(13)+ ne*nHp*(k_three_body(13)*ne + k_two_body(13) ) +
 Hn(1)*(k1_14*ne+k1_14_p*nHp_ex) + Hn(2)* ( ne*k214 + nHp_ex*k214_p ) + Hn(3)*( ne*k314
 + nHp_ex*k314_p) + Hn(4)*( ne*k414 + nHp_ex*k414_p) + Hn(5)*(ne*k514 + nHp_ex*k514_p)
+ Hn(6)*(ne*k614 + nHp_ex*k614_p) + Hn(7)*(ne*k714 + nHp_ex*k714_p) + Hn(8)*(ne*k814 +
nHp_ex*k814_p) + Hn(9)*(ne*k914 + nHp_ex*k914_p) + Hn(10)*(ne*k1014 + nHp_ex*k1014_p) +
 Hn(11)*(ne*k1114 + nHp_ex*k1114_p) + Hn(12)*(ne*k1214 + nHp_ex*k1214_p) + Hn(13)*(ne*
k1314 + nHp_ex*k1314_p) - Hn(14)*(ec(14,13)+ec(14,12)+ec(14,11)+ec(14,10)+ec(14,9)+ec
(14,8)+ec(14,7)+ec(14,6)+ec(14,5)+ec(14,4)+ ec(14,3)+ec(14,2)+ec(14,1)+ne*( k_ion_e(14)
+ k1420 + k1419 + k1418 + k1417 + k1416 + k1415 + k1413 + k1412 + k1411 + k1410 + k149
+ k148+ k147 +k146 + k145 + k144+ k143+ k142+ k14_1 ) + nHp_ex*( k_ion_p(14)+ k1420_p +
 k1419_p + k1418_p + k1417_p + k1416_p + k1415_p + k1413_p + k1412_p + k1411_p +
k1410_p + k149_p + k148_p + k147_p +k146_p + k145_p + k144_p + k143_p + k142_p +
k14_1_p ) ) + Hn(15)*(ec(15,14)+ne*k1514 + nHp_ex*k1514_p)+ Hn(16)*(ec(16,14)+ne*k1614+
nHp_ex*k1614_p) + Hn(17)*(ec(17,14)+ne*k1714+nHp_ex*k1714_p) + Hn(18)*(ec(18,14)+ne*
k1814+nHp_ex*k1814_p)+ Hn(19)*(ec(19,14)+ne*k1914+nHp_ex*k1914_p) + Hn(20)*(ec(20,14)+
ne*k2014+nHp_ex*k2014_p);
e15= k_dis_h2(14)*nH2*ne + ne*nH2p*kdr(14)+ ne*nHp*(k_three_body(14)*ne + k_two_body(14) ) +
 Hn(1)*(k1_15*ne+k1_15_p*nHp_ex) + Hn(2)* ( ne*k215 + nHp_ex*k215_p ) + Hn(3)*( ne*k315
 + nHp_ex*k315_p) + Hn(4)*( ne*k415 + nHp_ex*k415_p) + Hn(5)*(ne*k515 + nHp_ex*k515_p)
+ Hn(6)*(ne*k615 + nHp_ex*k615_p) + Hn(7)*(ne*k715 + nHp_ex*k715_p) + Hn(8)*(ne*k815 +
nHp_ex*k815_p) + Hn(9)*(ne*k915 + nHp_ex*k915_p) + Hn(10)*(ne*k1015 + nHp_ex*k1015_p) +
 Hn(11)*(ne*k1115 + nHp_ex*k1115_p) + Hn(12)*(ne*k1215 + nHp_ex*k1215_p) + Hn(13)*(ne*
k1315 + nHp_ex*k1315_p) + Hn(14)*(ne*k1415 + nHp_ex*k1415_p) - Hn(15) *( ec(15,14)+ec
(15,13)+ec(15,12)+ec(15,11)+ec(15,10)+ec(15,9)+ec(15,8)+ec(15,7)+ec(15,6)+ec(15,5)+ec
(15,4)+ ec(15,3)+ec(15,2)+ec(15,1)+ ne*(k_ion_e(15)+ k1520 + k1519 + k1518 + k1517 +
k1516 + k1514 + k1513 + k1512 + k1511 + k1510 + k159 + k158+ k157 +k156 + k155 + k154 +
 k153 + k152 + k15_1 ) + nHp_ex*(k_ion_p(15)+ k1520_p + k1519_p + k1518_p + k1517_p +
k1516_p + k1514_p + k1513_p + k1512_p + k1511_p + k1510_p + k159_p + k158_p + k157_p +
k156_p + k155_p + k154_p + k153_p + k152_p + k15_1_p ) ) + Hn(16)*(ec(16,15)+ne*k1615+
nHp_ex*k1615_p) + Hn(17)*(ec(17,15)+ne*k1715+nHp_ex*k1715_p) + Hn(18)*(ec(18,15)+ne*
k1815+nHp_ex*k1815_p)+ Hn(19)*(ec(19,15)+ne*k1915+nHp_ex*k1915_p) + Hn(20)*(ec(20,15)+
ne*k2015+nHp_ex*k2015_p);
e16= k_dis_h2(15)*nH2*ne + ne*nH2p*kdr(15)+ ne*nHp*(k_three_body(15)*ne + k_two_body(15) ) +
 Hn(1)*(k1_16*ne+k1_16_p*nHp_ex) + Hn(2)* ( ne*k216 + nHp_ex*k216_p ) + Hn(3)*( ne*k316
 + nHp_ex*k316_p) + Hn(4)*( ne*k416 + nHp_ex*k416_p) + Hn(5)*(ne*k516 + nHp_ex*k516_p)
+ Hn(6)*(ne*k616 + nHp_ex*k616_p) + Hn(7)*(ne*k716 + nHp_ex*k716_p) + Hn(8)*(ne*k816 +
nHp_ex*k816_p) + Hn(9)*(ne*k916 + nHp_ex*k916_p) + Hn(10)*(ne*k1016 + nHp_ex*k1016_p) +
```

```
      Hn(11)*(ne*k1116 + nHp_ex*k1116_p) + Hn(12)*(ne*k1216 + nHp_ex*k1216_p) + Hn(13)*(ne*
     k1316 + nHp_ex*k1316_p) + Hn(14)*(ne*k1416 + nHp_ex*k1416_p) + Hn(15) *(ne*k1516 +
     nHp_ex*k1516_p ) - Hn(16) *( ec(16,15)+ec(16,14)+ec(16,13)+ec(16,12)+ec(16,11)+ec
     (16,10)+ec(16,9)+ec(16,8)+ec(16,7)+ec(16,6)+ec(16,5)+ec(16,4)+ ec(16,3)+ec(16,2)+ec
     (16,1)+ ne*(k_ion_e(16)+ k1620 + k1619 + k1618 + k1617+ k1615 + k1614 + k1613 + k1612 +
      k1611 + k1610 + k169 + k168+ k167 +k166 + k165 + k164 + k163 + k162 + k16_1 ) + nHp_ex
     *(k_ion_p(16)+ k1620_p + k1619_p + k1618_p + k1617_p + k1615_p + k1614_p + k1613_p +
     k1612_p + k1611_p + k1610_p + k169_p + k168_p + k167_p + k166_p + k165_p + k164_p +
     k163_p + k162_p + k16_1_p ) ) + Hn(17)*(ec(17,16)+ne*k1716+nHp_ex*k1716_p) + Hn(18)*(ec
     (18,16)+ne*k1816+nHp_ex*k1816_p)+ Hn(19)*(ec(19,16)+ne*k1916+nHp_ex*k1916_p) + Hn(20)*(
     ec(20,16)+ne*k2016+nHp_ex*k2016_p);
e17= k_dis_h2(16)*nH2*ne + ne*nH2p*kdr(16)+ ne*nHp*(k_three_body(16)*ne + k_two_body(16) ) +
      Hn(1)*(k1_17*ne+k1_17_p*nHp_ex) + Hn(2)* ( ne*k217 + nHp_ex*k217_p ) + Hn(3)*( ne*k317
      + nHp_ex*k317_p) + Hn(4)*( ne*k417 + nHp_ex*k417_p) + Hn(5)*(ne*k517 + nHp_ex*k517_p)
     + Hn(6)*(ne*k617 + nHp_ex*k617_p) + Hn(7)*(ne*k717 + nHp_ex*k717_p) + Hn(8)*(ne*k817 +
     nHp_ex*k817_p) + Hn(9)*(ne*k917 + nHp_ex*k917_p) + Hn(10)*(ne*k1017 + nHp_ex*k1017_p) +
      Hn(11)*(ne*k1117 + nHp_ex*k1117_p) + Hn(12)*(ne*k1217 + nHp_ex*k1217_p) + Hn(13)*(ne*
     k1317 + nHp_ex*k1317_p) + Hn(14)*(ne*k1417 + nHp_ex*k1417_p) + Hn(15) *(ne*k1517 +
     nHp_ex*k1517_p ) + Hn(16) *(ne*k1617 + nHp_ex*k1617_p ) - Hn(17) *( ec(17,16)+ ec
     (17,15)+ec(17,14)+ec(17,13)+ec(17,12)+ec(17,11)+ec(17,10)+ec(17,9)+ec(17,8)+ec(17,7)+ec
     (17,6)+ec(17,5)+ec(17,4)+ ec(17,3)+ec(17,2)+ec(17,1)+ ne*(k_ion_e(17)+ k1720 + k1719 +
     k1718 + k1716 + k1715 + k1714 + k1713 + k1712 + k1711 + k1710 + k179 + k178+ k177 +k176
      + k175 + k174 + k173 + k172 + k17_1 ) + nHp_ex*( k_ion_p(17)+ k1720_p + k1719_p +
     k1718_p + k1716_p + k1715_p + k1714_p + k1713_p + k1712_p + k1711_p + k1710_p + k179_p
     + k178_p + k177_p + k176_p + k175_p + k174_p + k173_p + k172_p + k17_1_p ) ) + Hn(18)*(
     ec(18,17)+ne*k1817+nHp_ex*k1817_p)+ Hn(19)*(ec(19,17)+ne*k1917+nHp_ex*k1917_p) + Hn(20)
     *(ec(20,17)+ne*k2017+nHp_ex*k2017_p);
e18= k_dis_h2(17)*nH2*ne + ne*nH2p*kdr(17)+ ne*nHp*(k_three_body(17)*ne + k_two_body(17) ) +
      Hn(1)*(k1_18*ne+k1_18_p*nHp_ex) + Hn(2)* ( ne*k218 + nHp_ex*k218_p ) + Hn(3)*( ne*k318
      + nHp_ex*k318_p) + Hn(4)*( ne*k418 + nHp_ex*k418_p) + Hn(5)*(ne*k518 + nHp_ex*k518_p)
     + Hn(6)*(ne*k618 + nHp_ex*k618_p) + Hn(7)*(ne*k718 + nHp_ex*k718_p) + Hn(8)*(ne*k818 +
     nHp_ex*k818_p) + Hn(9)*(ne*k918 + nHp_ex*k918_p) + Hn(10)*(ne*k1018 + nHp_ex*k1018_p) +
      Hn(11)*(ne*k1118 + nHp_ex*k1118_p) + Hn(12)*(ne*k1218 + nHp_ex*k1218_p) + Hn(13)*(ne*
     k1318 + nHp_ex*k1318_p) + Hn(14)*(ne*k1418 + nHp_ex*k1418_p) + Hn(15) *(ne*k1518 +
     nHp_ex*k1518_p ) + Hn(16) *(ne*k1618 + nHp_ex*k1618_p )+ Hn(17) *(ne*k1718 + nHp_ex*
     k1718_p ) - Hn(18) *( ec(18,17)+ ec(18,16)+ ec(18,15)+ec(18,14)+ec(18,13)+ec(18,12)+ec
     (18,11)+ec(18,10)+ec(18,9)+ec(18,8)+ec(18,7)+ec(18,6)+ec(18,5)+ec(18,4)+ ec(18,3)+ec
     (18,2)+ec(18,1)+ ne*(k_ion_e(18)+ k1820 + k1819 + k1817 + k1816 + k1815 + k1814 + k1813
      + k1812 + k1811 + k1810 + k189 + k188+ k187 +k186 + k185 + k184 + k183 + k182 + k18_1
     ) + nHp_ex*(k_ion_p(18)+ k1820_p + k1819_p + k1817_p + k1816_p + k1815_p + k1814_p +
     k1813_p + k1812_p + k1811_p + k1810_p + k189_p + k188_p + k187_p + k186_p + k185_p +
     k184_p + k183_p + k182_p + k18_1_p ) ) + Hn(19)*(ec(19,18)+ne*k1918+nHp_ex*k1918_p) +
     Hn(20)*(ec(20,18)+ne*k2018+nHp_ex*k2018_p);
e19= k_dis_h2(18)*nH2*ne + ne*nH2p*kdr(18)+ ne*nHp*(k_three_body(18)*ne + k_two_body(18) ) +
      Hn(1)*(k1_19*ne+k1_19_p*nHp_ex) + Hn(2)* ( ne*k219 + nHp_ex*k219_p ) + Hn(3)*( ne*k319
      + nHp_ex*k319_p) + Hn(4)*( ne*k419 + nHp_ex*k419_p) + Hn(5)*(ne*k519 + nHp_ex*k519_p)
     + Hn(6)*(ne*k619 + nHp_ex*k619_p) + Hn(7)*(ne*k719 + nHp_ex*k719_p) + Hn(8)*(ne*k819 +
     nHp_ex*k819_p) + Hn(9)*(ne*k919 + nHp_ex*k919_p) + Hn(10)*(ne*k1019 + nHp_ex*k1019_p) +
      Hn(11)*(ne*k1119 + nHp_ex*k1119_p) + Hn(12)*(ne*k1219 + nHp_ex*k1219_p) + Hn(13)*(ne*
     k1319 + nHp_ex*k1319_p) + Hn(14)*(ne*k1419 + nHp_ex*k1419_p) + Hn(15) *(ne*k1519 +
     nHp_ex*k1519_p ) + Hn(16) *(ne*k1619 + nHp_ex*k1619_p )+ Hn(17) *(ne*k1719 + nHp_ex*
     k1719_p )+ Hn(18) *(ne*k1819 + nHp_ex*k1819_p ) - Hn(19) *( ec(19,18)+ ec(19,17) + ec
     (19,16)+ ec(19,15)+ec(19,14)+ec(19,13)+ec(19,12)+ec(19,11)+ec(19,10)+ec(19,9)+ec(19,8)+
     ec(19,7)+ec(19,6)+ec(19,5)+ec(19,4)+ ec(19,3)+ec(19,2)+ec(19,1)+ ne*(k_ion_e(19)+ k1920
      + k1918 + k1917 + k1916 + k1915 + k1914 + k1913 + k1912 + k1911 + k1910 + k199 + k198+
      k197 +k196 + k195 + k194 + k193 + k192 + k19_1 ) + nHp_ex*(k_ion_p(19)+ k1920_p +
     k1918_p + k1917_p + k1916_p + k1915_p + k1914_p + k1913_p + k1912_p + k1911_p + k1910_p
      + k199_p + k198_p + k197_p + k196_p + k195_p + k194_p + k193_p + k192_p + k19_1_p ) )
     + Hn(20)*(ec(20,19)+ne*k2019+nHp_ex*k2019_p) ;
e20= k_dis_h2(19)*nH2*ne + ne*nH2p*kdr(19)+ ne*nHp*(k_three_body(19)*ne + k_two_body(19) ) +
      Hn(1)*(k1_20*ne+k1_20_p*nHp_ex) + Hn(2)* ( ne*k220 + nHp_ex*k220_p ) + Hn(3)*( ne*k320
      + nHp_ex*k320_p) + Hn(4)*( ne*k420 + nHp_ex*k420_p) + Hn(5)*(ne*k520 + nHp_ex*k520_p)
     + Hn(6)*(ne*k620 + nHp_ex*k620_p) + Hn(7)*(ne*k720 + nHp_ex*k720_p) + Hn(8)*(ne*k820 +
     nHp_ex*k820_p) + Hn(9)*(ne*k920 + nHp_ex*k920_p) + Hn(10)*(ne*k1020 + nHp_ex*k1020_p) +
      Hn(11)*(ne*k1120 + nHp_ex*k1120_p) + Hn(12)*(ne*k1220 + nHp_ex*k1220_p) + Hn(13)*(ne*
     k1320 + nHp_ex*k1320_p) + Hn(14)*(ne*k1420 + nHp_ex*k1420_p) + Hn(15) *(ne*k1520 +
     nHp_ex*k1520_p ) + Hn(16) *(ne*k1620 + nHp_ex*k1620_p )+ Hn(17) *(ne*k1720 + nHp_ex*
```

```
            k1720_p )+ Hn(18) *(ne*k1820+ nHp_ex*k1820_p )+ Hn(19) *(ne*k1920+ nHp_ex*k1920_p ) -
            Hn(20) *( ec(20,19)+ ec(20,18)+ ec(20,17) + ec(20,16)+ ec(20,15)+ec(20,14)+ec(20,13)+ec
            (20,12)+ec(20,11)+ec(20,10)+ec(20,9)+ec(20,8)+ec(20,7)+ec(20,6)+ec(20,5)+ec(20,4)+ ec
            (20,3)+ec(20,2)+ec(20,1)+ ne*(k_ion_e(20)+ k2019 + k2018 + k2017 + k2016 + k2015 +
            k2014 + k2013 + k2012 + k2011 + k2010 + k209 + k208+ k207 +k206 + k205 + k204 + k203 +
            k202 + k20_1 ) + nHp_ex*(k_ion_p(20)+ k2019_p + k2018_p + k2017_p + k2016_p + k2015_p +
             k2014_p + k2013_p + k2012_p + k2011_p + k2010_p + k209_p + k208_p + k207_p + k206_p +
            k205_p + k204_p + k203_p + k202_p + k20_1_p ) ) ;



       HH=[e1;e2;e3;e4;e5;e6;e7;e8;e9;e10;e11;e12;e13;e14;e15;e16;e17;e18;e19;e20];


end
```